Title

Fire Whirls Over Liquid Fuels at Multiple Scales: Emissions, Burning Rates, and Sensitivity to Slick Thickness

ISBN
9798276023991

Author
Dowling, Joseph Lee

Publication Date
2025-12-06

Fire Whirls Over Liquid Fuels at Multiple Scales: Emissions, Burning Rates, and Sensitivity to Fuel Thickness

By

Joseph Lee Dowling

A dissertation submitted in partial satisfaction of the

requirements for the degree of

Doctor of Philosophy

in

Engineering- Mechanical Engineering

in the

Graduate Division

of the

University of California, Berkeley

Committee in charge:

Associate Professor Michael J. Gollner, Chair
Professor Van Carey
Assistant Professor Thomas Schutzius

Fall 2025

Fire Whirls Over Liquid Fuels at Multiple Scales: Emissions, Burning Rates, and Sensitivity to Fuel Thickness

Abstract

Fire Whirls Over Liquid Fuels at Multiple Scales: Emissions, Burning Rates, and Sensitivity to Fuel Thickness

By

Joseph Lee Dowling

Doctor of Philosophy in Engineering- Mechanical Engineering

University of California, Berkeley

Associate Professor Michael J. Gollner, Chair

Fire whirls have long been a fascination in the field of fire science, but few studies have been conducted with the intention of creating fire whirls at the field scale, and even fewer with associated measurements of emissions. Fire whirls are known to increase the flame length and burning rate for flames over liquid fuel pools, with recent research indicating that they reduce the amount of particulate soot emitted by the flame. These properties make it desirable for the process of *in-situ* burning, where air pollution and burning duration both must be minimized.

In this study, the sensitivity of fire whirl behavior and burning characteristics to the dimensions of a fixed-frame fire whirl generator were first investigated at the laboratory scale. Fire whirls were found to enhance burning rates and reduce emissions when burning slicks of crude oil over water when compared to pool fires, regardless of the thickness of the oil slick. Further increases in slick thickness improved the burning rate, but with diminishing returns. Flame lengths, burning rates, and quantities of particulate soot production were found to be sensitive to the height of the fire whirl generator's enclosure. Higher walls increased the burning rate and flame lengths while decreasing the emissions of soot to a minimum value. This is inferred to be due to an increase in effective circulation within the enclosure. This trend held until a critical wall height, above which the flame shrinks and weakens. This critical wall height is dependent on the size of the enclosure footprint.

One of the largest controlled fire whirl experiments was conducted at the field scale, with instrumentation used to collect the flame height, temperature, burning rate, emissions production, and heat flux. The desirable traits of the fire whirl were still present at this scale, with burning rates increased by a factor of up to 141% and reducing particulate soot emission to a minimum of 53% of the pool fire's soot emission per mass of fuel burned. However, these improvements were limited to specific cases as some tests experienced premature burnout.

To David Dowling, and Michael, Kevin and Jim Donahue,
Firefighters who inspired me to study fire and solve problems that help people

To Marie Dowling and Germaine Donahue,
who loved all five of us very much

To Samantha Moeckel,
who made sure I lived to see the end of this degree

Contents

List of Figures

List of Tables

Acknowledgments

This work would not have been possible without the guidance and support of Prof. Michael Gollner, who has been a mentor on all aspects of the research presented here as well as many aspects of life as an academic. The guidance and efforts of Prof. Elaine S. Oran, Prof. Hadi Hajilou and Dr. Wuquan Cui have been invaluable in doing this research and creating meaningful scientific achievement out of the very messy work of handling crude oil. Additionally, I would like to thank Mike Neufer and Daniel Paragas for manufacturing almost every piece of equipment used in the laboratory and managing the hazardous materials used in this research.

I have the utmost gratitude for my labmates who supported me for the five years I spent in California working on this dissertation. Christina, Melanie, Kelly, Mackenzie, and Bryce, and to my friends in the EBMP, you saved me from the greatest dangers of graduate school research — loneliness and burnout. I hope I have provided even half the companionship and inspiration you all have given me.

The research presented in this work was funded in part by the Bureau of Safety and Environmental Enforcement (BSEE) through contract number 40E0121C0004, with special thanks to Branch Chief Karen N. Stone. Some results of this work have been published in part as fulfillment of this contract in BSEE report OSRR-1124 AA "Efficient Remediation of Oil Spills Using Fire Whirls."

The author of this research gratefully thanks the Keith L. Markolf and Cristina T. Ruland Fellowship for supporting this research.

Chapter 2 has been published in *Fuel*, "Fire whirl emissions and burning rates for crude oil slicks of varying thicknesses," by J.L. Dowling, W. Cui, M. Hajilou, and M.J. Gollner, (2025) v. 393. The thesis author is the primary investigator in the publication

Chapter 3 is undergoing revision before its contents will be published in part in a journal yet to be determined, with authorship by J.L. Dowling as primary investigator, W. Cui, M. Hajilou, and M.J. Gollner.

Chapter 4 has been published in part in *Fuel*, "Large-scale experiments on enhancing In-situ burning with fire whirls," by W. Cui, J.L. Dowling, M. Hajilou, M. Huffman, B. Pawar, J. Aurell, Q. Wang, E.S. Oran, K. N. Stone, and M.J. Gollner, (2026) v. 403. The thesis author was one of the primary investigators and designers of the large scale experiments referenced in this chapter, as well as responsible for the data analysis in the portions of the published work written here. These sections are presented with consent from the first author and other contributors.

Chapter 1

Introduction

1.1 Motivation

The fire whirl phenomenon is both a spectacle and a hazard often present in wildland fires, causing destruction when they form and altering how the surrounding fire will behave [1]. Large scale wildland fires, such as those seen in recent years in California, can cause fire whirls to form at massive scales, endangering lives and property [2]. Historically, fire whirls have even occurred in urban conflagrations, though significantly more rarely [3]. A challenge is then presented to take the properties of the fire whirl which makes it such a hazard and use them in a beneficial manner.

This research was partially inspired by anecdotal evidence of fire whirls and whirling flame structures occurring spontaneously in the field, forming over layers of liquid fuels over water [4, 5]. The high heat fluxes and burning rates of fire whirls [6, 7] could be applied in the situation where consumption of a liquid fuel over water needs to be as fast and clean as possible, the *in-situ* burning of oil spills. Current forecasts predict a global consumption of crude oil of over 100,000,000 barrels of oil per day in 2025-2026 [8]. With 244 operational offshore oil rigs at time of writing, oil spills on the open ocean are a valid concern [9].

1.2 Background

In-situ Burning of Oil Spills

Oil spills over water can cause catastrophic damage to marine ecosystems [10]. One method of remediating a recent oil spill is to burn off the slick of oil before it can cause more damage to the ecosystem after mixing with the water; this process is known as *in-situ* burning. The most widely-known instance of *in-situ* burning as a remediation method for oil spills on water is likely the containment efforts for the 2010 Deepwater Horizon oil spill, during which over 400 individual burns removed up to 310,000 barrels of oil from the water surface [11]. Another high-profile instance of *in-situ* burning was the Exxon Valdez oil spill in 1990, during which up to 114,000 L of crude oil was burned and removed from the water surface [12]. The process of burning the oil off of the water surface is very efficient at removing the volume of oil spilled, removing up to 95% of the volume of the spilled oil depending on the initial thickness of the oil slick, but leaves a residue of the heaviest components of the oil [13–15]. The process is slow, with surface regression rates, which means the rate at which the oil slick is reduced in thickness, of approximately 0.06 mm/s [16]. The effective combustion of the fuel is hampered by the emulsification of the oil and the water surface, creating an oil slick that contains a large percentage of water that must be evaporated before the fuel can reach its ignition temperature [17]. *In-situ* burning operations combust the hydrocarbons that make up the oil slick and emit the products of combustion into the atmosphere. The emission of soot particles pose a health risk to those near the operation [18], visible as large plumes of dark smoke. The particles produced by *in-situ* burning are of a size small enough that they are respirable and may pass into the lungs of those that inhale the product gases

[19]. One of the goals of applying fire whirls to *in-situ* burning operations is to reduce the amount of particulate soot generated, particularly in the respirable range, that is emitted by burning the oil during a potential clean-up operation [20, 21].

Fire Whirl Behavior and Structure

Fire whirls form when ambient circulation is concentrated into a vortex column over a flame that serves as the source of buoyancy that drives the vortex. Two broad classes of fire whirl generator can be categorized based on the method used to impart this circulation: an Emmons-type fire whirl generator, which consists of a spinning mesh surrounding a fuel source [22], or a fixed-frame generator, which uses obstacles or walls to control the inflow of entrained air to create the fluid vortex [6, 23]. This research focuses on the fixed-frame fire whirl generator, which requires no moving parts to create a fire whirl. The fire whirl is taller and burns faster than a pool fire with a fuel source of an equivalent size [24]. The increase in burning rate for a fire whirl over a liquid fuel is the result of the vortex structure. The initiation of a radial inflow, akin to Ekman pumping [25], provides oxygen to the fuel vapor liberated from the liquid fuel surface. In addition to providing oxygen, this also forces the flame closer to the fuel surface, increasing heat transfer.

The fire whirl lengthens due to the direct effect of the vortex [23, 26], an increase in the burning rate [25], and the effect of turbulence dissipation [27]. The flame length of non-whirling flames depends upon the heat release rate of the flame [28], as a consequence of the presence of more fuel and the effect of buoyancy on the high temperature gases of the fire. Fire whirls similarly depend upon the heat release rate of the flame [29], but the flame length is also dependent upon the circulation imparted to the flame [26, 30]. The vortex is formed by the hot flame exhaust gases moving with some tangential velocity around the axis of the fuel source. This vortex concentrates the vorticity of the fluid and stretches the flame taller through this fluid dynamic effect [31]. The other factor influencing the height of the flame is the suppression of turbulent mixing. As there is a considerable tangential component to the fluid velocity, there is a radial stratification of gaseous components driven by a centrifugal force which inhibits the ability for the gases to mix [6, 27].

Emissions and Particulate Matter

Fire whirls have been shown in recent research to reduce the amount of soot produced in the combustion of a liquid fuel [20, 21], though the method by which this occurs is as yet poorly understood and is further investigated in this research. A pool fire is a form of nonpremixed flame wherein fuel vapors from the flammable liquid are transported via diffusion and fluid movement, encounter oxygen, and combust [32]. In diffusion flames, on the fuel rich side of the flame sheet, soot particles are formed, a process called soot inception. These particles become larger as they are convected through the flame, either through each particle becoming larger, a process known as surface growth, or from multiple particles attaching together, known as coagulation [33, 34]. At the same time, the soot particles are under chemical attack from oxidative species and radicals [35] which will reduce the size and number of soot particles as they are consumed before leaving the flame.

The factor that controls both the growth and oxidation of soot is the temperature of the flame near the soot particle [36, 37]. As the formation of soot is a multi-faceted process, the influence of temperature and of local species have complex and nonlinear effects on net soot production. As soot is responsible for the luminosity of the flame [35], more luminosity may indicate the presence of more soot, which causes the flame to radiate more heat, lowering the temperature of the flame [37]. Higher heat release rates are associated with higher soot production, as more fuel is consumed and therefore should produce more soot, assuming the quantity of emitted soot per unit of fuel consumed is constant. As the relative concentration of fuel increases, the propensity to form soot may increase, but this also limits the rate at which the fuel can burn, causing an implicit and complex system [38].

Measurement of Flame Characteristics

The primary products by mass of a diffusion flame are gaseous species produced by combustion. In particular, carbon dioxide (CO_2) and carbon monoxide (CO), the latter produced in greater quantities when combustion is inefficient or occurs at richer than stoichiometric conditions. A useful metric in describing the conditions of the flame is the modified combustion efficiency, MCE, calculated as:

$$MCE = \frac{\Delta CO_2}{\Delta CO_2 + \Delta CO} \tag{1.1}$$

where ΔCO_2 and ΔCO are the excess carbon dioxide and carbon monoxide in the flame product gases, respectively [39]. In this context, excess of a species refers to the amount by which the measured quantity of the species exceeds the quantity in ambient air, usually given in molar quantities. Measurement of these species, as well as oxygen, also allows for a measurement of the heat release rate of the flame by way of oxygen consumption calorimetry [40]. For pure fuels, like n-heptane, heat release rate can be calculated directly from the mass loss rate:

$$HRR = \dot{m}\Delta H_C \tag{1.2}$$

where $\dot{m}$ is the mass loss rate of the fuel and ΔH_C is the heat of combustion of that fuel. Additionally, throughout this work, a surface mass flux, SMF may be used instead of $\dot{m}$, where the mass loss rate has been normalized by the surface area of the fuel pool to give a value in mass per second per unit area.

1.3 Dissertation Outline

This work consists of five chapters, the first of which is an introduction to the concepts central to the rest of the paper. This consists of an introduction to fire whirls as a burning regime and their comparison to pool fires, the process of *in-situ* burning and the ways fire

whirls could enhance it, and the measurement of particulate and gaseous emissions from flames.
Chapter two consists of a laboratory-scale study on the effect of the thickness of an oil slick over a water layer on the formation of a fire whirl in a fixed-frame generator. An experimental investigation was conducted in which the thickness of an oil slick was varied between 3 and 11 mm and subjected to either a pool fire or a fire whirl. This investigation includes two different blends of crude oil. The heat flux to the fuel surface, the mass loss rate, and the particulate and gaseous emissions from the flame were recorded and analyzed. One phenomenon of interest in this investigation was boilover, during which the water layer begins to boil, causing bubbles to burst through the oil and violently increase burning rate. Increased slick thickness caused greater burning rates for the tested fire whirls until a critical slick thickness was reached, extending a trend seen in pool fires.

Chapter three consists of an experimental investigation into the effect of fixed-frame fire whirl generator dimensions on the produced flame. A modular four-walled fixed-frame fire whirl generator was constructed so that the height of the walls and the width of the generator enclosure could be varied. Mass loss rates, flame heights, and particulate emissions were recorded for the heptane-fueled flames produced in testing. A trend was found between enclosure height, flame height, and production of particulate emissions, such that an increase in enclosure height may increase the magnitude of circulation forming the fire whirl vortex, increasing its height and decreasing its emission of soot.

Chapter four is the culmination of chapters two and three into a large scale experiment that took place at Texas A&M. The large scale experiment investigated the practicality of forming fire whirls over crude oil fuel slicks at the field scale. Chapters two and three form the foundation of the scaling parameters needed to create the fire whirl generator at the size required in the field. The resulting fire whirls reached 1.5 m in diameter and nearly 5 m in height. These experiments are therefore some of the largest fire whirls created in a scientific investigation. While these experiments were successful in producing fire whirls that had consistent properties to those found at the small scale, the influence of wind at the large scale was found to greatly interfere with the steady formation of the fire whirl.

Chapter five is the conclusion of this work, providing a summary of the results of these experimental investigations and the hypotheses they support when viewed as a whole.

Chapter 2

Effect of Slick Thickness of Crude Oil on Emissions and Burning Rates of Fire Whirls

2.1 Introduction

Fire whirls are an extreme fire phenomenon often occurring in large wildland fires and urban conflagrations [1, 41]. They cause dramatically taller fires with higher burning rates, properties that make them dangerous in fire safety scenarios but have potential uses when induced under controlled conditions [5]. Fire whirls have been shown in past research to reduce $PM_{2.5}$ emissions and increase the burning rate of liquid fuel fires when compared to unaugmented pool fires [5, 20]. These properties may be useful for the *in-situ* burning of oil spills. In order for these properties to have practical value, these benefits must apply for a wide range of scenarios that can occur during these operations such as variations in fuel slick thickness or composition of the crude oil.

In the event of an oil spill, a priority of the clean-up effort is the removal of the oil slick from the surface of the water. *In-situ* burning is a process that is used to ameliorate the effect of the spilled oil by burning it off of the water surface before wave action and emulsification can mix the oil into the water, which would make the oil irretrievable and cause greater environmental harm [13, 42]. The process of *in-situ* burning is an effective tool for remediation, with a prominent example of its application being the Exxon Valdez oil spill in 1989, with the conservatively estimated removal of all but 1,136 L of the 56,000 to 114,000 L of oil spilled onto the surface of Prince William Sound [12]. The process of *in-situ* burning has a detrimental effect on nearby air quality, as smoke and soot is released from the burning slick into the atmosphere [42]. Gaseous products of combustion, such as polycyclic aromatic hydrocarbons (PAH), volatile organic compounds (VOC) and carbon monoxide (CO), are potentially hazardous, but may not form in quantities harmful to humans [13, 43]. The most prevalent hazard to health and air quality is the production of respirable particulate matter and its associated chemical constituents [13].

In-situ burning has been well characterized as a form of pool fire [44] with the addition of a water layer forming the bottom boundary of the fuel slick that changes the transfer and storage of heat in the fuel layer [45]. Pool fires are a type of diffusion flame where fuel vapor from the liquid fuel pool reacts with oxygen in the ambient air to form a flame sheet separating the fuel-rich core and the oxygen-rich ambient environment. Combustion continues as buoyancy draws the hot product gases up and away from the fuel surface and fresh air is drawn in to replace them, diffusing into the flame sheet [46]. The burning characteristics of a pool fire are determined largely by the implicit interaction between fuel vaporization and heat transfer from the flame. In the absence of external heating, greater heat transfer from the flame leads to greater vaporization rates of the fuel, leading to greater fuel availability in the gas phase and therefore a higher burning rate. This heat feedback cycle continues until heat losses to the environment and the heat required to continue pyrolysis balance the increases in heat availability and a steady burning state is reached [40, 46]. The presence of a water layer beneath the fuel pool in *in-situ* burning events and experimental investigations thereof provide an additional method of heat loss from the fuel surface. Additionally, the presence of the water layer causes a phenomenon known as boilover, where the water at the interface with the fuel layer reaches its boiling point and causes vapor bubbles to burst through the fuel layer and increase the burning rate [45, 47]. The formation of soot in the pool fire is controlled by the mixing of fuel and oxidizer, but net soot production by the flame is reduced as the soot particles oxidize, resulting in a dependence on the residence time of soot particles in the reacting regions of the flame [46].

Fire whirls increase the burning rate of a liquid fuel due to increased heat transfer at the fuel surface [6]. The imbalance of centripetal and radial forces at the base of the vortex structure cause a net radial inflow of air similar to Ekman pumping [22, 25]. This enhances the fuel-air mixing at the base and brings the flame sheet closer to the fuel surface, increasing heat transfer to the surface, increasing the burning rate due to increased heat feedback and mass transfer [24, 25]. The increase in fuel evaporation and burning rate elongate the visible flame due to the increase in flammable gases [25, 27] while the formation of the vortex further stretches the flame vertically [6, 48]. While the generation of fire whirls in nature often relies on surrounding topology and vegetation to provide the initial vorticity for the generating eddy [48, 49], the generation of fire whirls in the laboratory typically relies on either a spinning mesh [22] to induce the vortex, or on a fixed-frame imparting tangential velocity to the air that is naturally entrained by the flame [41]. Recent research by [20] indicates that particulate soot production is reduced by the formation of a fire whirl over what would otherwise be a pool fire. The mechanisms by which this is achieved are not thoroughly understood, but may rely on improved mixing, increased temperatures, oxygen availability [20], potential changes to the relative size of the fuel-rich core of the pool fire [46], or alterations to fundamental soot production parameters such as particle residence time [35, 50, 51]. Previous research was conducted into the practicality of generating fire whirls at scale by determining the critical heights of obstacles used in a fixed-frame fire whirl generator [52], but did not address the characteristics of the fuel layer at scale.

The current understanding of the effect of fire whirls on emissions from liquid fuels does not take into account the thickness of the fuel layer supporting the flame. In a practical implementation of *in-situ* burning, the thickness of the oil slick does not remain constant, and the heat transfer to the oil layer is affected by the cold water layer. This research investigates the effect of varying the slick thickness of two blends of crude oil over water on the particulate emissions and combustion efficiency of the resulting flame. Three slick thicknesses are tested for each oil type to investigate trends in particulate matter production and mass loss rate. The flame behavior is monitored by way of the instantaneous mass of remaining fuel and the heat flux received by the fuel surface, while the efficiency of combustion is estimated by the production of gaseous species and particulate matter.

2.2 Experimental Apparatus and Methods

To generate fire whirls, a three-wall fixed-frame fire whirl generator [6, 41] was constructed. This generator deviates from previous four-wall square fire whirl generators [20] or multi-vaned [23] fire whirl generators used in previous research, but was chosen to avoid the potential for diagonal cross-flows across the fuel pool that might disturb vortex formation.

Additionally, qualitative comparisons of the four-wall and three-wall generators found a reduced effect of flame wander [53] during the brief formation period of the conical fire whirl when the three-wall generator was used, while no difference in steady-state behavior was discerned. The base of the fire whirl generator formed an equilateral triangle with side length $S = 52cm$, with three 60 cm high walls forming the boundary of the enclosure. Buoyancy from the fire plume causes air to enter the enclosure through a 10 cm wide gap in the left side of each wall, forming a vortex which spins clockwise when viewed from above. At the center of the triangular enclosure, a 10 cm diameter fuel dish was placed within the base of the apparatus such that the fuel surface would be flush with the enclosure floor to preserve laminar flow at the base of the flame. The fuel dish used in this investigation is 5.0 cm deep, with each test volume of oil added to the fuel dish floating over a layer of water such that the fuel surface would be as close as possible to flush with the enclosure floor. This water layer also provides a cold and nearly isothermal reservoir at the base of the fuel layer for better analysis of the oil layer's heating [45, 47]. A top-down schematic of the enclosure is shown in Figure 2.1.

Three slick thicknesses, approximately 3.5, 7, and 11 mm, were used in pool fire and fire whirl experiments for each of two oil blends, Alaskan North Slope (ANS) and Hoover Offshore Oil Platform System (HOOPS) crude oil. These thicknesses were chosen as they represent a thickness that is near the lower boundary of ignitability for crude oil [13], a thickness beyond which pool fires have similar surface mass fluxes independent of slick thickness[14, 45], and a thickness near the midpoint of these values. A CHN analysis was conducted to quantify the components of the crude oils used in these experiments, with ANS crude oil composed of 86.0% carbon, 12.3% hydrogen, 0.7% nitrogen, and 1.0% oxygen, and HOOPS crude oil composed of 85.8% carbon, 8.2% hydrogen, 0.9% nitrogen, and 5.1% oxygen by weight. These values match well with those described in literature [54, 55].

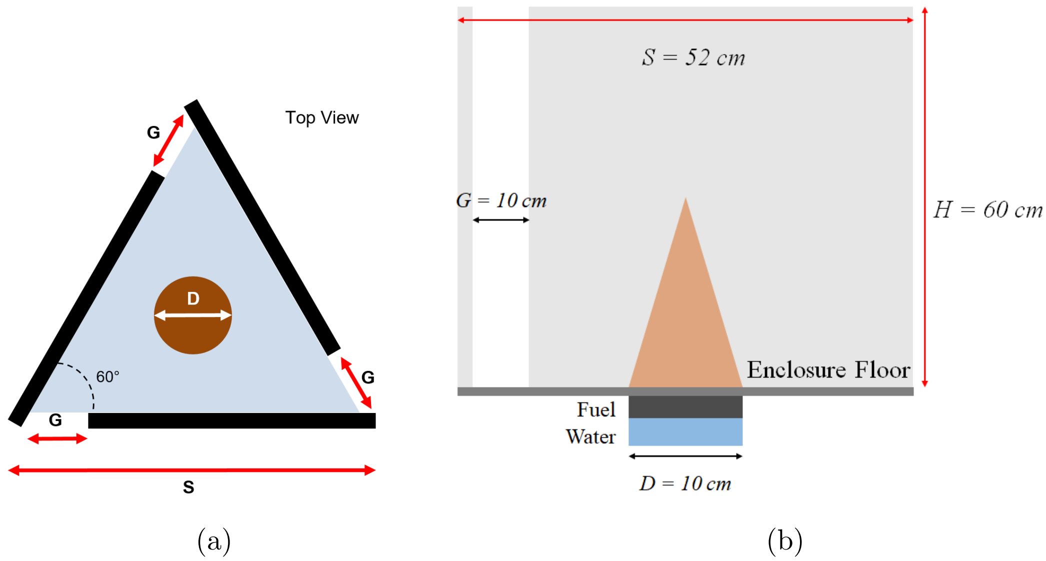

Figure 2.1: Diagram of three-wall generator enclosure, with gap size $G = 10cm$, pool diameter $D = 10cm$, and side length $S = 52cm$ with a) top-down view and b) profile view.

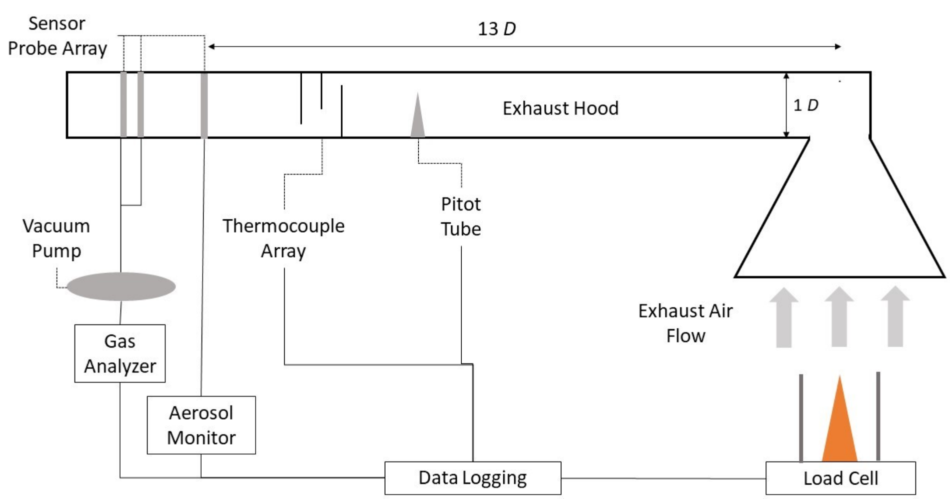

Figure 2.2: Instrumentation used for data collection, including DustTrak DRX 8534 aerosol monitor, CAI ZPA gas analyzer, and Mettler-Toledo load cell.

For each unique combination of fuel, flame configuration, and slick thickness, a minimum of five tests were performed, save at the thickest tests with ANS crude oil for which only three tests per data point were performed. The instantaneous mass of the fuel dish was monitored at a frequency of 1 Hz via a Mettler-Toledo load cell with an accuracy of 0.01g. The emissions from the fire whirls and pool fires generated were captured by an overhead exhaust instrumentation system, diagrammed in Figure 2.2. A Sony RX10 series digital camera was used to capture images of the flame for qualitative analysis. A volumetric flow of approximately 0.4 cubic meters per second drew the gaseous products of combustion into the exhaust hood, which has a diameter of approximately 23 cm. Sampling probes were inserted into the exhaust flow system approximately 3 meters downstream from the system inlet, which would allow for full mixing of the sampled gases. System volumetric flow was monitored during all tests using a Veris Verabar pitot tube combined with three thermocouples to provide accurate gas temperatures. A TSI DustTrak DRX 8534 optical aerosol monitor was used to measure the mass of fine respirable particles, those with diameters that are 2.5 micrometers and smaller ($PM_{2.5}$), emitted by the flames as a function of time. An internal pump drew gas from the sampling probe at a rate of 2 SLPM. The $PM_{2.5}$ measurements were calibrated using gravimetric measurements of soot captured by a filter cassette with 0.8 micron pores to accurately represent the density of collected soot. A California Analytical Instruments CAI ZPA NDIR/O_2 gas analyzer was used to measure the concentrations of CO_2, CO, and O_2 in the exhaust air from the tested flames, with ranges 0-10%, 0-1%, and 0-25% respectively. Samples were drawn from the probe through a filtered line at a rate of 0.5 SLPM. The measurements of CO_2 generation rate, O_2 consumption rate, and particulate matter generation rate at every second for a sample experiment are shown in Figure 2.3a for an 11 mm thick ANS pool fire, with smoothing in the form of a ten-point moving average for the species measurements.

The mass of remaining fuel at each second for this experiment is in Figure 2.3b with the instantaneous mass loss rate, as smoothed by a ten-point moving average.

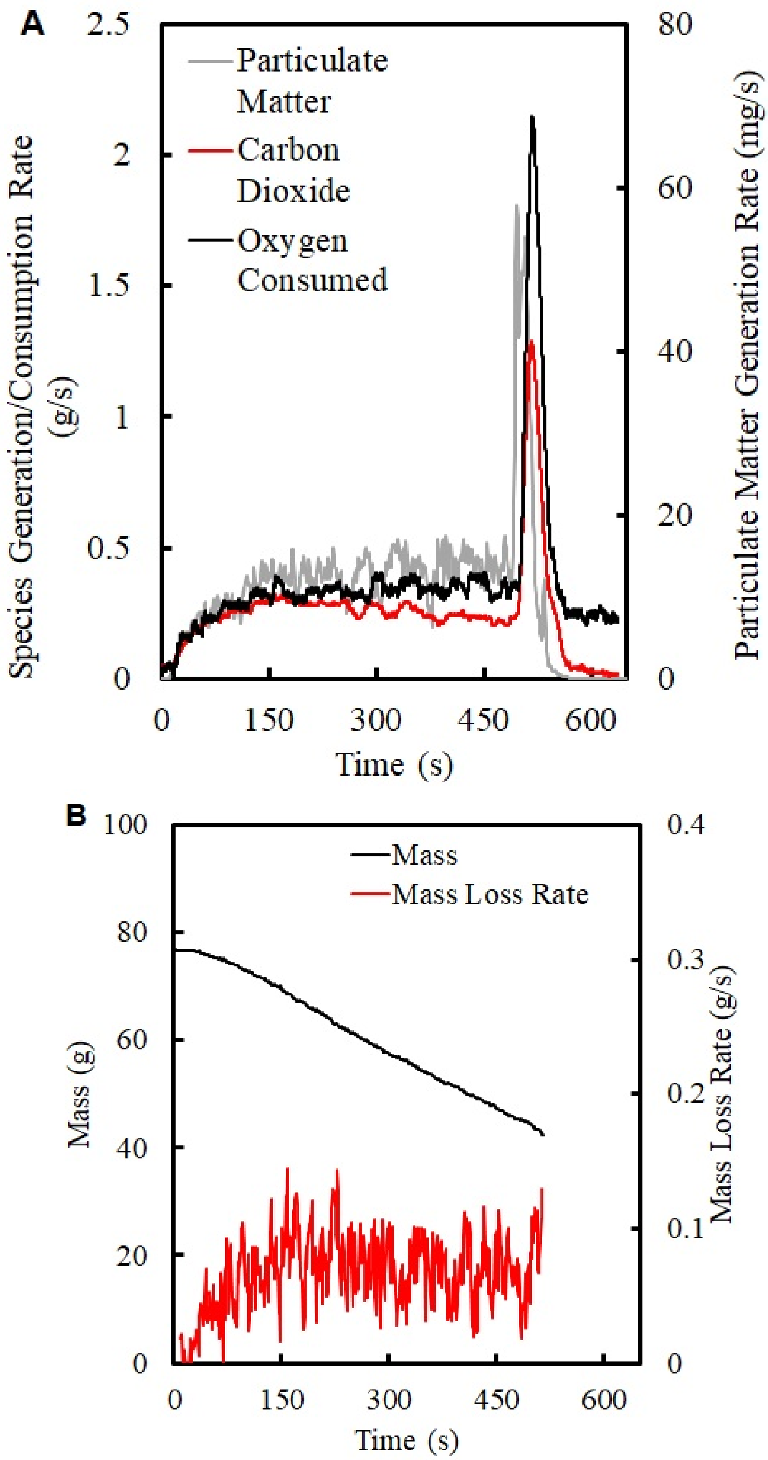

Figure 2.3: Representative data collected during an experiment observing an 11 mm thick ANS pool fire, including a) the gaseous species emissions, smoothed by a ten-point moving average, and the $PM_{2.5}$ emissions and b) the instantaneous mass and mass loss rate, smoothed by a ten-point moving average.

A California Analytical Instruments Hydrogen Flame Ionization Detector (HFID) was used to monitor the emission of unburnt hydrocarbons, but despite the 0-40 ppm range, the test results were indistinguishable from baseline, indicating negligible unburnt hydrocarbon production at this scale for these experiments. Separate experiments were undertaken to monitor the temperature of the oil layer, oil-water interface, and bulk water layer using submerged K-type thermocouples, as the conditions of these tests allowed for the oil-water interface to reach boiling. Additional experiments were conducted using a Hukseflux water-cooled Schmidt-Boelter/Gardon heat flux gauge located at the center of the pool, approximately 5 mm above the fuel surface, to record the heat flux from the flame to the center of the fuel pool for the thinnest and thickest oil slicks tested in this experiment. These supplemental tests were conducted to observe the heat flux to the fuel surface at the minimum viable slick thickness for ignition in *in-situ* burning [13], the 3 mm slick thickness, for the pool fire and the fire whirl with ANS fuel. Observations of heat flux at the 11 mm slick thickness are intended to record differences in heat feedback to the fuel surface between pool fires and fire whirls at the slick thickness beyond which additional fuel does not increase the burning rate for pool fires [45, 47].

2.3 Results

Experiments began with the ignition of the fuel layer using a pre-mixed butane torch. Heating from the flame leads to sustained burning of the fuel layer. In the case of the pool fire, the flame forms a traditional plume structure including regular puffing action. In tests where the generator is implemented, air entrainment is limited to directions tangential to the fuel pool, which increases circulation. The effect of this entrainment is first to stretch the flame into a rotating tilted plume [56] before forming a tall conical fire whirl. The flame continues to burn in this regime for the rest of the steady burning duration. The steady burning duration ends when boilover phenomena begin. For both crude oils, heating from the flame conducts through the fuel layer into the water below. Boilover phenomena occur when the thin ($\leq$ 5 mm) layer of water in contact with the bottom of the fuel layer will reach its boiling point, at which time bubbles of water vapor will rise through the fuel layer and burst. The bursting of these bubbles atomizes the fuel and causes a rapid increase in fuel mass loss rate of between 500 and 1000%, an increase in heat release rate by between 280-330% and an increase in particulate matter generation by up to 240%.

Heat Flux

The heat flux received by the fuel surface was calculated as the average of the heat flux received by the sensor during the steady burning period for ANS pool fires and fire whirls. The heat flux calculated this way for each experiment is shown in Figure 2.4 as a function of time. The average heat flux at each second is shown as a solid line in Figure 2.4, while the shaded regions represent the full range of recorded heat flux across all tests. The average results of this experiment and other relevant burn characteristics are shown in Table 2.1. These results indicate that the surface of the fuel subjected to a fire whirl is receiving nearly double the amount of heat at the center of the fuel pool compared to one subjected to a pool fire of the same size.

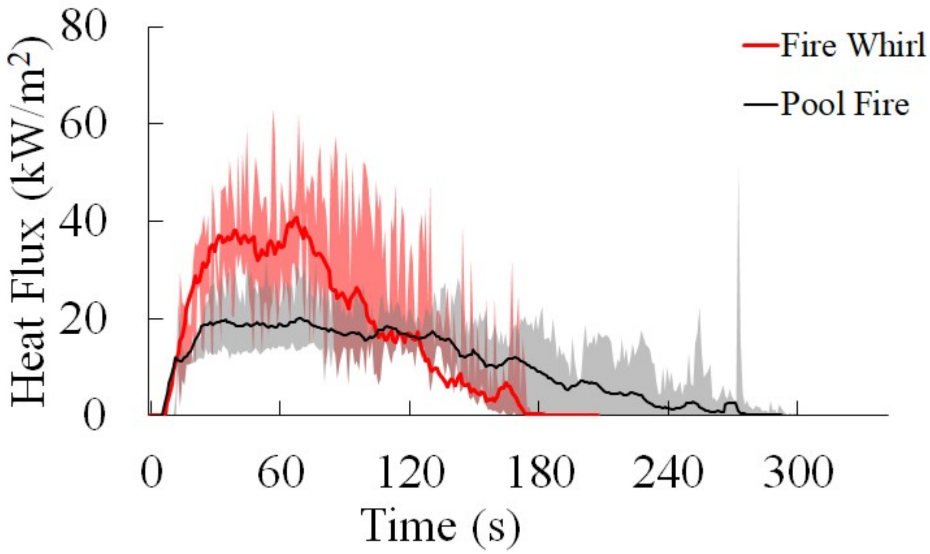

(a)

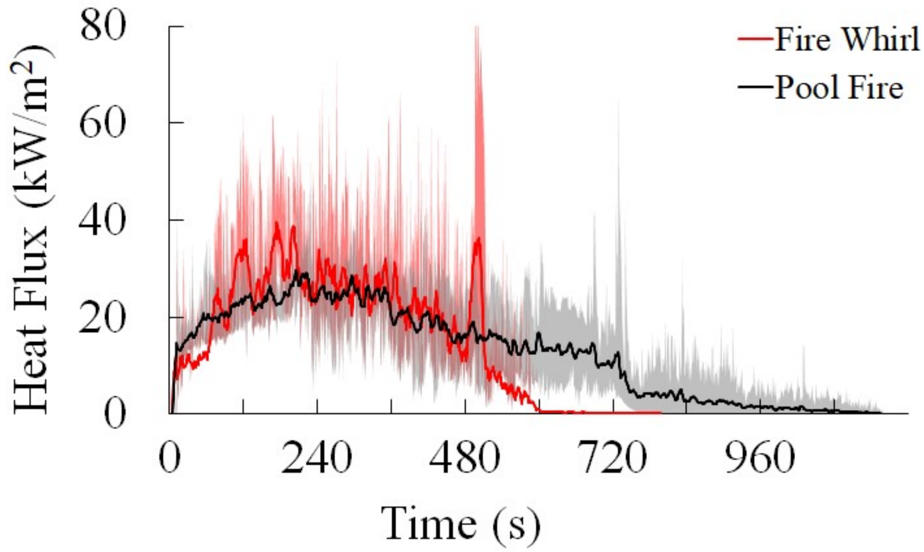

(b)

Figure 2.4: Average heat flux recorded during the burning of a) 3.5 mm thick slick ANS pool fires and fire whirls b) 11 mm thick slick ANS pool fires and fire whirls. Shaded regions represent the full range of values across the averaged tests.

Table 2.1: Average burning characteristics for slicks of ANS crude oil with 95% confidence intervals.

Configuration	Pool Fire			Fire Whirl		
Slick Thickness (mm)	3.5	7	11	3.5	7	11
Mass Loss Rate (mg/s)	53 ± 4.4	68 ± 8.9	69 ± 2.9	101 ± 24	139 ± 1	142 ± 19
Surface Mass Flux (g/m^2-s)	6.8 ± 0.6	8.4 ± 1.1	8.8 ± 0.4	12.8 ± 3.1	17.4 ± 1.7	18.0 ± 2.4
Slick Reduction Rate (mm/min)	0.47 ± 0.04	0.59 ± 0.08	0.61 ± 0.03	0.89 ± 0.21	1.21 ± .11	1.25 ± 0.17
Heat Flux (kW/m^2)	17.5 ± 3.8	-	20.3 ± 1.7	31.5 ± 1.3	-	29.0 ± 2.9
Heat Release Rate (kW)	2.41± 0.65	2.87 ± 0.71	4.00 ± 0.35	3.76 ± 0.86	4.93 ± 0.28	7.74 ± 2.65

Mass Loss Rate

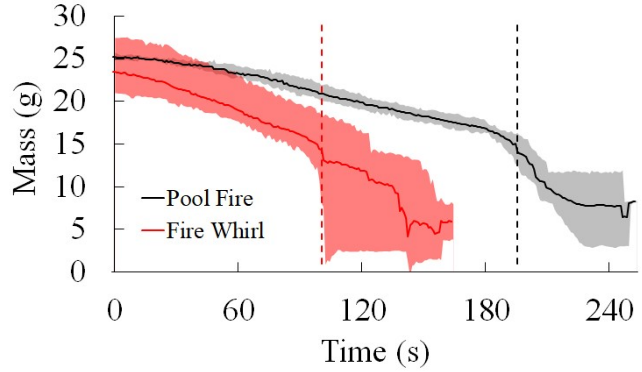

(a)

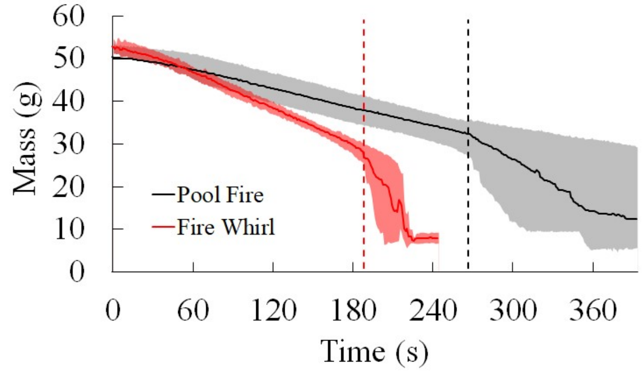

(b)

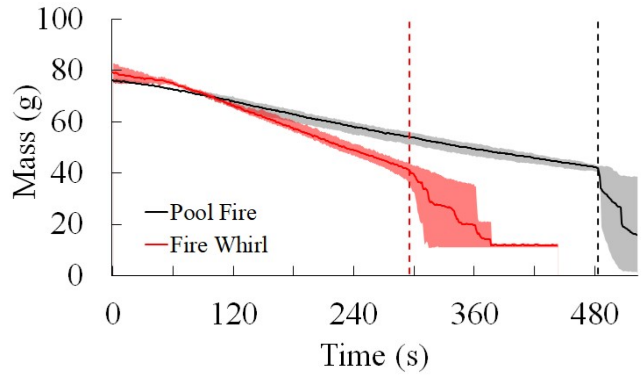

(c)

Figure 2.5: Average instantaneous mass of ANS fuel slicks over time for pool fires and fire whirls over slicks a) 3.5 mm thick b) 7 mm thick c) 11 mm. Dashed lines indicate the beginning of boilover. Shaded regions represent the full range of experimental results. Note the scale of the vertical axis is adjusted for each plot.

The instantaneous mass of remaining fuel was recorded over the burn duration, shown for ANS in Figure 2.5, exhibiting the shallow slope of the steady burning period and the steep drop as boilover occurs.

The mass loss rate for each experiment was taken as the average of the forward difference in mass at each second during the steady burning period, and is shown in Figure 2.6 with error bars representing a 95% confidence interval using Student's t-Test. For these experiments, the steady burning period is the duration of the test between ignition and the onset of boilover, during which the mass loss rate is relatively constant. As noted in section 2.3 and elaborated on in section 2.3, the onset of boilover causes increased heat feedback that greatly increases the burning rate for a short duration before flame extinction.

The mass loss rates for all pool fires, as shown in Figure 2.6, stay nearly constant as fuel slick thickness is increased. This is expected behavior for pool fires of constant diameter above a critical slick thickness [14, 45, 57]. The mass loss rates of fire whirls formed with these fuels has a positive correlation with slick thickness. For the thickest fuel layer, the ratio of fire whirl mass loss rate to pool fire mass loss rate nears two. Little variation in mass loss rate is seen between ANS and HOOPS crude oil. Pool fires had more repeatable mass loss rate values, evidenced by the comparatively small error bars. More variation is seen between tests for fire whirls, especially at low slick thicknesses, as the steady burning duration is shorter than for larger slicks and the behavior of the flame has less time to reach a stable state.

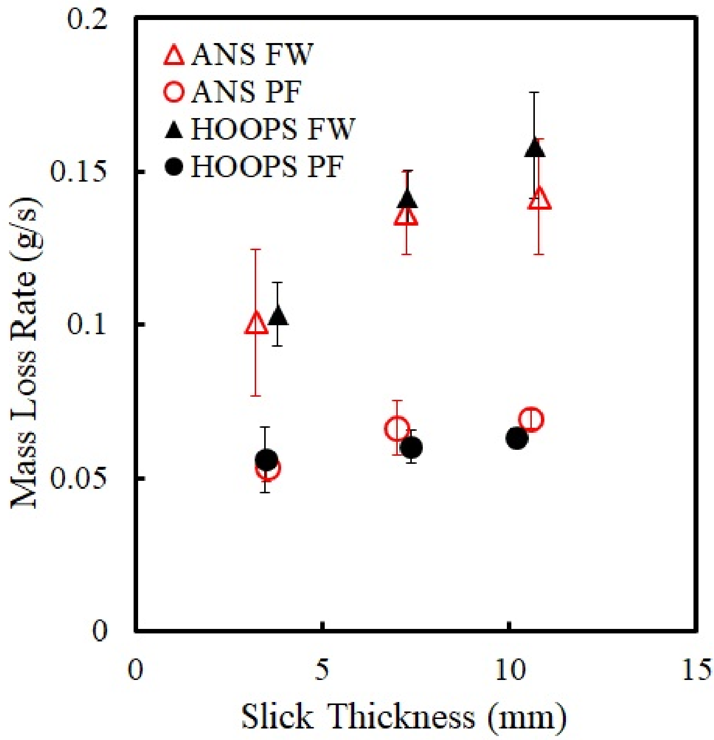

Figure 2.6: Average mass loss rate during steady burning for fire whirls and pool fires with ANS and HOOPS crude oil for varying slick thicknesses, shown with a 95% confidence interval.

Table 2.2: $PM_{2.5}$ generation rate and $EF_{PM2.5}$ for all tested configurations with 95% confidence intervals.

Fuel	Configuration	Slick Thickness	$PM_{2.5}$ Generation Rate (mg/s)	$EF_{PM2.5}$ (g/kg)
ANS	Fire Whirl	3.5 mm	8.2 ± 1.27	80.3 ± 5.7
		7 mm	11.2 ± 0.7	101.5 ± 5.4
		11 mm	14.8 ± 3.0	129.3 ± 26.8
	Pool Fire	3.5 mm	4.8 ± 0.9	142.3 ± 4.9
		7 mm	6.0 ± 1.1	151.1 ± 9.5
		11 mm	12.5 ± 0.3	167.8 ± 3.4
HOOPS	Fire Whirl	3.5 mm	6.2 ± 0.5	48.7 ± 8.3
		7 mm	10.4 ± 0.5	65.1 ± 11.1
		11 mm	6.4 ± 0.8	72.0 ± 5.8
	Pool Fire	3.5 mm	8.8 ± 0.8	69.0 ± 14.2
		7 mm	6.9 ± 0.3	99.6 ± 16.9
		11 mm	6.8 ± 1.1	119.5 ± 18.5

Emissions

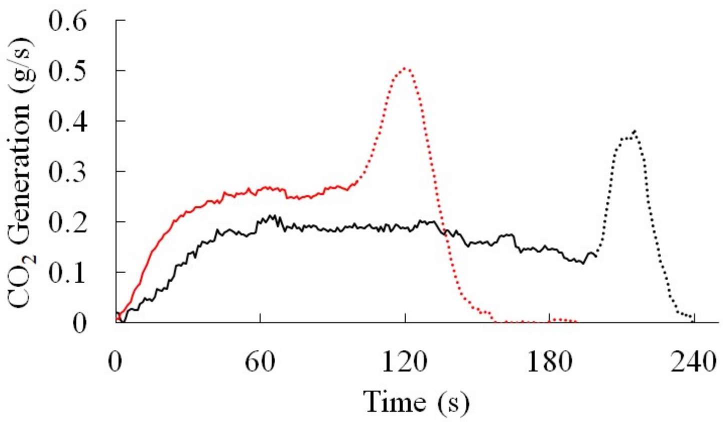

(a)

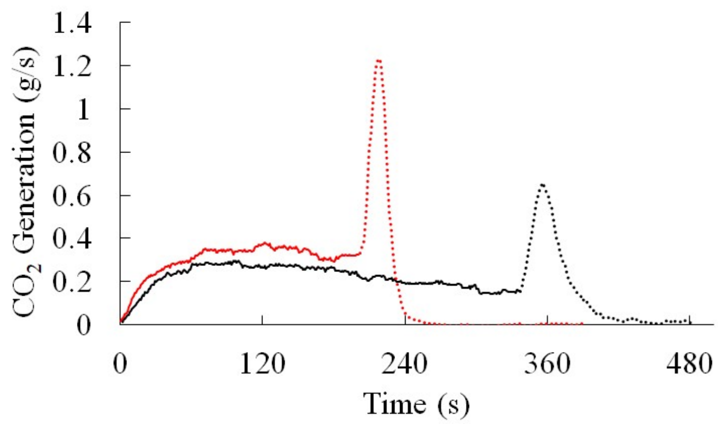

(b)

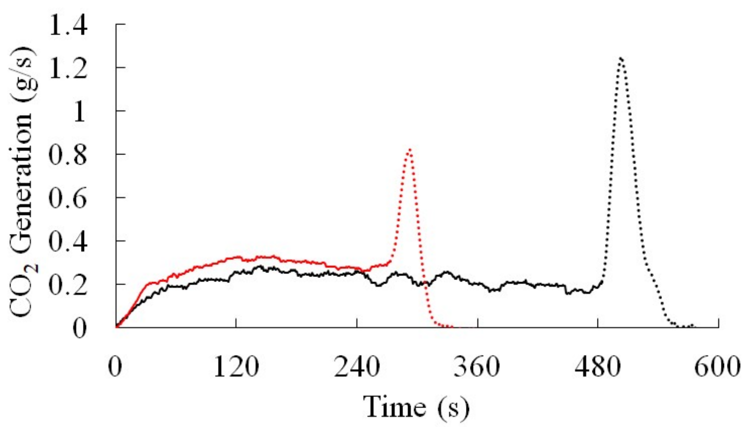

(c)

Figure 2.7: Instantaneous CO_2 mass generation rate for representative pool fires and fire whirls with a starting ANS fuel slick thickness of a) 3.5 mm b) 7 mm c) 11 mm. Dotted regions represent the duration of boilover.

Carbon species were captured during the burning period to assess completeness of combustion. Instantaneous rates of carbon dioxide generation, as shown for ANS crude oil in Figure 2.7, were captured at a rate of 10 HZ. Notable in Figure 2.7 are the spikes in CO_2 production that indicate the rapid onset of boilover. The concentrations of carbon species in the exhaust hood flow were measured as time dependent quantities and multiplied by the flow rate in the hood to produce rates of carbon species emissions by mass. These rates were then forward summed to produce a value for total mass of emitted carbon species. The emissions factor of the carbon species, EF_{CO2} and EF_{CO}, were defined as the ratio of the emitted mass of the carbon species to the mass of fuel lost during the steady burning period, and are shown in Table 2.3. Table 2.3 shows that the overall carbon species emissions do not vary greatly between scale, between fuels, or between configurations, despite comparatively large differences in particulate matter emissions as test conditions vary. Error in the measurement of EF_{CO} is very large compared to the measured values as the small quantities of CO produced by the flames were further diluted by the hood exhaust flow and the resulting concentrations were close to the limit of detection. The overall modified combustion efficiency, MCE, was calculated for each test condition as follows

$$MCE = \frac{\frac{m_{CO2}}{MW_{CO_2}}}{\frac{m_{CO2}}{MW_{CO_2}} + \frac{m_{CO}}{MW_{CO}}} \tag{2.1}$$

where m_X is the total mass of substance X emitted, and MW_X is the molar mass of substance X. Table 2.3 shows the results of this calculation for the tested fuels and slick thicknesses. The variations in MCE are very small between test configurations and slick thicknesses, indicating that all tests had very completeness of combustion.

Table 2.3: Emission Factors of Carbon Species and Modified Combustion Efficiencies during steady burning period shown with 95% confidence intervals.

Fuel	Configuration	Slick Thickness	EF_{CO2} (g/g)	EF_{CO} (g/g)	MCE
ANS	Fire Whirl	3.5 mm	1.71 ± 0.60	0.0212 ± 0.010	0.977 ± 0.0058
		7 mm	1.99 ± 0.44	0.0226 ± 0.027	0.970 ± 0.0043
		11 mm	2.30 ± 0.60	0.0316±0.0044	0.976 ± 0.0010
	Pool Fire	3.5 mm	2.81 ± 0.27	0.0275 ± 0.017	0.985 ± 0.0048
		7 mm	2.82 ± 0.20	0.0360 ± 0.011	0.981±0.0046
		11 mm	2.79 ±0.12	0.0323 ± 0.0062	0.982± 0.0015
HOOPS	Fire Whirl	3.5 mm	1.55 ± 0.32	0.0157± 0.0087	0.987±0.0047
		7 mm	1.64 ± 0.15	0.0166 ± 0.0048	0.984 ± 0.0033
		11 mm	1.98 ± 0.16	0.0345 ± 0.0095	0.982 ± 0.0030
	Pool Fire	3.5 mm	1.71 ± 1.1	0.0116 ± 0.0054	0.986 ± 0.0027
		7 mm	2.00 ± 0.56	0.0177 ± 0.0074	0.987 ± 0.0055
		11 mm	2.39 ± 0.44	0.0194 ± 0.013	0.979 ± 0.0086

$PM_{2.5}$ emission rates for pool fires and fire whirls were collected once per second during the burn duration, as shown for ANS crude oil in Figure 2.8. The spikes in $PM_{2.5}$ shown in Figure 2.8 are the result of the boilover phenomenon increasing the burning rate. The flat tops of these spikes are artifacts of sensor saturation and not physical phenomena. The average rate of $PM_{2.5}$ production during the steady burning period is shown in Table 2.2.

The time-dependent concentration of $PM_{2.5}$ in milligrams per cubic meter, calibrated via gravimetric weighing of samples captured in 2.5 micron filters, was multiplied by the exhaust flow rate and forward summed to produce a value for $PM_{2.5}$ mass emission. The emission factor of $PM_{2.5}$, $EF_{PM2.5}$, is shown for the steady burning period of each test condition in Table 2.2. This emission factor was calculated as the mass of $PM_{2.5}$ emitted from the flame before the onset of boilover, divided by the total mass lost over the same time period.

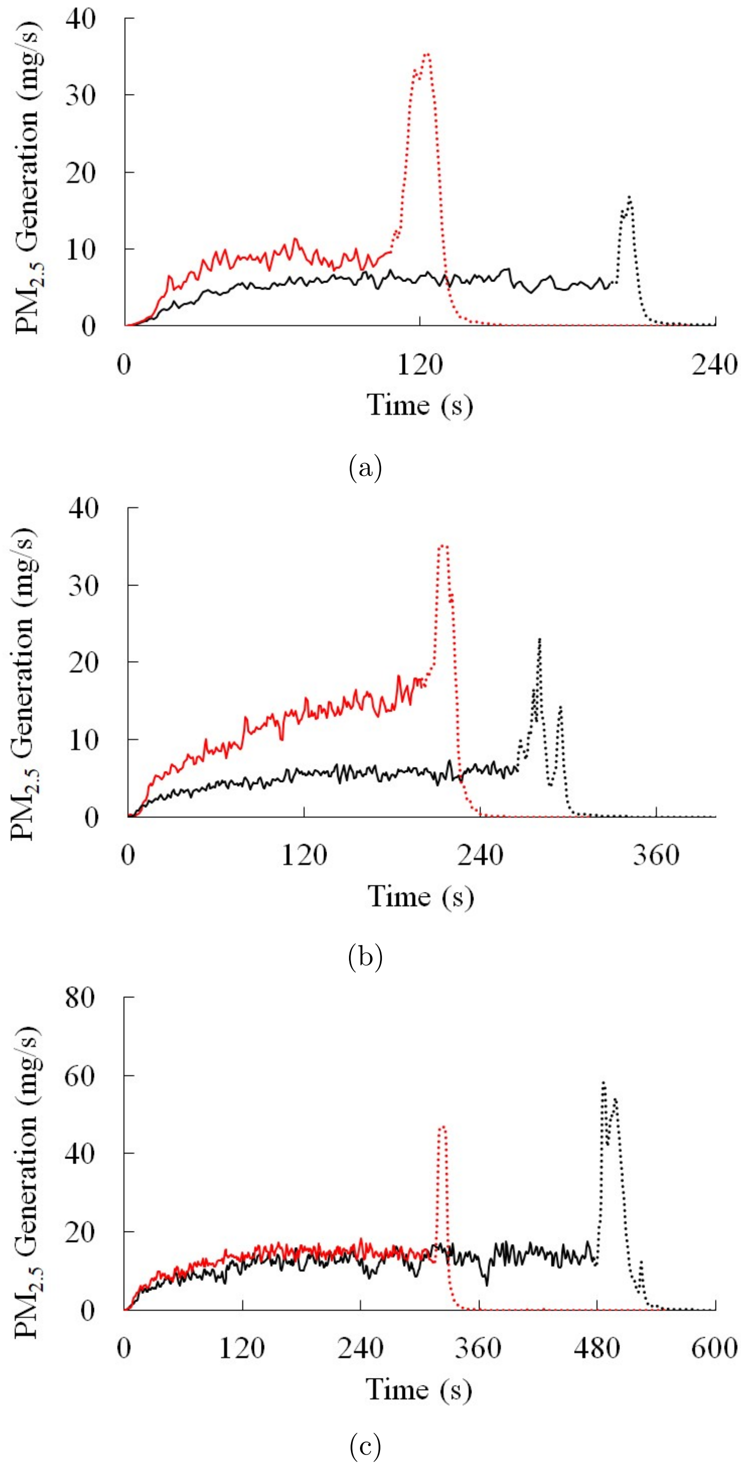

Figure 2.8: Instantaneous $PM_{2.5}$ mass generation rate for representative pool fires and fire whirls with starting ANS fuel slick thicknesses of a) 3.5 mm b) 7 mm c) 11 mm. Dotted regions represent the duration of boilover.

For all test conditions, $EF_{PM2.5}$ has an increasing trend with slick thickness, as shown in Figure 2.9. This is expected based on results from [43] showing an increase in soot aerosols with increasing slick thickness, but does not show the same magnitude as the values in [43], which depict the doubling of aerosol mass per gram fuel as fuel slick thickness changed. For all slick thicknesses and for both fuels, fire whirls showed a lower $EF_{PM2.5}$, indicating a potentially more complete combustion, with less of the fuel mass being converted to soot. For ANS crude oil, the pool fires show a very slight increasing trend for $EF_{PM2.5}$ with slick thickness, whereas for HOOPS crude oil this trend is very prominent. Inversely, the fire whirls that formed over ANS crude oil showed a much stronger trend between $EF_{PM2.5}$ and slick thickness than those formed over HOOPS crude oil. Values of $EF_{PM2.5}$ have comparatively small 95% confidence intervals, with the exception of the thickest slicks of ANS subjected to the fire whirl, which had much more variability in results. Also shown in Figure 2.9 is the tendency for ANS crude oil to soot more heavily than HOOPS crude oil in all tested conditions.

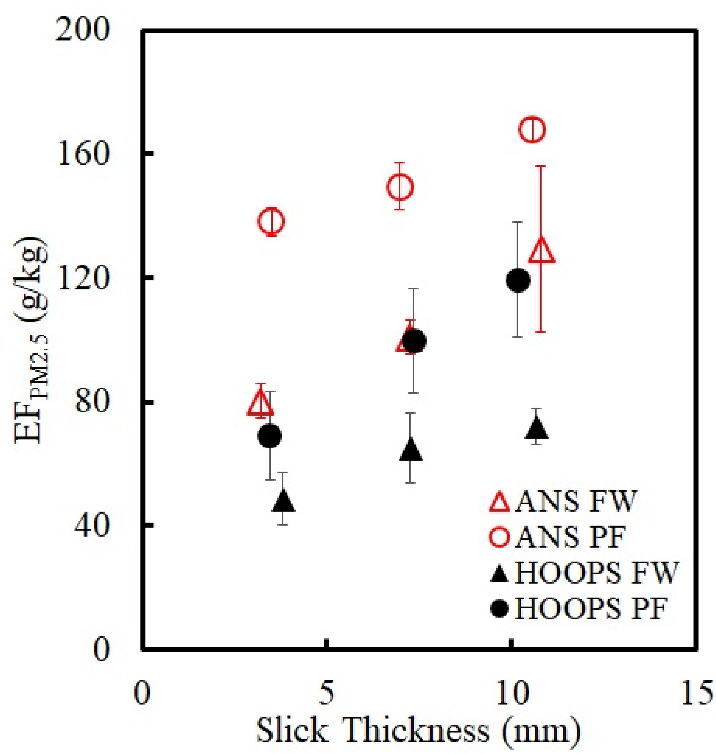

Figure 2.9: Emissions Factor of $PM_{2.5}$ as compared to mass of fuel burnt during the steady burning period by slick thickness for ANS and HOOPS crude oil, with error bars denoting a 95% confidence interval.

Qualitative Observations on Boilover Phenomena

In the majority of experiments, heating from the flame led to water just under the oil interface to reach its boiling point. The resulting boilover phenomenon causes a rapid increase in burning rate and particulate matter production as vigorous mixing ensues and oil droplets are ejected from the fuel layer. ANS crude oil causes a much more violent boilover event, including audible boiling of higher intensity than the HOOPS crude oil under the same conditions. For this reason, data in sections 2.3 through 2.3 have been separated into the steady burning period before boilover and the subsequent boilover to extinction region. Visual differences in flame behavior, such as flame size and particle ejection from the fuel surface, are typified by Figure 2.10. Seen in Figure 2.10, the flame becomes much more intense, violent, and turbulent in the boilover regime, drastically changing the flame characteristics for the short duration before extinction.

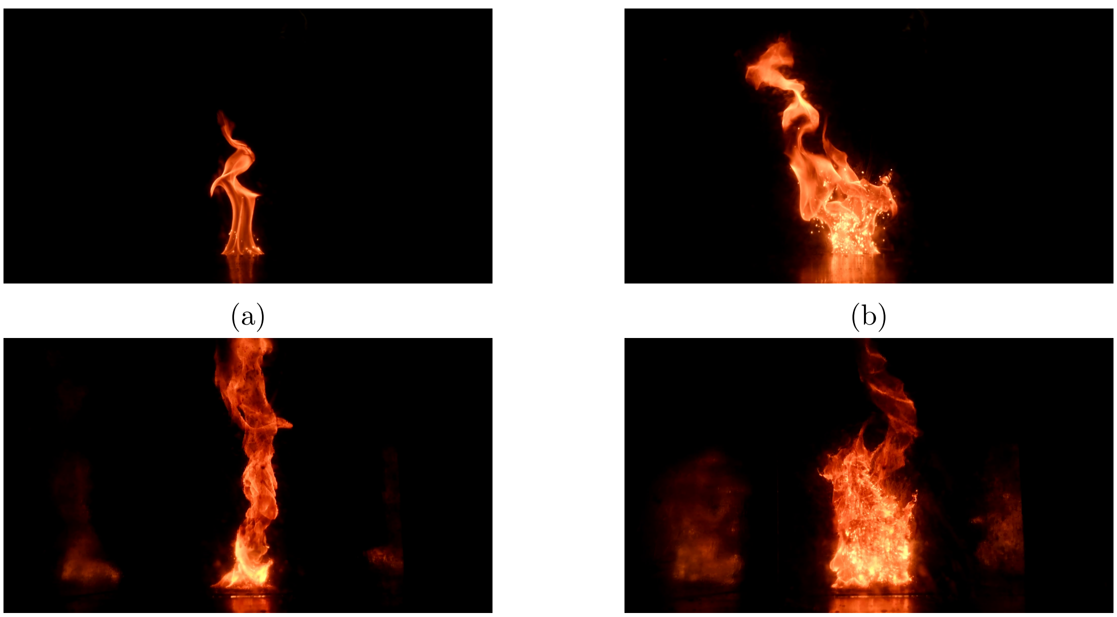

(a) (b) (c) (d)

Figure 2.10: An ANS pool fire a) before boilover and b) during boilover compared to an ANS fire whirl c) before boilover and d) during boilover, both over a 7.5 mm thick fuel slick.

The temperature of the oil layer, oil water interface, and bulk water layer are shown evolving with time for an example ANS fire whirl in Figure 2.11, where the excess temperature is defined as the increase in temperature above initial conditions. Heat from the flame is transferred through the burning oil layer and into the water layer, but this heat is primarily confined to the thin region nearest the fuel-water interface due to insulation from the bulk of the water layer. The oil layer temperature was recorded by a thermocouple 5 mm below the surface of the oil, the interface temperature was recorded by a thermocouple 12 mm below the surface of the oil at the start of the water sublayer, and the water temperature was recorded by a thermocouple 15 mm below the oil-water interface. As seen in Figure 2.11, the water sublayer temperature increased only slightly even as the interface layer reached boiling. This boilover event briefly uncovered the oil layer and interface thermocouples and exposed them to air, creating the dip shown in Figure 2.11 after the interface exceeds 373 K.

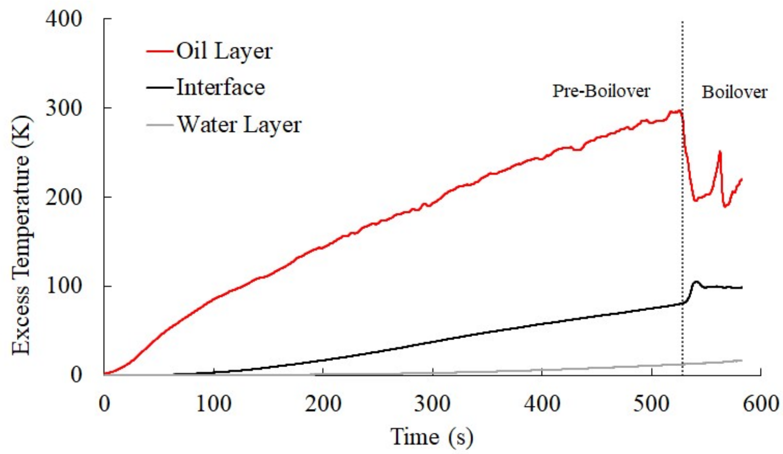

(a)

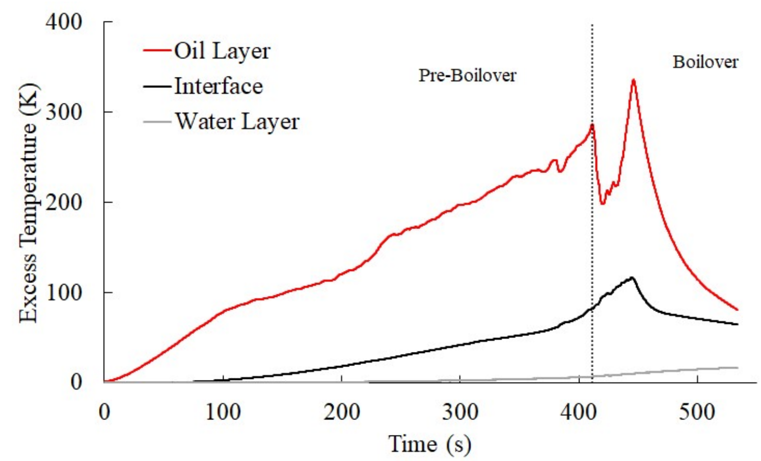

(b)

Figure 2.11: Temperature in the oil layer, at the oil-water interface, and in the bulk water layer for a) a pool fire and b) a fire whirl, both over an 11 mm thick ANS slick.

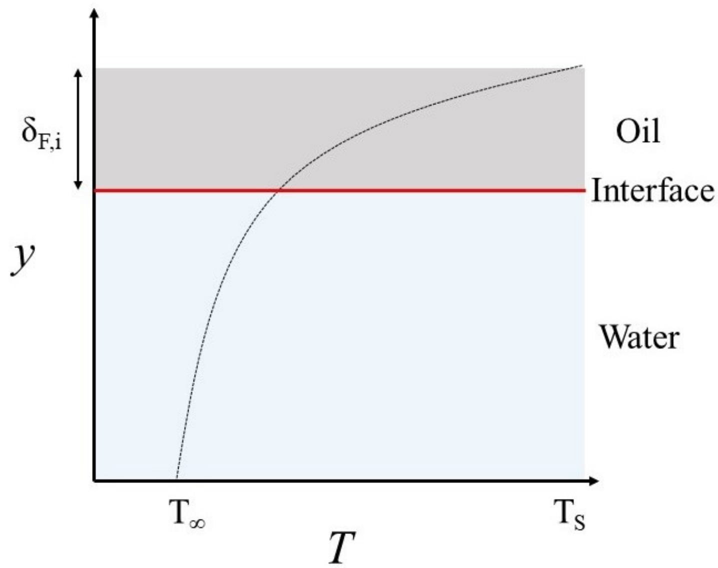

Figure 2.12: Visual depiction of the conditions required to formulate the model described in equation 2.2.

2.4 Discussion

Mass Loss Rate

Analysis of the mass flux from the fuel surface, taken to be the fuel mass loss rate divided by the surface area of the pool, compares well to values predicted by literature for burning pools over water [45]. Garo et. al [45] create an analytical estimate for the burning rate of the thin oil slick assuming the oil and water substrate together comprise a semi-infinite solid, with a heat flux to the fuel surface proportional to the heat of combustion of the fuel and the diameter of the pool. A visual depiction of the conditions assumed by the model is shown in Figure 2.12. The equation used to produce the estimated fuel surface mass flux, $\dot{m}''$, modified from [45], which present the same results in terms of slick thickness reduction rate, is

$$\dot{m}'' = \frac{1}{H_V}\left(\chi(\frac{4\rho_\infty C_p(T_\infty g(T_f - T_\infty))^{\frac{1}{2}}}{\pi})d^{\frac{1}{2}} - \frac{\alpha_F \lambda_F (T_S - T_\infty)}{\delta_{F,i}(\sqrt{\alpha_F} + \sqrt{\alpha_w})^{\frac{1}{2}}}\right) \tag{2.2}$$

where H_V is the heat of vaporization of the crude oil, χ is the fraction of the heat released by combustion returned to the fuel layer, empirically determined to be 3.9×10^{-3} by [45], ρ_∞ is the density of ambient air, C_P is the specific heat of fuel, T_∞ is the temperature of ambient air, g is the acceleration due to gravity, T_f is the temperature of the flame, d is the diameter of the fuel pool, α_F and α_w are the thermal diffusivity of fuel and water respectively, λ_F

is the thermal conductivity of the fuel, T_S is the vaporization temperature of the fuel, and $\delta_{F,i}$ is the initial fuel layer thickness. The fraction of heat released by combustion that is returned to the fuel layer, which can be referred to as the fraction of heat feedback, differs for varying fuels, with the value used here being the maximum value in the investigations of Garo et al. (1999)[45]. This model was used by [14] and matched well with results for a variety of oil-fueled pool fires with slick thicknesses encompassing the range tested in these experiments.

Comparisons between the pool fires and fire whirls from this investigation are compared to the expectations of this analytical model are shown in Figure 2.13.

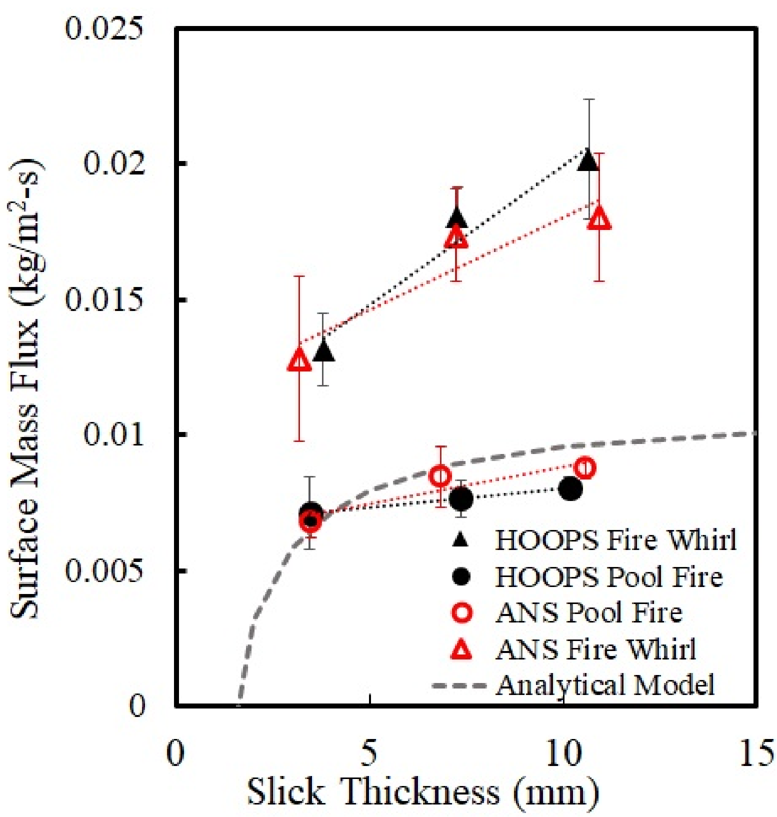

Figure 2.13: Average surface mass flux of pool fires and fire whirls at varying slick thicknesses shown with a standard error, compared to analytical predictions from [45]

The surface mass fluxes of tested pool fires match well with the values expected from the analytical model. The data for pool fires also matches well with the results from [14] burning pools of Russian Export Blend Crude Oil (REBCO) and Grane crude oil with similar slick thicknesses. Fire whirls, however, greatly exceed the expected surface mass flux from this model. This shows that the behavior of the fire whirl deviates from the expected behavior of the pool fire in ways for which this analytical model does not account. Of note, flame temperature, surface temperature, and fraction of heat feedback may need to be altered to account for the formation of the fire whirl, as these factors do not as yet account for the increased heat flux to the fuel surface of the fire whirl.

The fire whirl in this scenario receives 179% of the heat flux that the pool fire of the same size receives, and consequently has a mass loss rate 189% higher, as the excess heat is used in the fuel pyrolization process.

Increases in slick thickness caused little effect on the received heat flux to the pool surface, irrespective of configuration as shown in Table 2.1, allowing for some error introduced by the physical presence of the sensor within the fuel layer. As described in [45], the effect of increasing the fuel layer thickness over a water reservoir is to provide insulation for the surface of the heated fuel. This insulation allows the same heat flux to have greater effect on the fuel temperatures at the slick surface. Higher surface mass fluxes are recorded for these thicker slicks, as shown in Table 2.1, indicating how effective this insulating process is even at the small scale.

The duration of the steady burning period can be used to infer the rate of thermal penetration by assessing the time taken for the surface of the water layer to boil. The penetration of heat flux to the fuel surface into the bulk of the oil layer is determined both by the depth of the remaining oil layer and the rate of slick thickness reduction determined by the mass loss rate [47, 58]. By plotting the steady burning duration versus the initial oil slick thickness, a method used by [47], a value in millimeters per second can be determined from the slope of the graph. Figure 2.14 shows this process applied to the experimental data, with well-fit linear slopes. To isolate the influence of thermal penetration, the slick thickness reduction rate is subtracted from this value to obtain a thermal penetration rate, shown in Figure 2.15, with a 95% confidence interval calculated from the average slick thickness reduction rate for each test as compared to the slope of the fit trend line in Figure 2.14. Explicitly, as the fuel layer is supported by the water layer, the thermal penetration rate is a measure of how fast the water in contact with the fuel layer can be brought to its boiling point under a given thickness of fuel. The thermal penetration rate can, in this sense, be used as a measure of how far below the fuel surface can the bulk liquid be affected by increased heating at the surface.

The thermal penetration rate of fire whirls exceeds that of pool fires for both fuels, while ANS shows a lower thermal penetration rate than HOOPS for both configurations.

These differences in thermal penetration rate and surface mass flux can be attributed to the greater heat flux received by the fuel surface during the fire whirl regime of combustion.

Emissions

Particulate matter and gas species emissions indicate a preferable combustion environment occurs inside the fire whirl. Heat flux to the fuel surface is increased in the fire whirl regime, as indicated in Table 2.1 and corroborated in literature [20, 24, 25]. Improved convective mass transfer [24] is one factor potentially increasing the combustion efficiency of the fire

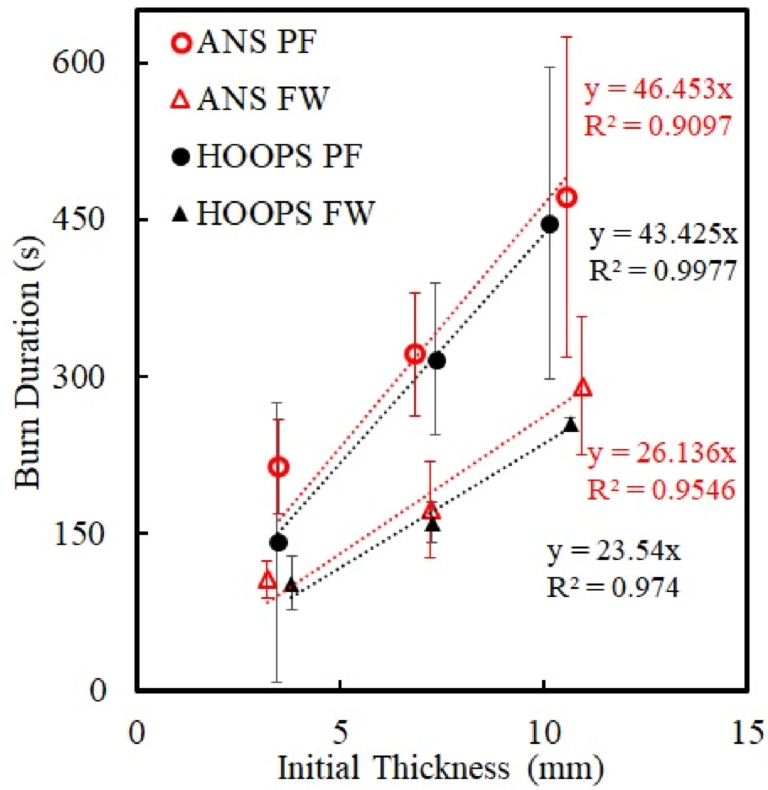

Figure 2.14: Duration of steady, pre-boilover burning by initial slick thickness for both fuels and configurations shown with 95% confidence interval.

whirl and affecting particulate soot formation. The relative availability of oxygen [35] and residence time of soot particles [50] have great effect on the production of soot. The presence of the radial inflow boundary layer [25, 48] pumping ambient air into the base of the fuel layer can increase the availability of oxygen and reduce the residence time of any potentially formed particles. As shown in Figure 2.9, the fire whirl shows a lower $EF_{PM2.5}$ than the pool fire for all cases, but both regimes show an increasing trend with slick thickness. Since the surface mass flux of fuel from a fire whirl also increases with slick thickness, a comparison between the emissions of particulate matter for varying surface mass fluxes is shown in Figure 2.16. In this figure, it is clear that slight variations in the surface mass flux correlate to large variations in $EF_{PM2.5}$ for pool fires. The opposite correlation appears for fire whirls, as $EF_{PM2.5}$ increases slowly with increasing surface mass flux. Since Table 2.3 shows very little variation in the emissions of CO and CO_2 between the fire whirl and pool fire configurations, the change in particulate emissions may not be entirely explained by the changes in mixture composition at the flame base. The shape of a flame has great effect on the quantity of produced particulate emissions, due to changes in local oxygen availability [21] and chemical kinetics leading to soot formation [36]. The "over-rotation" [21] of a fire whirl under imposed

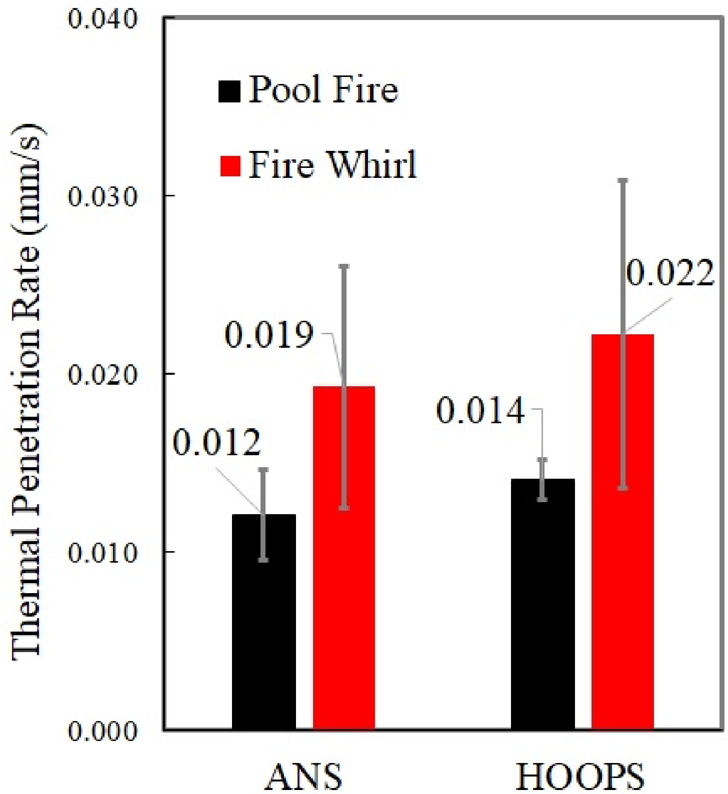

Figure 2.15: Thermal penetration rate in millimeters per second, shown with 95% confidence interval.

circulation causes the formation of a turbulent cylindrical fire whirl [59] which produces more visible smoke than the typical conical fire whirl. The difference in soot emissions may be more strongly influenced by soot consumption and potentially reduced residence time of particles in the relevant flame regions, which can effect the production of soot in laminar diffusion flames [35, 50].

2.5 Conclusions

Fire whirls formed over small scale oil slicks show an increase in mass loss rate and a decrease in particulate emissions when compared to pool fires of the same diameter without any obvious signs of impaired combustion efficiency. As the slick thickness of oil increases, the magnitude of these deviations from pool fire behavior increases, with thicker slicks showing a greater increase in mass loss rates and greater decrease in particulate matter emission factors. Insulation from thicker layers of oil allow for higher mass loss rates to be reached at the surface of the oil, increasing until a critical thickness of insulation is reached, and

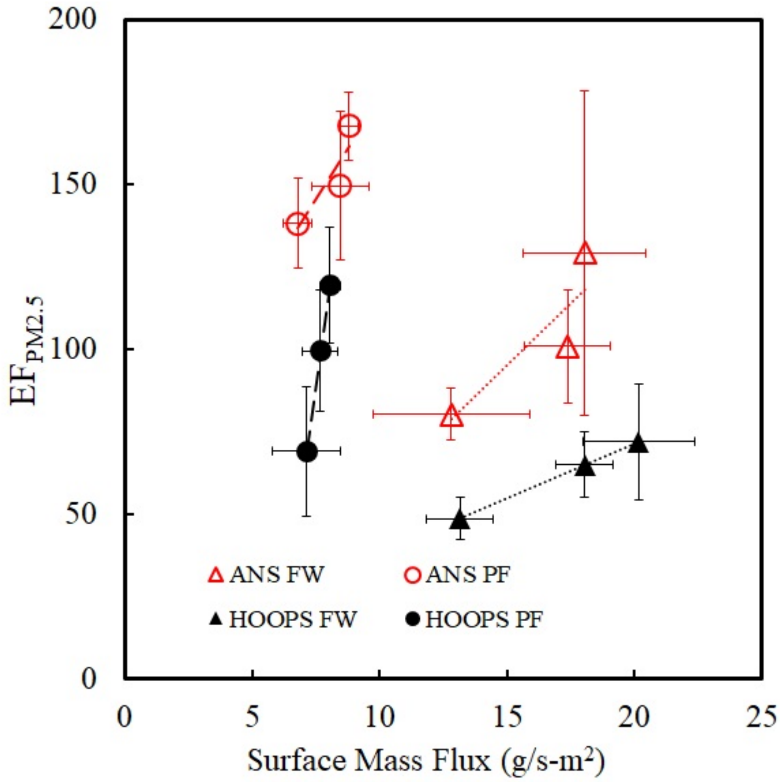

Figure 2.16: $EF_{PM2.5}$ by surface mass flux for both fuels and configurations, shown with line of best fit to describe trends and with a 95% confidence interval for all variables.

this critical thickness is higher for fire whirls than for pool fires. The thermal penetration rates through the oil layer were greater for experiments involving the generation of the fire whirl than for the pool fire, in some cases approaching a near doubling of thermal penetration rate. This is attributable to the higher heat flux to the fuel surface in the fire whirl configuration. The emission of PM2.5 increased with increasing fuel slick thicknesses for all cases, fire whirls and pool fires, but fire whirls showed significantly reduced particulate emissions compared to pool fires at all slick thicknesses. Little change in modified combustion efficiency was observed, leading to speculation that the changes in soot production may be more attributable to changes in soot precursor and particulate lifespan within the flame than the present but lower magnitude effect on fuel-air mixing. Further research into the effects of fire whirl generation on emissions and products of combustion should focus on the influence on the mechanisms of soot generation and presence of unburnt hydrocarbons liberated from the fuel surface. Future work should additionally focus on the scalability of these results as the pool diameter and generator footprint size are increased.

Chapter 3

Effect of Laboratory-Scale Fire Whirl Generator Dimensions

3.1 Introduction

Fire whirls forming in uncontrolled wildland fires can pose a serious hazard as their effects dramatically change the characteristics of the flame in ways that make the fire more dangerous, namely via taller flames and increased burning rates [3, 6]. To understand the behavior and structure of fire whirls, they are often generated at a smaller scale in the laboratory where they can be carefully controlled and studied in detail [60, 61]. Previous research has shown that fire whirls not only produce more extreme fire behavior, but also that they can decrease the production of particulate matter emissions for a given flame [20]. This has introduced the concept of intentionally inducing fire whirl formation during *in-situ* burning of oil spills to limit their effect on local air quality [7, 62]. Whether used for study at the laboratory scale or for practical implementation, fire whirls are inherently sensitive to the methods used to generate them.

Fire whirls are formed when ambient circulation is centralized over a flame, where the buoyant plume acts as a sink, allowing for the formation of a vortex [1]. For a pool of liquid fuel, the burning rate is influenced by the resulting flame structure, as the flame sheet is brought closer to the fuel surface, enhancing heat and mass transfer [25]. The flame structure and burning characteristics are then strongly dependent on the circulation in the surrounding air that creates the fire whirl structure [30]. The mass loss rate of the fuel is controlled in part by the flame structure, implicitly relating it to the circulation through the movement of the flame sheet and mass transfer into the plume [25, 30]. The shape of the flame also depends upon the flow structure. Lei et. al demonstrate this in [26], in which multiple distinct regimes of inclined flame and fire whirl were observed as the imposed circulation was increased.

The fire whirl generators used at the laboratory scale can be categorized into two broad groups based on the method used to induce the vortex. In the spinning-mesh or Emmons-type fire whirl generator, circulation is directly imparted by spinning a porous mesh around the flame at some distance, allowing for direct control of the imposed circulation [22]. The other category is the fixed-frame fire whirl generator, where the circulation is generated by the tangential component of the velocity of the air entrained by the flame [63]. In the fixed-frame fire whirl generator, circulation cannot be controlled, as it arises naturally from a balance of air entrainment and heat release from the flame [6].

The formation of the fire whirl reduces the amount of particulate matter emitted from the flame when compared to a pool fire of the same size [7, 20, 62]. The creation of the fire whirl intentionally may then have practical uses, such as an application for *in-situ* burning of oil spills [52, 62]. For field-scale practical application, then, it is paramount to understand the effect that scaling the size of the fire whirl generator will have on the produced flames.

The objective of this study is to investigate the effect of the dimensions of a fixed-frame fire whirl generator on the burning rate, flame height, and particulate emissions of the resulting flame. The height of the enclosure is varied in order to isolate the minimum wall height required to form a fire whirl, and study the effects that further increases in the enclosure height may have on the flame height. Also varied is the width of the enclosure, in order to quantify the relationship between enclosure width and height that allows for the scaling of the fire whirl generator.

Literature Review

Fire whirls are known to extend the flame length of pool fires (without added circulation) of similar diameter [22]. For the case of a liquid fuel, this increase in flame length is due to a combination of an increase in fuel vapor emitted from the surface due to increased surface heat transfer and the fluid dynamic effect of the vortex to stretch the flame [6, 64]. One effect of circulation is to draw the flame sheet closer to the fuel surface by Ekman pumping [25], which increases convective heat transfer to the fuel surface, allowing for increased rates of evaporation from the liquid fuel [24]. For a fire whirl with a gas burner fuel source, the increase in flame height is due solely to fluid dynamic effects suppressing the mixing of fuel and air [65]. The dominating term in determining the flame height, then, is the circulation term [30, 61, 65]. Lei et al. [26] categorize fires under imposed circulation into inclined flames, weak, conical, transitional, cylindrical, and curved cylindrical fire whirls, and unstable flames. These categories are defined by the intensity of the imposed circulation and the heat release rate of the flame. For the fixed-frame fire whirl generator, where walls and positioned gaps are used to induce formation, circulation cannot be directly imposed as buoyancy dictates air entrainment which, in turn, controls the velocity of the incoming air [24], but the qualitative differences in flame geometry between these categories can be useful in describing the flame behavior. The inclined flame is of particular interest, as it is formed at low circulation and is characterized by the flame revolving about the interior of the generator [56]. This behavior can be observed at the early stages of fire whirl formation in fixed frame generators [7].

The inflow boundary layer controls much of the combustion behavior of the fire whirl, with the air entrainment in this near-wall layer supplying sufficient air for complete combustion [30]. This inflow layer has a thickness defined by the circulation imparted in the flow as well as the distance from the fire whirl axis at which the circulation is induced [48]. The final height of the fire whirl and its behavior beyond the boundary layer are determined by the type and size of the generator forming the fire whirl [61, 66].

In the design of the spinning mesh, or Emmons-type, fire whirl generator, circulation can be controlled directly, and for a fire whirl over a gas burner, this allows for a complete decoupling of the fire whirl's heat release rate and the circulation in the ambient fluid [22, 65]. These fire whirl generators allow for the creation of a cylindrical fire whirl, as categorized by [56], with high ratios of circulation to burning rate. Other methods of inducing fire whirl formation rely on passive methods of generating circulation, most prominently in the form of lee vortices, which can form from interactions with terrain at the large scale [1] or with other large fires [3, 67]. At the laboratory scale, a fixed-frame generator is used to generate vorticity by limiting air entrainment to predominantly azimuthal flow via the placement of obstacles. These obstacles can take the form of vanes directing the angle of flow [23], offset hemicylinders [29, 65], or walled structures with three [7, 62], four [20, 24], or more sides [61].

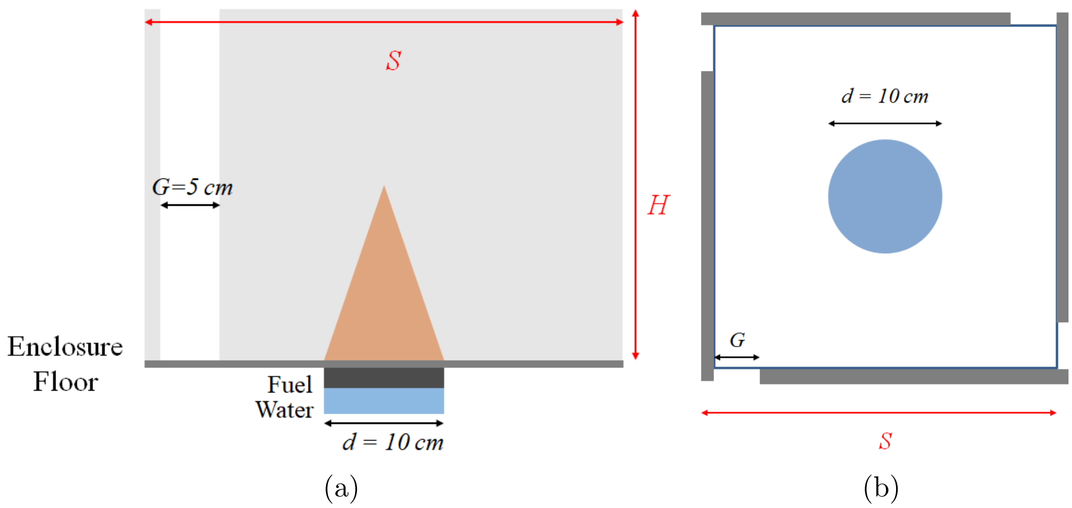

Figure 3.1: Fixed-frame four-wall fire whirl generator with variable wall height H and side length S with fixed gap size G. Section view (a) and plan view (b)

Obstacles need only prevent the radial entrainment of air [61], so fire whirl generators can also be constructed with air jets forming the obstacles instead of solid walls [68], although this is uncommon. Despite a plethora of studies investigating different fire whirl generation apparatus at the laboratory scale, few if any studies investigate the effects of apparatus height and configuration on fire whirl formation and behavior.

3.2 Experimental Apparatus and Methods

A modular system of four enclosure walls were used to create fixed-frame fire whirl generators of various dimensions to be used in this investigation. The base of these generators was a smooth metal base plate into which a 10 cm fuel dish could be placed such that the surface of the liquid fuel layer was kept flush with the base plate. The modular enclosure walls were then arranged in a square centered around the fuel dish. Each side of the square enclosure had a gap of $G = 5$ cm on the left side of the wall to allow for air entrainment into the enclosure, as shown in Figure 3.1. As buoyancy draws exhaust gases away from the fuel surface, ambient air is entrained into the fire whirl, creating a vortex that spins clockwise when viewed from above.

In this investigation, wall heights of $H = 5, 15, 20, 35, 45, 60,$ and 80 cm were arranged to create square enclosure footprints with side lengths $S = 20, 30,$ and 40 cm. Each wall height was tested for each enclosures with side lengths $S = 20$ or 30 cm. For the enclosure with side length $S = 40$ cm, tests were only conducted with wall heights $H = 45, 60,$ and 80 cm. The test for each wall height and enclosure side length combination was repeated a minimum of three times.

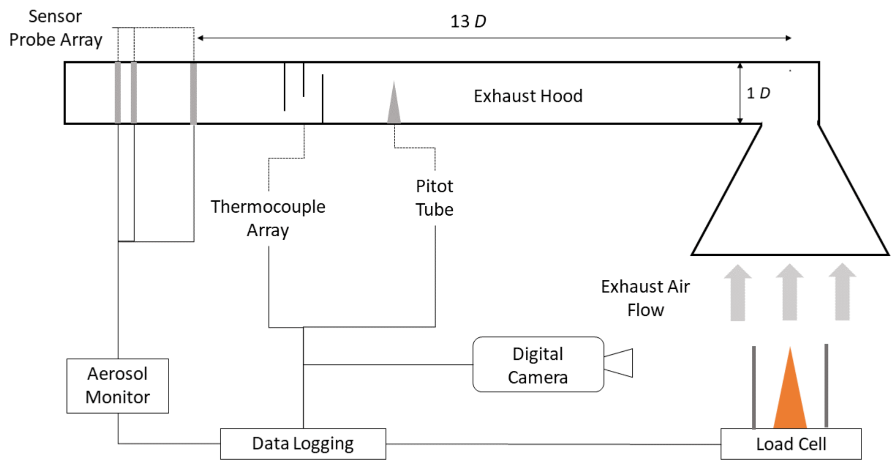

Figure 3.2: Diagram of sensoria used in experiments, including TSI DustTrak aerosol monitor, Sony RX10 II digital camera, and Mettler-Toledo MS6002TS load cell

The fuel for each test consisted of 30 mL of n-heptane floating over a cold water layer that was ignited with a sparking igniter. The instantaneous mass of fuel remaining in the fuel dish was captured at a frequency of 1 Hz for the duration of burning via a Metler-Toledo load cell model MS6002TS with an accuracy of ±0.02 g.

Emissions from the flame were captured by an exhaust ventilation system consisting of an exhaust hood 1.85 m above the fuel surface with an inlet diameter of 23 cm, which drew in exhaust gases at a rate of approximately 0.3 m^3/s, shown in Figure 3.2. The concentration of 2.5 micron particulate matter in the exhaust gases was obtained by a TSI DustTrak DRX Handheld Optical Aerosol Monitor at a rate of 1 Hz. The mass of $PM_{2.5}$ emissions was calculated based on this concentration, the flow rate of the exhaust gases, and a gravimetric calibration factor for the density of heptane soot. The volumetric flow rate of exhaust gases was monitored by a Veris Verabar pitot tube system with a thermocouple array to account for changes in exhaust gas temperature. All sensors in the exhaust gas system were located at a distance of at least 300 cm from the exhaust inlet to allow for adequate mixing before sampling.

Videos of the flame were captured with a Sony RX10 II digital camera at an average frame rate of 30 Hz with an aperture speed of 1/800, an ISO value of 800 and an F-stop value of 5.6. These videos were scaled to a reference image to calculate the ratio of length in pixels to length in millimeters. Images of the flame were binarized using Otsu's method, implemented through MatLab's Computer Vision Toolbox, so that the flame would be the only visible bright pixels in the image. For each image, the largest continuous group of bright pixels, representing the continuous flame length, had an oval fit to encompass the pixel mass. The major axis of this fit oval was taken to be the flame length. A verification of

(a) $\{S, H\} = \{20, 10\}$ cm (b) $\{S, H\} = \{20, 45\}$ cm (c) $\{S, H\} = \{20, 80\}$ cm

Figure 3.3: Images of the fire whirls generated in an enclosure with a side length of 20 cm for shown wall heights. A reference scaling length for 10 cm is shown as the white bar in each image

this method was produced by comparing the lengths calculated by this method to the flame height calculated by finding the longest column of pixels with an intensity of greater than 55%. Flame lengths equaled or exceeded the flame height calculation by a factor of no more than 1.8.

3.3 Results

For higher wall heights, $H > 35$ cm, fire whirls quickly formed and remained stable for the entire test duration, with little variation in mass loss rate or flame height before extinction. For lower heights, $H \leq 35$ cm, fire whirl formation was unsteady, often involving long periods where the flame formed a precessing inclined flame sweeping the inside of the generator enclosure. This led to greater variations in flame height and correlated with lower mass loss rates.

Mass Loss Rate

The mass of remaining fuel was sampled from the load cell below the fuel dish at a rate of 1 Hz for the duration of each experiment. The fuel mass remaining as a function of time is shown for three representative tests in Figure 3.4. In Figure 3.4 a relatively constant mass loss rate is shown as nearly linear decreases in mass with time, but as shown in subfigure (b), the lowest wall height, $H = 10$ cm, causes a much lower mass loss rate than the other wall heights, taking more than 150 seconds to burn 18 grams of fuel.

The average mass loss rate for each test was taken as the average of the forward difference of the instantaneous mass at each second. The average mass loss rate for each condition is shown in Figure 3.5 with error bars representing one standard deviation. This figure shows the mass loss rate for the tested fire whirl generators compared to the mass loss rate of the unaugmented pool fire, shown by the dotted gray line at 0.109 g/s. For the enclosure with side lengths $S = 30$ cm, the mass loss rate continues to increase as H increases. For the widest enclosure, $S = 40$, the mass loss rate was not significantly different than that of a pool fire for wall heights $H = 45$ and $H = 60$ cm, but increased dramatically at $H = 80$ cm to 0.256 ± 0.008 g/s. For both of the wider enclosures, a noticeable jump in mass loss rate is observed beyond $H = \{45, 60\}$ cm for $S = \{30, 40\}$ cm rather than a smooth increase. Notably, the greatest mass loss rates for the tested wall heights were similar for both $S = 30, 40$ cm, both occuring at $H = 80$ cm. For the narrowest enclosure, $S = 20$ cm, the increase in H causes an increase in mass loss rate until $H = 35$ cm, beyond which the mass loss rate has a slightly decreasing trend. This gives evidence that the flame may be oxygen starved at these dimensions due to obstruction of air entrainment from narrow openings.

Flame Height

For the duration of burning, starting at ignition, a video of the flame was recorded with images captured at a frequency of approximately 30 frames per second through the front sidewall. Every 15 frames, or at rate of 2 Hz, an image of the flame was binarized by Otsu's method of image thresholding and an oval was fit around the largest region of bright pixels, which represents the continuous flame region. The major axis of the fit oval was taken to be the length of the flame in that frame. The intermittent flame length, IFL, was taken as the 50th percentile greatest flame length from ignition to extinction. This definition is modified from [28], in which the intermittent flame height was determined as the height the flame reached for a minimum of 50% of the observed time.

The IFL for each tested wall height and enclosure side length is shown in Figure 3.6 with error bars representing one standard deviation. Figure 3.6 also depicts the average IFL for the pool fires measured in this study, which is shown as a dashed grey line for comparison. To eliminate the sensitivity of the choice of intermittency percentage, a 75th percentile flame length,L_{75th} was also calculated by the same method. The values of L_{75th} are shown in Figure 3.7 with comparison to the pool fire shown by the grey dashed line and with error

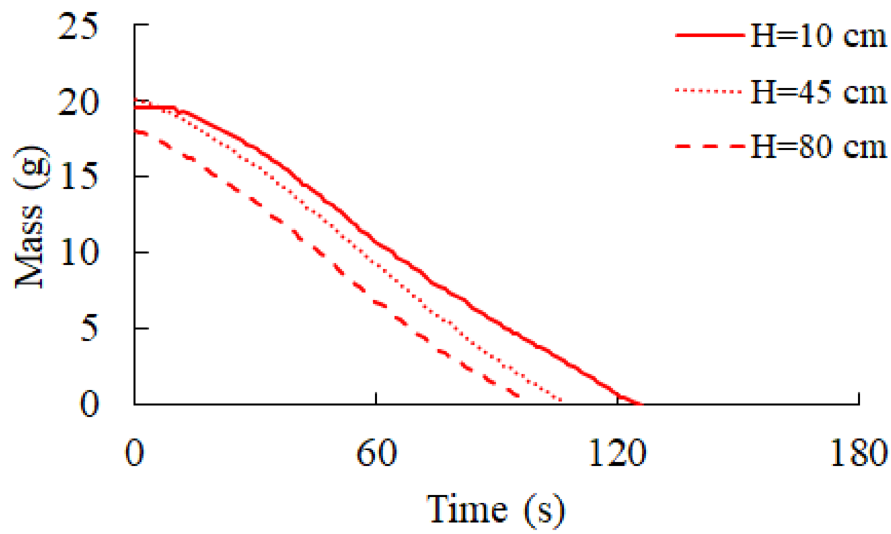

(a)

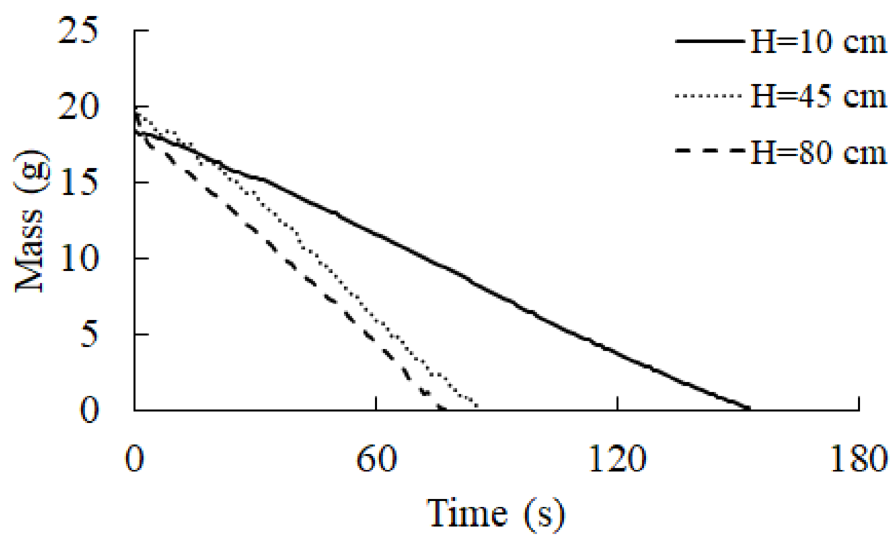

(b)

Figure 3.4: Instantaneous fuel mass remaining from representative tests for fire whirl generators with wall heights $H = 10, 45, 80$ cm and side length a) $S = 20$ cm in red and b) $S = 30$ cm in black.

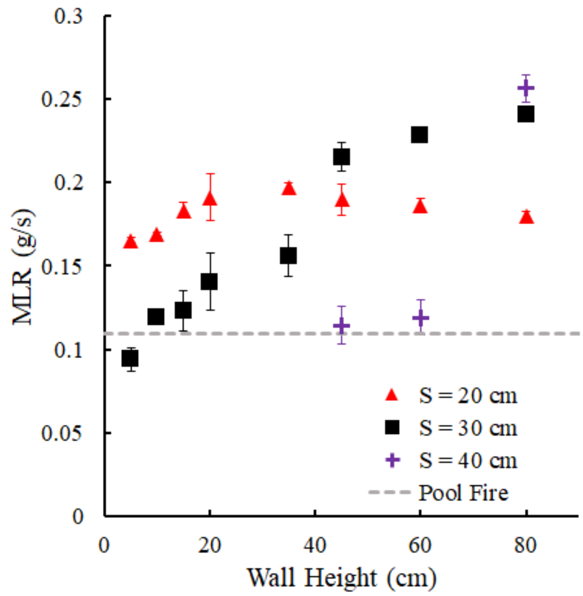

Figure 3.5: Average instantaneous mass loss rates for fire whirl generators with side lengths $S = 20, 30, 40$ cm, compared to that of an unaugmented pool fire. Error bars represent one standard deviation.

bars representing one standard deviation. The growth and decay phases of the flame are of negligible duration as the surface of the liquid n-heptane ignited homogeneously, so any variation in the flame height is due to fluctuations in the flow structure of the generated flame.

For the narrower enclosures, with $S = 20, 30$ cm, IFL is positively correlated with the height of the enclosure until the height of the enclosure exceeds $H = 60$ cm, beyond which point the IFL shrinks. For low H the IFL is similar to that of the unaugmented pool fire. For the widest enclosure, $S = 40$ cm, the IFL is below that of the flame length of the unaugmentented pool fire until the wall height reaches $H = 80$ cm, at which point the flame length nearly doubles. For the enclosures with $S = 20, 30$ cm, the IFL exceeds the height of the generator walls for $H < 45, 35$ cm, respectively. The IFL also exceeds the wall height for $S = 30$ cm at $H = 60$ cm, which is the maximum IFL observed in this investigation at a flame length of 694 ± 6 mm. For the enclosure with $S = 40$ cm, the IFL never exceeds the height of the generator walls. Similar trends are shown for L_{75th} in Figure 3.7, with a notable difference in that the greatest value of L_{75th} occurs at the greatest wall height and for the greatest enclosure width.

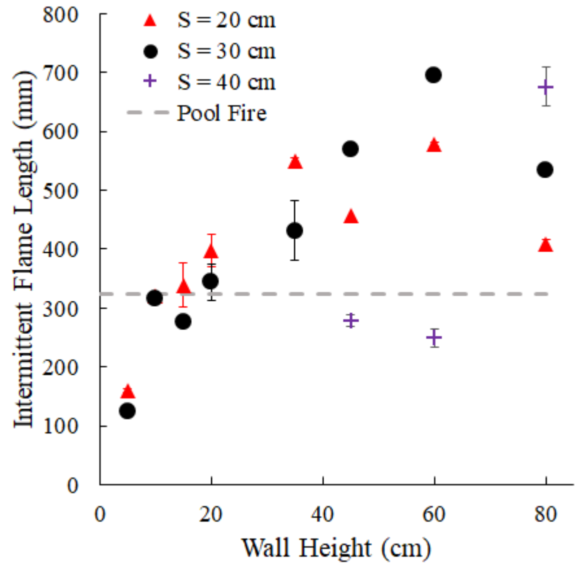

Figure 3.6: Intermittent flame length (IFL) for fire whirl generators with $S = 20, 30, 40$ cm at all tested wall heights, compared to that of the pool fire, represented by the dashed grey line. Error bars represent one standard deviation.

Particulate Matter Emissions

The emissions of each test were captured and passed through an aerosol particle analyzer to determine the concentration of particulate matter with diameters of at least 2.5 microns, $PM_{2.5}$, in the exhaust gas. The concentration of $PM_{2.5}$ and the flow rate of exhaust gases allowed for the calculation of total $PM_{2.5}$ production per second. The production rates of $PM_{2.5}$ are shown in Figure 3.8 for the same representative tests as in Figure 3.4.

The average production rate of $PM_{2.5}$ is shown for each test in Figure 3.9 with error bars representing one standard deviation. The generation rate of $PM_{2.5}$ for most fire whirl generators are either comparable to or exceeding the $PM_{2.5}$ generation rate of the pool fire. The exceptions to this are at the greatest wall heights, $H \geq 60$ cm, for $S = 30, 40$ cm, which have lower rates of particulate matter generation with a minimum of 2.76 ± 0.14 mg/s for $S = 40$ cm at $H = 80$ cm. The maximum rate of particulate matter generation occurs at $H = 5$ cm for $S = 20$ cm, with a magnitude of 6.25 ± 0.12 mg/s.

The emissions factor of $PM_{2.5}$, $EF_{PM2.5}$, was calculated for each test as the total mass of particulate matter produced divided by the mass of n-heptane fuel consumed. The value of $EF_{PM2.5}$ is shown for each test in Figure 3.10 with a comparison to the unaugmented pool fire, with error bars representing the combined standard deviation.

For the enclosure with side length $S = 20$ cm, the lowest wall height $H = 5$ cm shows an overall $EF_{PM2.5}$ greater than that of the unaugmented pool fire, at 41.62 ± 0.42 mg/g. As

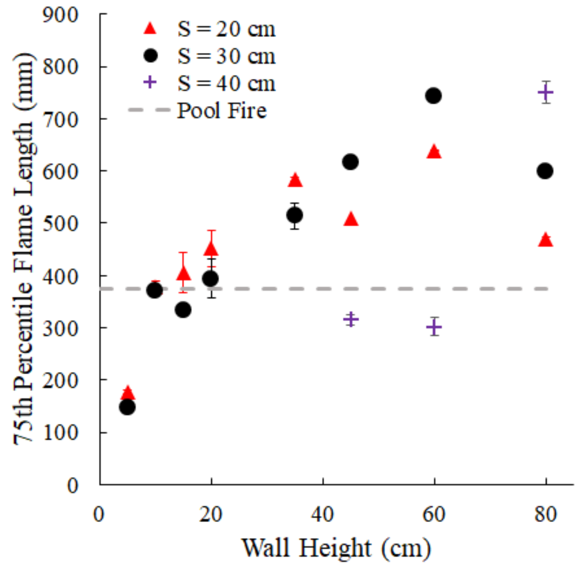

Figure 3.7: 75th percentile flame height for fire whirl generators with $S = 20, 30, 40$ cm at all tested wall heights, compared to that of the pool fire, represented by the dashed grey line. Error bars represent one standard deviation.

H increases, the $EF_{PM2.5}$ decreases until a minimum value of 21.00 ± 0.86 mg/g at $H = 45$ cm, beyond which the emission factor begins to increase. This implies that beyond some critical wall height, the flame is being choked due to an inability to entrain sufficient unburnt air. The enclosure with $S = 30$ cm also has an $EF_{PM2.5}$ greater than that of the pool fire at $H = 5$ cm, reaching a maximum of 39.79 ± 1.26 mg/g. For all greater values of H, the decreasing trend of $EF_{PM2.5}$ with H continues until the minimum value of 12.72 ± 0.16 mg/g at $H = 80$ cm. This minimum value is similar to the minimum value observed for the widest enclosure. The widest enclosure, $S = 40$ cm, did not show a sloping trend with H at the tested resolution, but instead a steep drop in $EF_{PM2.5}$ beyond $H = 60$ cm to the minimum value of $EF_{PM2.5}$ for all tested generator dimensions at 11.00 ± 0.21 mg/g. The $EF_{PM2.5}$ is lower for most fire whirl generators than for pool fires despite their higher rate of $PM_{2.5}$ generation due to the much shorter burn duration.

3.4 Discussion

As the height of the generator walls increased, an increase in mass loss rate and flame length were observed, as well as a decrease in the emission of particulate matter. This trend holds for wall heights up to $H = 60$ cm, beyond which the flame length and mass loss rate of the fire whirl decreased for the enclosures with side length $S = 20$ or 30 cm. This indicates that

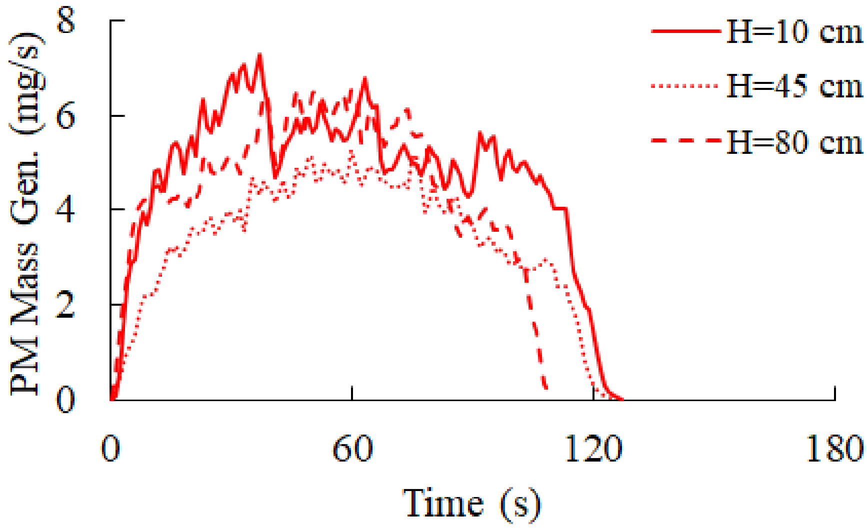

(a)

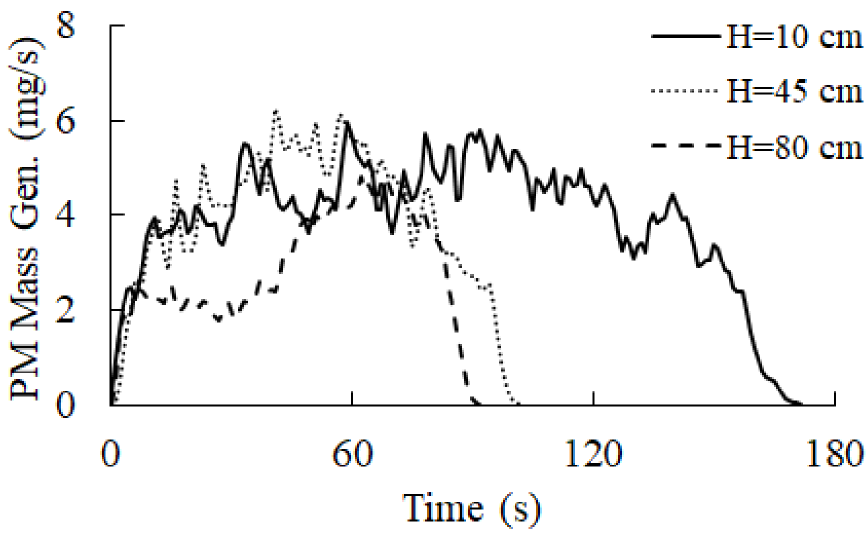

(b)

Figure 3.8: Instantaneous rate of $PM_{2.5}$ generation from representative tests for fire whirl generators with wall heights $H = 10, 45, 80$ cm and side length a) $S = 20$ cm in red and b) $S = 30$ cm in black.

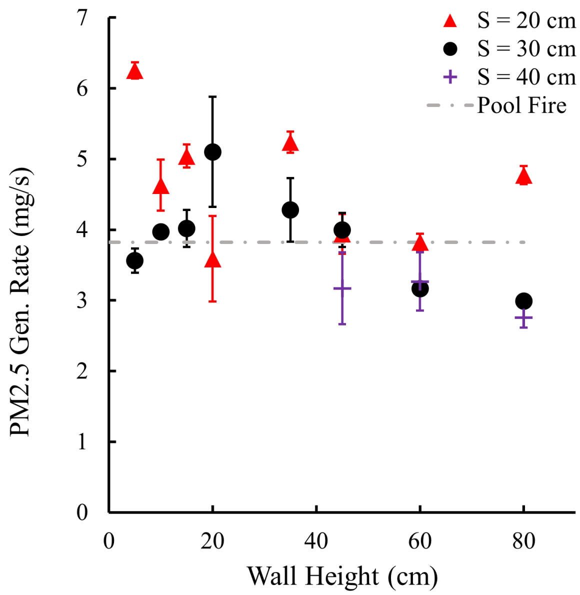

Figure 3.9: Average generation rate of $PM_{2.5}$ for each tested wall height, compared to the generation rate of $PM_{2.5}$ for a pool fire shown as a dotted line. Error bars represent one standard deviation.

the fire whirl is weaker, potentially due to lack of sufficient oxygen for combustion.

The generation of the fire whirl augments the behavior of a pool fire due to the formation of the vortex encompassing the flame. The flame height of a pool fire is directly related to the heat release rate of the flame, as the visible flame length is the result of buoyancy carrying red-hot soot particles away from the fuel and into the cooler ambient air, forming a fire plume. This buoyancy results from the lower density of the high-temperature flame gases, with the heat released from combustion causing the increase in gas temperature. Additionally, for a liquid-fueled fire, the presence of soot in the flame to create the luminous region is determined in part by the quantity of fuel vapor emitted from the liquid surface, which is determined by the heat flux fed back to the fuel surface from the flame. This creates an implicit relationship between the flame height and the heat release rate of the flame which can be empirically determined, resulting in correlations such as the following correlation by Heskestad [69].

$$\frac{L}{D} = -1.02 + 3.7Q^{*2/5} \tag{3.1}$$

where L is the length of the flame, D is the diameter of the fuel dish, and Q^* is the nondimensional heat release rate.

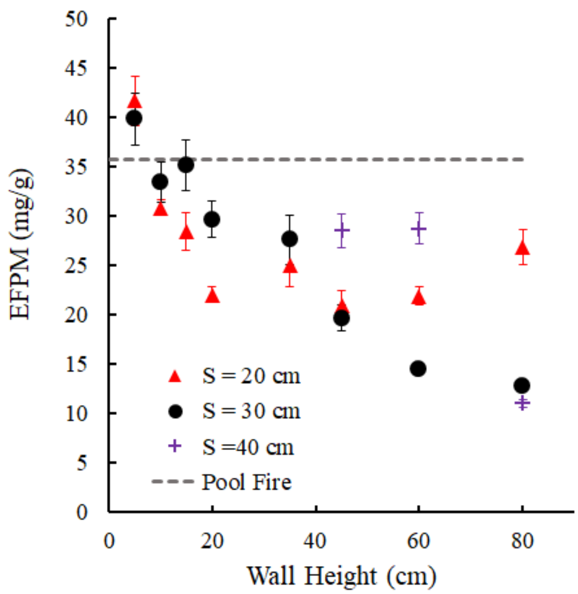

Figure 3.10: $EF_{PM2.5}$ for fire whirl generators with side lengths $S = 20, 30, 40$ cm, with a dashed line representing the average $EF_{PM2.5}$ of the pool fires. Error bars represent one standard deviation.

The nondimensional heat release rate is calculated by

$$Q^* = \frac{\dot{m}\Delta H_C}{\rho_\infty T_\infty c_p \sqrt{gD^5}} \tag{3.2}$$

where $\dot{m}$ is the mass loss rate of fuel, ΔH_C is the heat of combustion of the fuel, ρ_∞ is the density of ambient air, T_∞ is the temperature of ambient air, c_p is the specific heat of air, and g is the acceleration due to gravity. Zukoski uses a similar nondimensional heat release rate in his correlation for flame height, also with a power of 2/5 [28]. These correlations assume that the mass flux into the fire plume is due to entrainment of air into the fire plume and the heating and mixing of this fresh air [28] , but they do not account for the effect of circulation on the flow around the flame. Figure 3.11 shows a nearly linear correlation between the nondimensional flame length, $Z^* = H/d$ and the nondimensional heat release rate, Q^*, for the results of these experiments rather than the 2/5 power dependency in [28, 69]. Zhou et al. [30] attribute the difference between the flame height of a pool fire and that of a fire whirl entirely to the effect of circulation, with the empirically fit equation

$$\frac{H_{FW}}{H_{PF}} = 0.36\Gamma^{*1.11} \tag{3.3}$$

where H_{FW} is the height of the fire whirl, H_{PF} is the height of a pool fire with the same fuel

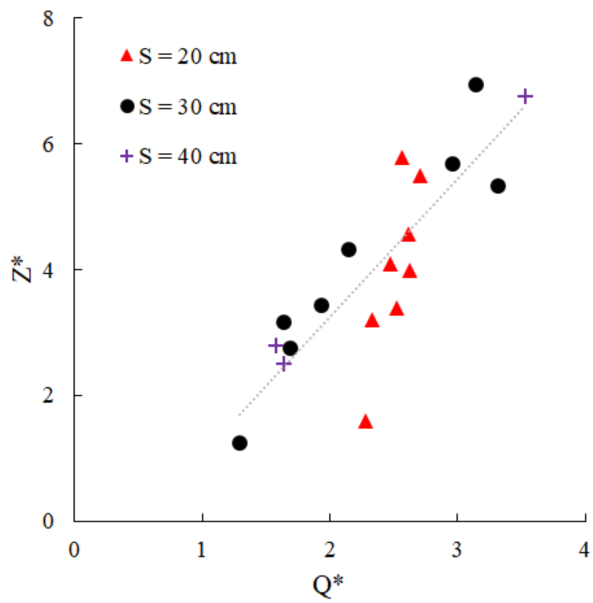

Figure 3.11: Nondimensional flame length, Z^* as a function of nondimensional heat release rate Q^* for all tested conditions, with line of best fit shown with $R^2 = 0.7222$.

pool diameter, and Γ^* is the nondimensional circulation

$$\Gamma^* = \frac{\Gamma}{\sqrt{gD^3}} \tag{3.4}$$

with Γ being the circulation. Applying this to the experimental results in this investigation, nondimensional circulation can be estimated from the flame lengths, which are shown in Figure 3.12. If these nondimensional values are accurate and used to obtain a dimensional value for circualtion in m^2/s based on equation 3.4, the circulation varied between 0.10 and 0.49 m^2/s, placing them in the weak fire whirl and inclined flame regimes of [26].

In Figure 3.12, the calculated nondimensional circulation, Γ^*, shows a region of increasing trend with increasing wall heights for $S = 20, 30$ cm, coincident with the region in which stable fire whirls form. Below $H = 10$ cm, there is very little circulation imparted by the surrounding air, likely because air entrainment can be drawn over the short walls. At $H = 80$ cm, the nondimensional circulation drops for $S = 20, 30$ cm, which is due to the corresponding drop in IFL, and with the drop in MLR for $S = 20$. Instead, the value for $H = 80$ cm $S = 40$ cm seems to fit this increasing trend. This means that the width of the enclosure will become the limiting factor for the generation of larger and stronger fire whirls in a given generator.

The $\text{EFPM}_{\text{PM2.5}}$ is shown as a function of Q^*, as calculated by equation 3.2, in Figure 3.13. In this figure, an inverse relationship between heat release rate and particulate matter

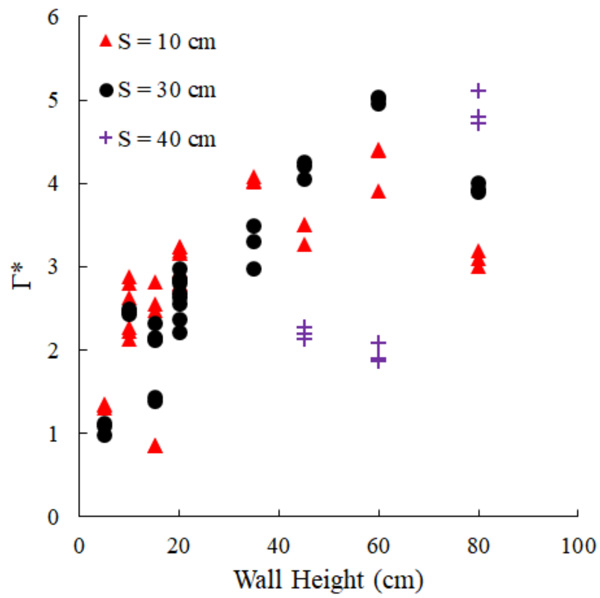

Figure 3.12: Nondimensional circulation, Γ^* calculated from eq. 3.3 for each experiment for all wall heights.

production is clear. The increased mass flux from the fuel surface does not result in an abundance of incompletely combusted soot particles. The increased heat release rate then shows that more of the soot particles are being consumed in the larger fire whirls. Similarly, Figure 3.15 shows an inverse relationship between the flame height and the emission of particulate matter. This relationship is nearly linear, save for a notable outlier at $Q^* = 2.28$ and $EF_{PM2.5} = 41.6$ mg/g, which corresponds to the lowest wall height for the narrowest enclosure, $\{S, H\} = \{10, 5\}$ cm. At this height and width combination, the flame is unstable, neither producing a fire whirl nor remaining an axisymmetric pool fire.

The decreasing trend of soot emission with heat release rate in Figure 3.15 is counterintuitive at first glance. The visible flame height is the result of glowing of soot particles, with the limit of the visible flame height determined by the distance over which soot burns out and cools [35]. One would assume then that more soot being emitted from the fuel surface would increase the visible flame length, but this is not the case in the observed tests. The decrease in $EF_{PM2.5}$ with Q^* indicates that the increase in flame length is not due to an overabundance of soot particulate lengthening the flame, but instead that the particulate soot is more fully consumed in the longer flames.

The decrease in $EF_{PM2.5}$ with Γ^* is shown in Figure 3.14 with a linear fit line that has an R^2 value of 0.8177. This figure shows that the increase in circulation provided by higher walls correlates to lower emission of particulate matter. For a fixed-frame fire whirl, the range of circulation possible to generate with the fire whirl is dependent on the heat release rate of the

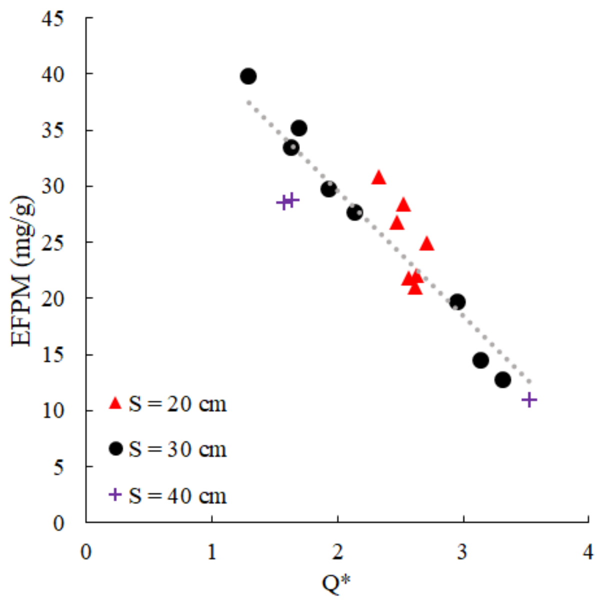

Figure 3.13: Emission factor of $PM_{2.5}$ for flames with a given Q^*. Data points are grouped by generator width. The line of best fit for the entire data set is shown, with an R^2 value of 0.8652

flame, so the range of tested values is limited. For future experiments in an Emmons-type fire whirl generator, where circulation is decoupled from heat release rate, a change in this trend may occur as applied circulation exceeds the circulation naturally established in the fixed-frame generator.

3.5 Conclusions

In this work the effects of a fixed-frame fire whirl generator's dimensions on the produced flame's characteristics were investigated. An increase in the height of the walls forming the fire whirl generator's enclosure correlates with an increase in the ambient circulation, leading to increases to the flame's length and burning rate, until a critical point is reached, beyond which the flame appears to weaken. This critical point is dependent on the width of the enclosure, leading to the hypothesis that the apparent weakening of the flame is due to issues of oxygen availability. The emission of 2.5 micron particulate matter from the flame is inversely correlated with the height of the enclosure walls. Higher walls create flames with lower soot emissions until a minimum emissions factor is reached for a given enclosure width. The production of particulate soot emissions is therefore also inversely correlated with the flame length and circulation, indicating that the extended flame length is consuming particulate soot before it can escape the flame tip. Future work should investigate

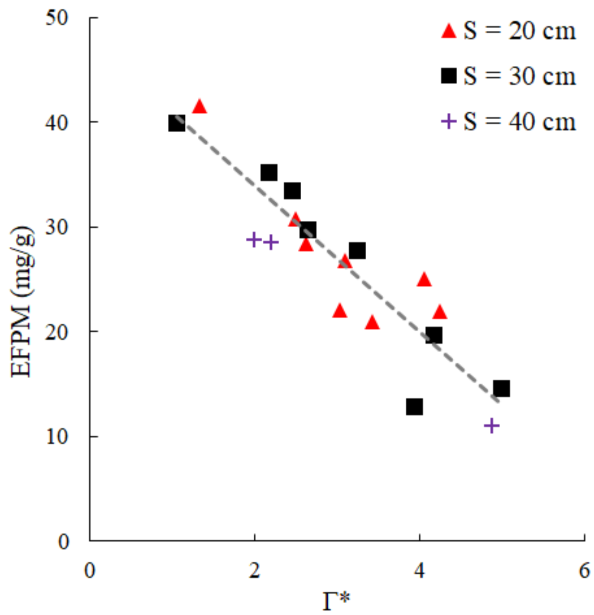

Figure 3.14: Average $EF_{PM2.5}$ and $\Gamma*$ for each tested combination of H and S shown with a linear fit with an R^2 value of 0.8177

the relationship between net particulate matter production and circulation in a fire whirl generator that decouples the circulation from the burning rate of the fuel.

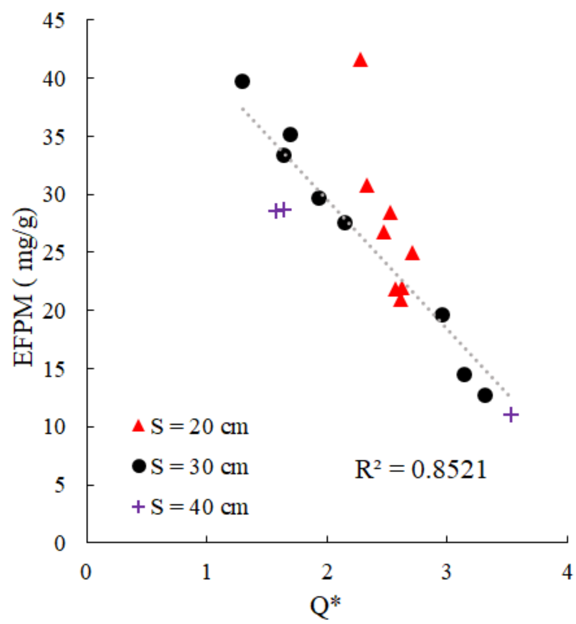

Figure 3.15: IFL for each flame with its associated $EFPM_{PM2.5}$. Data points are grouped by generator width. A line of best fit is shown with an R^2 value of 0.7086

Chapter 4

Large-Scale Field Experiments on Enhancing *In-Situ* Burning with Fire Whirls

4.1 Introduction

Oil spills pose significant threats to marine environments, causing both immediate and long-term ecological impacts [10, 70]. These catastrophic events can lead to acute mortality of marine life through toxic exposure and smothering, as well as chronic effects that persist for years or even decades after the initial spill [70, 71]. In-situ burning has emerged as a potential effective and cost-efficient method for cleaning up oil spills, particularly in remote areas or under challenging conditions [16, 72, 73]. This technique can rapidly remove up to 95% of spilled oil from the water surface, reducing the risk of oil penetrating sediments or drifting to contaminate adjacent habitats [72]. However, in-situ burning is not without limitations. The process produces a visible smoke plume containing soot and other combustion products, raising concerns about air pollution and potential health risks to response personnel and nearby populations [18]. Accordingly, the primary focus in enhancing in-situ burning involves improving burning characteristics, shortening the burning operation time, and minimizing emissions released into the atmosphere.

The most common in-situ burning technique can be classified as controlled pool fires [46]. Extensive research has been conducted to understand the factors influencing the burning characteristics of in-situ burning, including slick thickness, pool diameter, ambient wind conditions, and fuel properties [14, 74–76]. Studies on slick thickness have revealed that initial slick thickness significantly affects burning efficiency, with maximum efficiency typically achieved at thicknesses exceeding 10-20 mm for crude oils [14, 74]. The influence of pool diameter has also been investigated, with research indicating that burning efficiency does not increase significantly for diameters larger than 1 m [47, 74, 75]. A key insight from related in-situ burning research is the potential for improving burning characteristics by modifying conditions that affect the fire. One approach involves increasing heat fluxes to the fuel surface, such as the Flame Refluxer which uses a metal substrate in the oil layer to increase heating [77]. Larger pool fires are often limited in efficiency by a lack of available oxygen near the center of the fuel pool. Enhancing ventilation has the possibility of reducing airborne emissions. For instance, studies on varying the fire boom shape, such as line configurations, have shown reduced emission factors of soot [78]. As research continues to evolve, there is a growing interest in novel approaches like the use of fire whirls in oil spill remediation, because fire whirls are particularly promising due to their inherent ability to increase heat flux to the fuel surface and improve air circulation naturally, without the need for external mechanical ventilation [5, 20, 21].

Fire whirls are formed when circulation is introduced to or generated by a buoyant fire plume, creating a vortex that leads to a taller, more defined flame structure and enhanced combustion [6]. The generation of fire whirls can be achieved through a variety of mechanisms and setups, such as an open configuration like L-shaped fire sources with cross-flow [3, 79], and enclosed stationary configurations like wall structures with slits [21, 25, 31, 68, 80–84] , half-cylinders with offset slits [64], circular intakes [85], and rotating screen setups known as an Emmons type [22, 26, 59]. The majority of fire whirl studies are conducted on a limited scale within laboratory settings, offering precise control over variables to investigate fundamental mechanisms. However, fire whirls in natural settings have been observed on a significantly larger scale; for example, the tallest recorded fire whirl during a wildland fire reached a staggering height of 5200 m [86], and a pool fire under cross wind conditions produced a 21-meter-high fire whirl lasting 9 seconds [87]. Conducting controlled large-scale experiments is necessary for a comprehensive understanding of fire whirl dynamics and their practical applications. Given that recent laboratory-scale experiments have demonstrated the capability of fire whirls to enhance burning characteristics and diminish soot emissions per unit of fuel consumed [7, 20], this study aims to investigate the scalability, reliability, and effectiveness of utilizing fire whirls for the remediation of oil spills in large-scale field scenarios, thereby advancing our understanding of this method's practicality.

In this paper, we report on large-scale field experiments that aim to enhance the in-situ burning technique through the application of fire whirls, representing one of the largest-to-date experiments in fire whirl research, and the first study to bridge the knowledge gap between laboratory and field-scale utilization of fire whirls for in-situ burns. Our objective was to study the combustion efficiency of large-scale crude-oil fire whirls for use in in-situ burning. Experiments involving fire whirls and pool fires were conducted using two distinct crude oil slick thicknesses (15 mm and 40 mm) atop a water surface, encircled by a 1.5-meter-diameter fuel ring. Observations and measurements of fire whirl and pool fire dynamics included flame geometry, flow velocity, temperature profiles, heat flux, mass consumption, and gas and particulate emissions. Comparative analyses spanning fire whirl and pool fire configurations, variations in oil slick thicknesses, divergent ambient conditions, and correlative assessments with prior laboratory-scale experiments provide invaluable insights conducive to improving in-situ burning methods for enhanced combustion efficacy and reduced environmental emissions.

4.2 Experimental Methods

The field experiments were conducted at the Brayton Fire Training Field of the Texas A&M Engineering Extension Service (TEEX) in College Station, Texas from May 15 to 19, 2023. The site plan and facilities at the experimental field are shown in Figure 4.1. A 3-meter square in-ground pool filled with water to a depth of 1.2 m was used to emulate the open-water conditions of an oil spill. A custom-built metal ring with a 1.5 m diameter was suspended at the water surface to enclose the fuel for the in-situ burning experiments. Figure 4.1(c) shows a photo of a typical fire whirl and pool fire formed in the large-scale experiments.

The fire whirl configuration plan and instrument locations are illustrated in Figure 4.2. A three-wall structure was constructed around the pool based on the design in laboratory experiments to generate fire whirls [7]. The wall structure was fabricated using fire-retardant wallboards that formed a 5 m $\times$ 5 m surface area, with steel frames providing structural support at the back. The three walls were arranged in an equilateral triangle configuration centered on the metal ring, with a 1.5 m gap on each side to allow for tangential air entrainment during the fire whirl experiments. After the fire whirl experiments, the wall structure

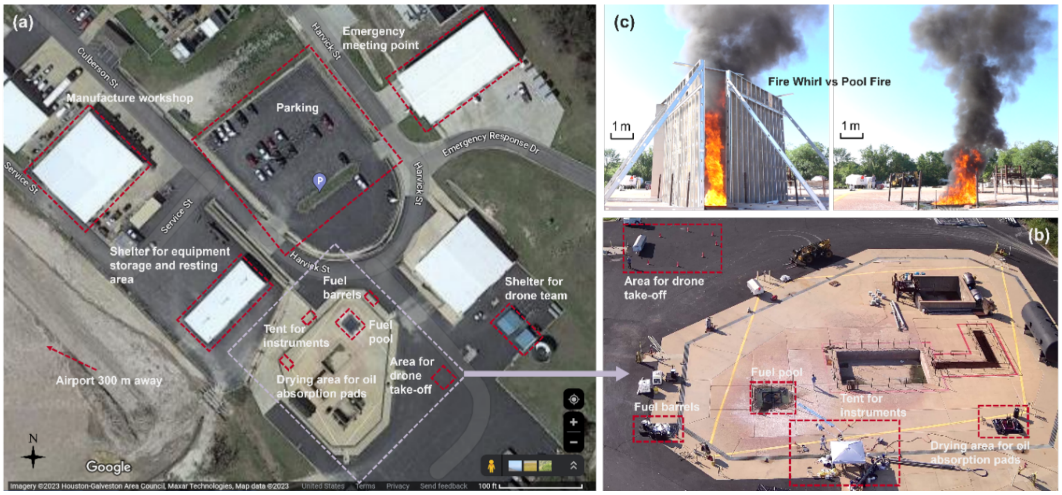

Figure 4.1: (a) TEEX site plan for the large-scale field experiment. The site is located at N 30deg 34’40” and W 96deg 21’16” (Source: Google Map). Red rectangles are used to highlight the main facilities utilized in the experiment. Easterwood Airport is 300 m away from the experimental site. All burning activities and drone activities were communicated with the airport tower. All experimental activities followed the safety regulations of the TEEX site. (b) An aerial photo depicting the experimental site layout (Photo: USGS). There are four fuel pools at the site encircled by a yellow line on the ground. It is required for all participants to refrain from crossing the demarcated yellow line while fire experiments are in progress. The pool used in the experiment is enclosed by a red rectangle. (c) Photos of a successfully formed fire whirl and pool fire during the large-scale experiment.

was dismantled to accommodate the subsequent pool fire experiments.

For the fire whirl experiments, five hot-wire anemometers (Testo 405i) were used to measure the inlet flow velocity into the test section. Three anemometers were stationed at location A on the wall structure at heights of 0.25 m, 0.5 m, and 1.5 m, and one anemometer was positioned at each of locations B and C, 0.25 m above ground level. The probe of each anemometer was positioned perpendicular to the wall, with a 0.4 m distance from the wall surface. Figure 4.2(a) and 4.2(c) indicate the specific placements of the anemometers during the fire whirl experiments. For the pool fire experiments, an anemometer was mounted on a pole, positioned 0.25 m above the ground near location A. The Testo 405i anemometer features a portable design with an extendable probe shaft (maximum length: 40 cm) and wireless data transmission capabilities, making it well-suited for field measurements. The anemometer also measures temperature within the range of -20 to 60 ℃. However, its operating temperature range is limited to -20 to 50 ℃, which can affect the accuracy of velocity measurements when the ambient temperature exceeds 50 ℃. Furthermore, a portable weather station (Kestrel 5200 with rotating vane mount) was installed 20 m east of the fuel ring. This weather station continuously monitored the ambient conditions, including wind

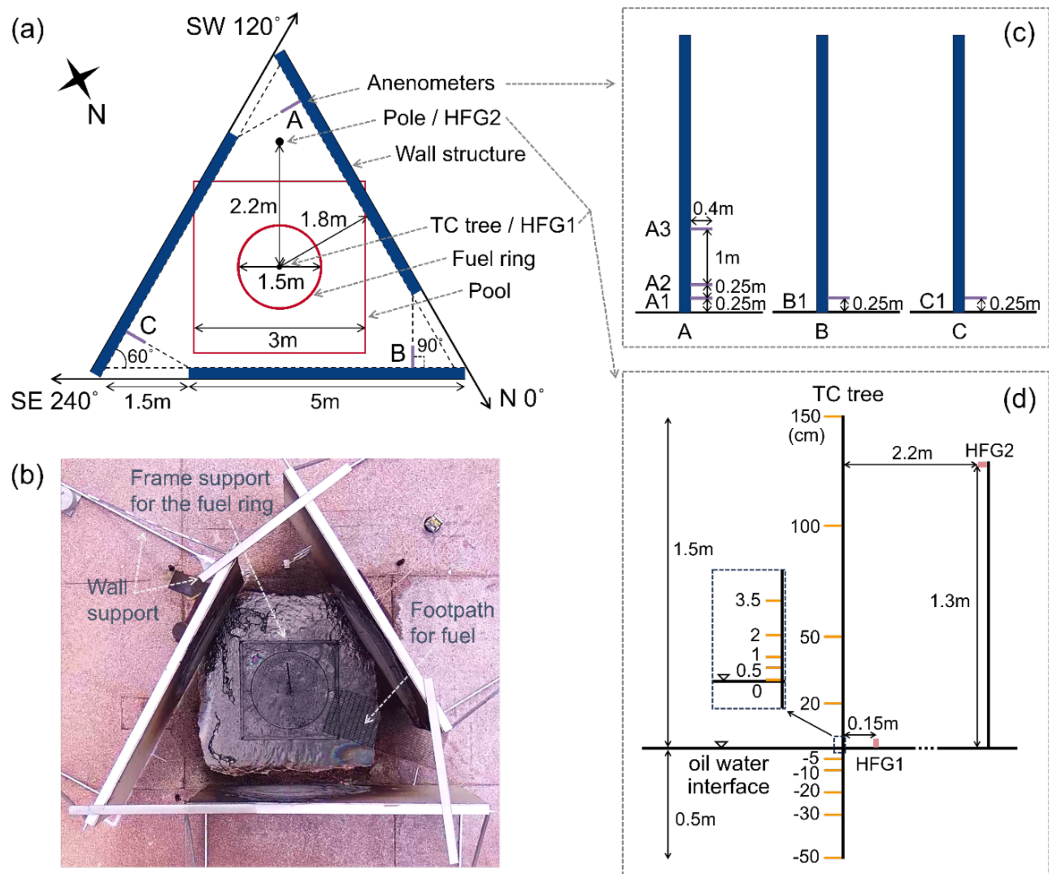

Figure 4.2: Fire whirl structure configuration and instrumentation. (a) Schematic of the three-wall structure to generate fire whirls and the locations of instruments. The directions of the three walls were measured by a mobile compass. (b) Aerial photo of the three-wall structure on site (Photo: USGS). To simplify the schematic, the frame support for the fuel ring suspended at the water surface, the support for the wall, and the footpath to reach the fuel ring shown in (b) are not depicted in (a). (c) Schematic showing the locations of anemometers at inlet A, B and C. (d) Schematic showing the thermocouple locations along the thermocouple tree (TC tree) and positions of the two heat flux gauges (HFG). Thermocouples are marked with numbers showing the distance from the thermocouple to the water surface (in cm).

speed and direction, humidity, and temperature, throughout the experimental period. The TEEX site also had its own weather station, which provided real-time forecasts of environmental changes, such as lightning and precipitation, as well as additional wind condition data as a reference.

A thermocouple tree was constructed, originating from the center of the fuel ring, to measure the temperature variations in the generated flame, the oil slick, and the underlying water. Fourteen K-type thermocouples were installed along the thermocouple tree, with their specific locations illustrated in Figure 4.2(d). Two water-cooled total heat flux gauges (Medtherm Schmidt-Boelter type) were also used. One heat flux gauge (HFG1) was installed on the thermocouple tree, offset by 15 cm and protruding up from the fuel slick surface, to capture heat flux feedback from the flame. The second heat flux gauge was mounted on a 1.3 m pole, positioned 2.2 m from the center of the fuel ring, to measure the radiation from the flame to the surroundings. The specific locations of the heat flux gauges are shown in Figure 4.2(a) and 4.2(d). The heat flux gauges had a rated measurement range of 0 to 150 kW/m2 and were calibrated against a reference gauge using a cone calorimeter at the Berkeley Fire Research Lab prior to the experiments.

Various action and high-speed cameras were installed around the test area to capture images and videos of the fire whirls and pool fires. The layout of the six deployed cameras is depicted in Figure 4.3.

Camera 1 (GoPro action camera), 2 (Sony high-speed camera), and 3 (Casio high-speed camera) were positioned at distances of 6 m, 12 m, and 12 m, respectively, from the center of the fuel ring to capture video footage of the flames. Camera 4 (SJCAM action camera) was mounted on the wall's edge, 1.7 m above the ground, and directed towards the fuel ring to document the formation of fire whirls. (Note: Camera 4 was not used in the pool fire tests.) Camera 5 (DJI action camera) was mounted on a drone to capture aerial footage. Camera 6 (Canon 5D) was used to photograph the flames throughout the experiments.

Hoover Offshore Oil Pipeline System (HOOPS) blend crude oil, a medium-weight crude oil typical of the Gulf of Mexico, served as the primary fuel for experiments. Prior to commencing experiments with HOOPS crude oil, preliminary tests with diesel, a surrogate fuel, were carried out to determine the feasibility of the experimental setup. Experiments involving two oil slick thicknesses – 15 mm and 40 mm – were conducted to investigate the impact of slick thickness on burning rate, fuel consumption efficiency and emissions. The 15 mm thickness represented the minimal case sufficient to sustain combustion, whereas the 40 mm thickness was indicative of a more realistic scenario encountered in open water burning [88]. In each experiment, TEEX staff ignited the fuel in the fuel ring by applying a propane torch to the fuel surface for 5 seconds. For each slick thickness, two fire whirl experiments and one pool fire experiment were conducted using HOOPS crude oil. The mass of crude oil deployed for each experiment was quantified on-site using a platform scale (Model S-SK 60/L150, Teraoka Seiko Co. Ltd.). The crude oil residues were collected using 3M sorbent pads and subsequently weighed after air-drying overnight to determine the remaining mass post-burning. After the experiments, samples of the raw crude oil and the residues from each condition were transported to the UC Berkeley Microanalytical Lab

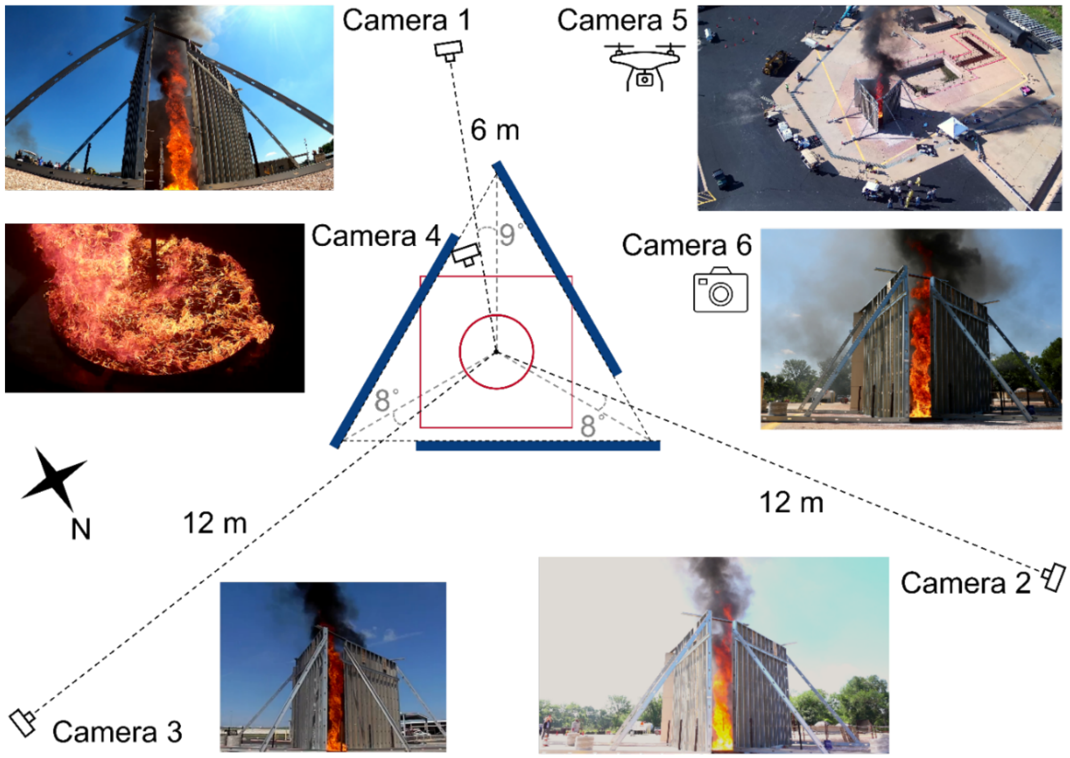

Figure 4.3: The placement of six cameras used in the experiments. Cameras 1, 2, and 3 were positioned at distances of 6 m, 12 m, and 12 m, respectively, from the center of the fuel ring to record both the complete wall structure and parts of the emitted smoke. The cameras were angled to minimize obstruction by the wall structure to the view of the flame. Representative photographs from these cameras are included in the figure for reference.

for elemental analysis, which included carbon, hydrogen, nitrogen, and sulfur (C/H/N/S) analysis using the ThermoFisher Flash Smart Elemental Analyzer.

In these experiments, emission measurements were conducted by the Environmental Protection Agency (EPA), with drone piloting support from the US Geological Survey (USGS). A lightweight emission sampling package developed by EPA named "Kolibri" was carried by a DJI M600 drone to be flown in the plume at altitudes of up to 122 m [89]. The target emission compounds include carbon dioxide (CO2), carbon monoxide (CO), particulate matter with aerodynamic diameter of 2.5 micrometers or less (PM2.5) and elemental/organic/total carbon (EC/OC/TC) in PM2.5. CO2 was measured by using a CO2 Engine® K30 Fast Response sensor (SenseAir), employing non-dispersive infrared absorption (NDIR) with a response time of less than 10 seconds and an accuracy within a 5% error margin. The CO measurements utilized an e2V EC4-500-CO electrochemical sensor (SGX Sensortech) with a response time of less than 30 seconds and an accuracy within a 10% error margin. Both gas sensors were calibrated on a daily basis. PM2.5 sampling utilized a Personal Environmental

Table 4.1: Experimental Matrix for Large-Scale Experiments

Test	Date	Time	Fuel	Configuration	Targeted Slick Thickness (mm)	Fuel Weight (kg)
15FW1	5/17	09:06:55-09:13:57	HOOPS	FW	15	36.1
15FW2		16:13:40-16:20:08				36.2
40FW1		10:49:31-10:58:51			40	65.5
40FW2		14:00:34-14:09:04				63.6
15PF	5/18	08:35:12-08:44:47		PF	15	37.3
40PF		10:14:00-10:30:40			40	65.6
d15FW	5/16	14:05:32-14:14:16	Diesel	FW	15	31.8
d15PF	5/18	13:06:48-13:15:54		PF		31.8

Monitor (PEM) impactor (SKC Inc.), along with a 37 mm tared Teflon filter. Sampling of EC/OC/TC employed a PM2.5 Personal Modular Impactor (PMI) coupled with a 37 mm quartz filter. Both impactors were facilitated by a calibrated micro air pump (C120CNSN, Sensidyne) to ensure a constant flow rate (10 L/min for PEM and 3 L/min for PMI). Filter mass was measured before and after sampling to determine the PM2.5 concentration. EC/OC/TC analysis was conducted by EPA via a modified thermal-optical analysis (TOA) method in the laboratory following field collection. More details of the emission measurements in this large-scale experiment are available in a technical report prepared by the EPA [90].

In total, eight experiments were performed in this study with six experiments using HOOPS crude oil and two experiments using diesel. The experimental conditions are summarized in Table 4.1, including the date of the experiment, time duration from ignition to burnout, fuel type, configuration, targeted slick thickness and measured mass. All experiments had the following measurements taken: temperature, heat flux, air entrainment velocity, mass consumed, video, emissions, and ambient condition, with the exception of tests d15FW and d15PW, which did not have data for mass consumption as the diesel fuel was near fully consumed and the residual mass was irretrievable. In experiments using HOOPS crude oil, four fire whirl experiments and two pool fire experiments were conducted, with two fire whirl and one pool fire experiments using 15 mm slick thickness (named as 15FW1, 15FW2, and 15PF) and two fire whirl and one pool fire experiments using 40 mm slick thickness (named as 40FW1, 40FW2, and 40PF). One fire whirl and one pool fire experiment were conducted using a 15 mm slick of diesel (d15FW and d15PF) for comparison.

4.3 Results and Discussion

Ambient Conditions and Air Entrainment

All fire whirls specified in the experimental plan were successfully generated, encompassing one with diesel and four with HOOPS crude oil. These experiments represent one of the largest controlled fire whirl studies conducted to date. The analysis focused on four fire whirl experiments conducted on the same day using crude oil, with results from pool fires used for comparison. Video footage from cameras 1, 2, and 3 were analyzed to extract the flame height and flame length, which was only analyzed for pool fires. The Python-based software called "Flame Tracker", developed by the UC Berkeley Fire Research Lab, enabled precise measurement of flame characteristics by identifying the red coloration in footage from cameras 1, 2, and 3, thereby quantifying flame height and width [91]. Regarding flame height, the upper portion of the flame was often obscured by smoke. To minimize the obfuscating effect of smoke, the maximum height value obtained from the three camera views was used as the flame height at each time step. In pool fires, the elongation effect of wind on flame length is more significant than in fire whirls, so flame length was specifically analyzed in the pool fire experiments. As the flame inclination in the two pool fire experiments was mainly perpendicular to the view of camera 2, the distance from the identified point for flame height to the center of the pool was calculated as the flame length. For fire whirls, the standardized section of measurement for flame width was set at $z = 1.2$ m, where the flame exhibited relative stability, minimal smoke interference, and reduced inclination from aerodynamic forces. Camera 1 footage provided the primary source for flame width data due to minimal visual obstructions from the wall structure. Figure 4.4 presents data on flame height and width, complemented by camera 1's photographs capturing distinct moments in the development of fire whirls.

Figure 4.4a shows the flame geometry observed in experiment 15FW1, the first experiment conducted in the morning. The first sight of a fire whirl was recorded at $t = 17$ s, with a progressive increase in height which stabilized by $t = 35$ s. From $t = 45$ s, the flame height matched the height of the wall structure, and a relatively steady fire whirl structure ensued with comparably lighter smoke until $t = 157$ s. The period from $t = 157$ s to $t = 175$ s witnessed perturbed stability with darker smoke generated, but a reinstatement of stability transpired post $t = 175$ s. The interval between $t = 267$ s and $t = 294$ s saw intermittent fire whirl occurrences, marked by compromised stability and relatively more black smoke production. The period extending from $t = 295$ s to $t = 408$ s was characterized by a consistent fire whirl with diminished smoke opacity. Subsequent to this duration, the fire whirl

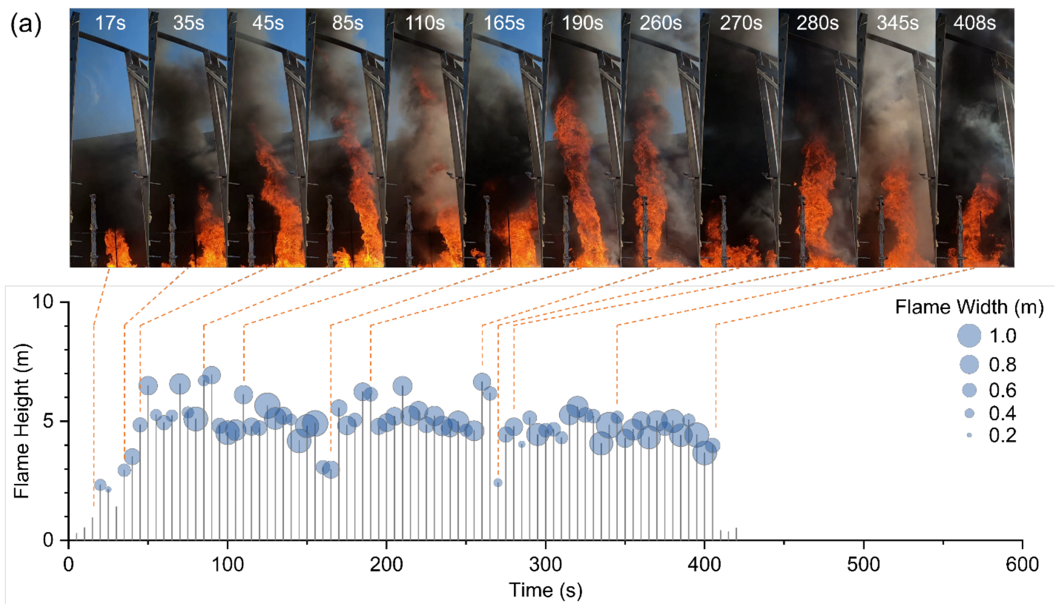
(a)
17s
35s
45s
85s
110s
165s
190s
260s
270s
280s
345s
408s
Flame Height (m)
Time (s)
Flame Width (m)
1.0
0.8
0.6
0.4
0.2

(a)

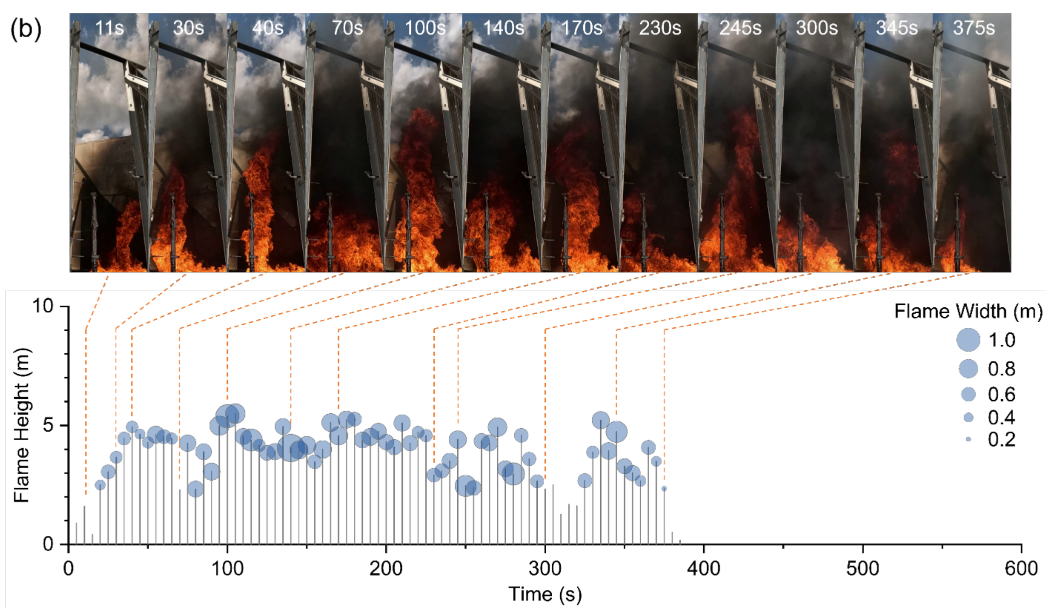
(b)
11s
30s
40s
70s
100s
140s
170s
230s
245s
300s
345s
375s
Flame Height (m)
Time (s)
Flame Width (m)
1.0
0.8
0.6
0.4
0.2

(b)

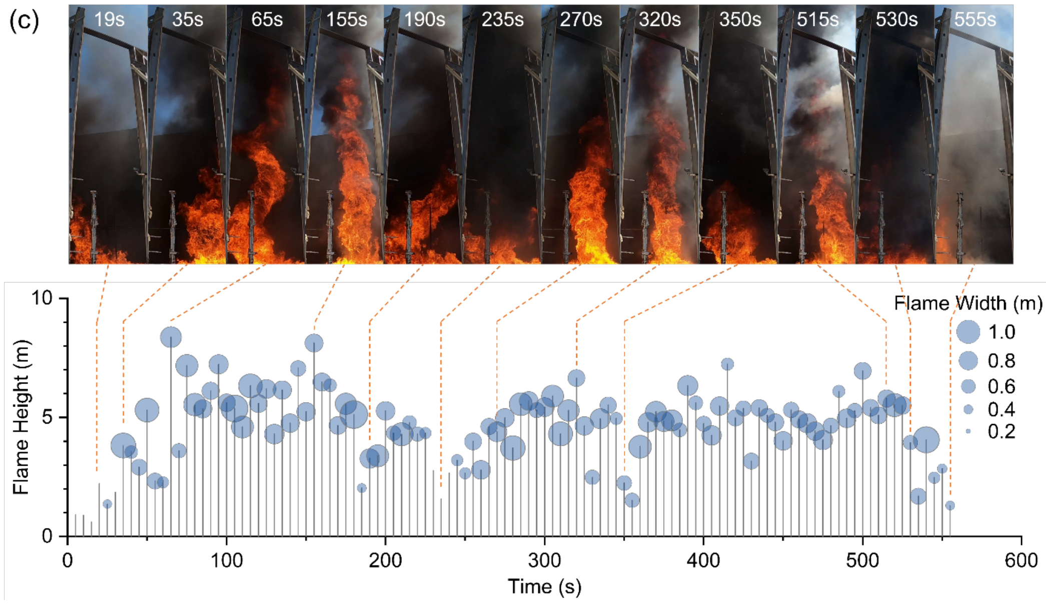

(c)

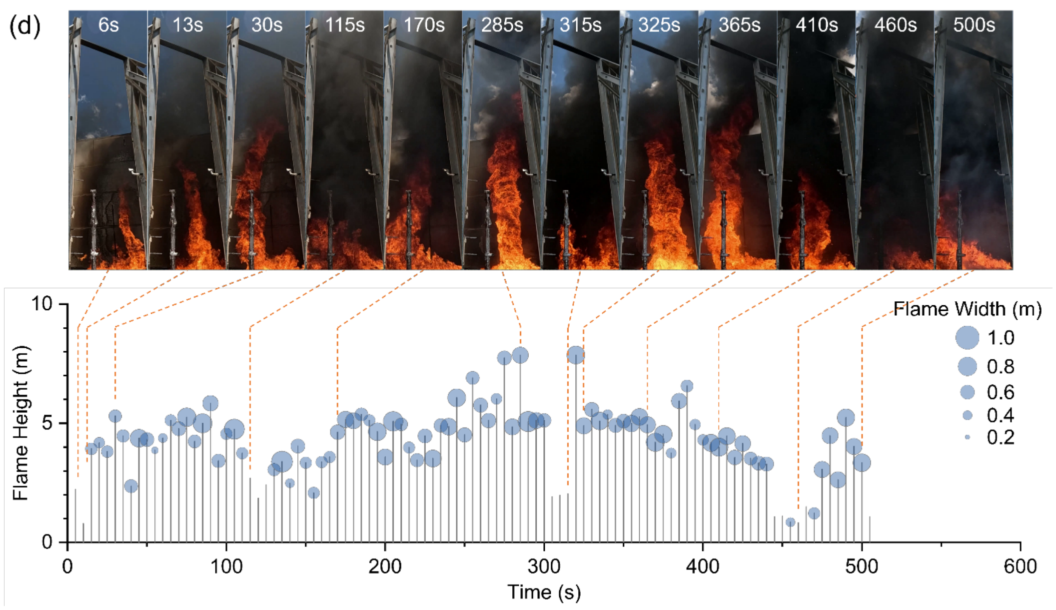

(d)

Figure 4.4: Quantitative visual analysis of flame dynamics in fire whirl experiments: (a) 15FW1, (b) 15FW2, (c) 40FW1, and (d) 40FW2. The bars' lengths correspond to the flame heights, and the circles' diameters represent the flame widths at respective time steps. Bars without circles means no fire whirls recognized from the footage at that time step. Ancillary photographs from Camera 1 are provided to capture the distinct moment in fire whirl development.

decayed, and the flame was extinguished within a span of 13 seconds.

Figure 4.4b shows the flame geometry observed in experiment 15FW2, conducted later in the afternoon under increased wind conditions. Unlike in 15FW1, this fire whirl demonstrated decreased stability with a more pronounced generation of black smoke. Rapid onset of the fire whirl occurred at t = 11 s, achieving relative stability from t = 30 s. Two significant fire whirl disruptions were observed: t = 66 s to t = 71 s, and t = 296 s to t = 324 s, characterized by wind gusts displacing black smoke from the upper region of inlet A, resulting in a visually irregular flame. In general, the fire whirl was visually shorter and less stable in 15FW2. After t = 375 s, the fire whirl ceased, with flame extinction occurring within 12 seconds.

Figure 4.4c shows the flame geometry observed in experiment 40FW1, the second experiment conducted in the morning. The first sight of a fire whirl was recorded at t = 19 s, leading to sustained formation from t = 35 s. Early stages displayed instability, with a notable curved fire whirl structure emerging at t = 65 s. Starting at t = 72 s, the fire whirl transitioned to a stable phase, exhibiting robustness and reduced black smoke emission until t = 182 s. Instability resumed briefly between t = 183 s and t = 191 s, and a major fire whirl disruption occurred from t = 227 s to t = 243 s. Subsequently, two short-lived episodes of instability were recorded, one around t = 350 s and another towards the end of the burning. The final observation of the fire whirl was at t = 555 s, with extinguishment of the flame following in a rapid 3-second period. It is noteworthy that the fastest flame extinguishment following fire whirl was observed in experiments 40FW1 and 40FW2, distinct from 15FW1, 15FW2 and pool fire experiments by substantial release of whitish water vapor from the pool surface.

Figure 4.4d shows the flame geometry observed in experiment 40FW2, the first experiment conducted in the afternoon under increased wind conditions. The rapid formation of the fire whirl, the fastest among all tested, was noted at t = 6 s, potentially facilitated by advantageous ambient wind towards inlet B promoting circulation. From t = 13 s, the fire whirl sustained. Notable disruptions were observed at three intervals: from t = 113 s to t = 127 s, t = 305 s to t = 317 s, and t = 441 s to t = 470 s. Post t = 470 s, marked instability was evident, and following the last sighting of the fire whirl at t = 501 s, flame extinction occurred within 7 seconds. Wind gusts notably angled the black smoke towards the upper portion of inlet A. Overall, this experiment was characterized by less stable fire whirls with intensified black smoke emission.

Contrasting with pool fires, fire whirls notably exhibit increased flame heights attributable to a higher burning rate and the fluid dynamics of a vortex. Figure 4.5 shows the mean flame heights or lengths calculated as the 50% probability of the flame heights or lengths across the burn duration [92, 93].

The data indicates that experiments 15FW1 and 40FW1, conducted in the morning under milder wind conditions, yielded higher mean flame heights than their afternoon counterparts, experiments 40FW2 and 15FW2, which faced stronger winds. Moreover, fire whirls on 40 mm slick thickness of crude oil attained peak flame heights that exceeded those with a 15 mm oil slick. In this study, the mean flame heights of fire whirls were nearly twice

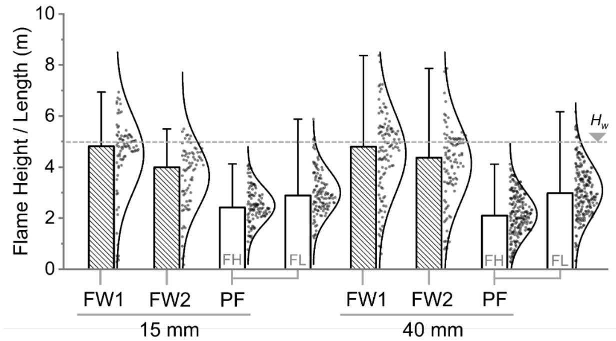

Figure 4.5: Comparative flame height or length in fire whirl and pool fire experiments. Bars denote mean flame height or length values, while whiskers correspond to the observed maximum flame height or length values. Both flame height and flame length are included for pool fire experiments marked as FH and FL. Only flame height is shown for fire whirls. The dashed line represents the height of the wall structure.

that of pool fires. Considering the elongation effect of wind on flame length, the mean flame lengths of pool fires were still at least 40% shorter than those of fire whirls. In a controlled laboratory setting devoid of wind, previous research on fire whirls found transient flame wander yet confirmed its mean position as centralized over the fuel pool's axis [53]. Our field experiments, however, have demonstrated a pronounced deviation of fire whirl flame displacement from the pool center, markedly influenced by prevailing wind conditions. Specifically, at z = 1.2 m, representing the continuous flame region, experiments 15FW2 and 40FW2 showed significant flame displacement towards inlet B (see Figure 4.2(b)), from which the wind originated. In contrast, the intermittent flame and plume regions were observed to lean in the opposite direction. In comparable wind intensity scenarios during pool fire experiments, the flame and plume were consistently pushed away from the wind's origin. This distinct pattern of flame displacement in fire whirls indicates a highly fuel-rich burning environment, with the flame actively moving towards a fresh supply of oxygen to sustain the combustion process. Notably, experiments 15FW1 and 40FW1, conducted under less intense wind conditions, showed the fire whirls remaining relatively closer to the center of the pool.

It is important to note that achieving repeatability of fire whirl experiments is indeed possible in laboratory-controlled environments. However, variations in outdoor environmental conditions, particularly wind speed and direction, naturally influence fire whirl dynamics. These variations do not indicate a lack of experimental stability. Rather, we have carefully quantified these environmental conditions and analyzed their relationship with fire dynamics in the following section.

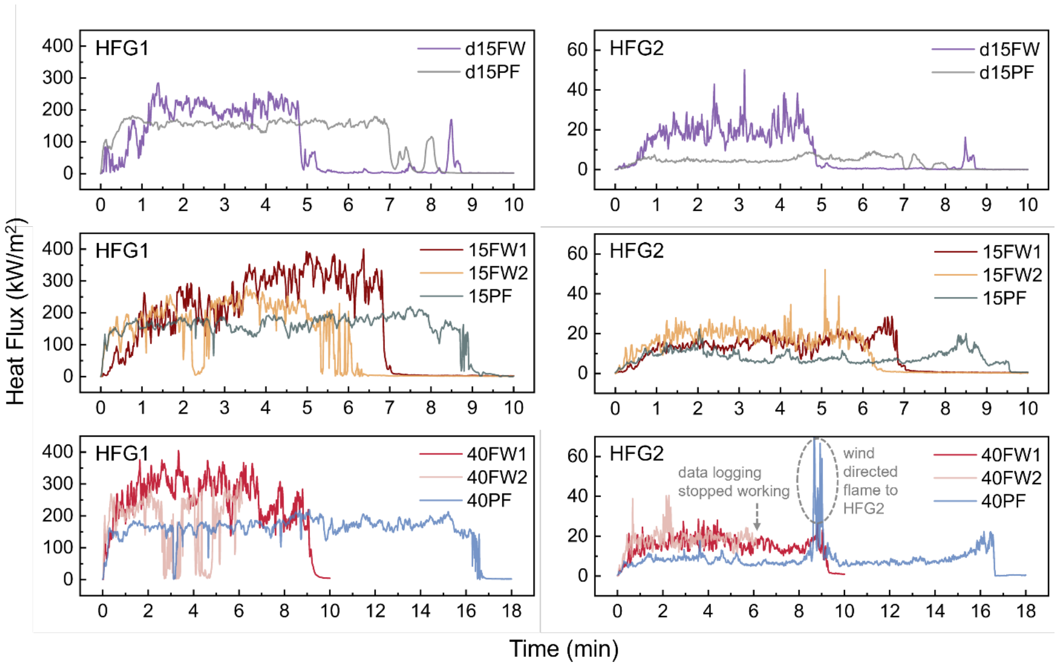

Figure 4.6: Heat flux measured by HFG1 and HFG2 for all experiments.

Burning Parameters and Fuel Consumption

Figure 4.6 illustrates the total heat flux measured by HFG1 positioned near the center of the flame above the fuel surface, and HFG2 located 2.2 m away from the center facing the flame. The results show that the measured total heat flux received by HFG1 in fire whirl experiments is significantly higher than that in pool fires due to the elongated flame and potential for re-radiation within the enclosure. Additionally, the fluctuation in the recorded heat flux during fire whirl experiments can be attributed to the dynamic flame displacement and stability, which are contingent upon the prevailing ambient conditions. Figure 4.7(a) presents a statistical comparison of heat flux readings at the center of the fuel pool for experiments using HOOPS crude oil. It reveals that the averaged heat flux in fire whirl experiments 15FW1 and 40FW1, recorded at 233 kW/m2 and 249 kW/m2 respectively, is significantly elevated - approximately 52% higher – compared to the pool fire experiments 15PF and 40PF, which measured 153 kW/m2 and 164 kW/m2. Moreover, the maximum heat flux values recorded in 15FW1 and 40FW1 are exceptionally high, reading at 400 kW/m2 and 405 kW/m2, an increase of 83% and 84% over their pool fire counterparts - 15PF at 219 kW/m2 and 40PF at 220 kW/m2. The contrast in heat flux between fire whirl experiments 15FW2 and 40FW2 and their respective pool fire counterparts revealed a marginal increase in average heat flux – under 10%. This modest enhancement contrasts with significantly higher maximum heat flux values, registering 30% and 46% above experiments 15PF and 40PF, respectively. It is posited that the marginal average increase is attributable

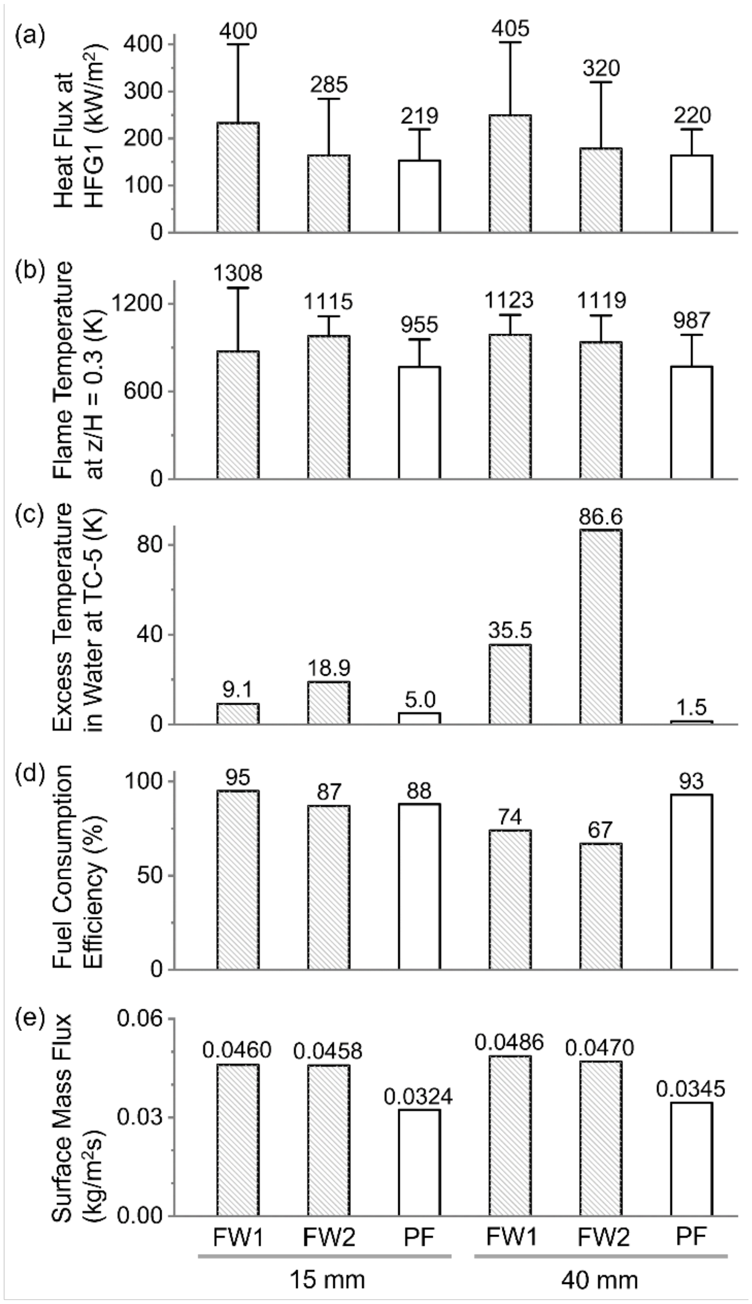

Figure 4.7: Burning parameters measured in fire whirl and pool fire experiments using crude oil. The bars and whiskers in (a) and (b) represent the mean value and the maximum value. Calculated uncertainties from instrument resolution and error propagation were too small to be visibly represented in (c), (d), and (e). Given the unique nature of the large-scale setup, each test is inherently unique due to environmental factors. Therefore, rather than combining replicates and showing sample spread with statistical tests, the results of each individual test are presented.

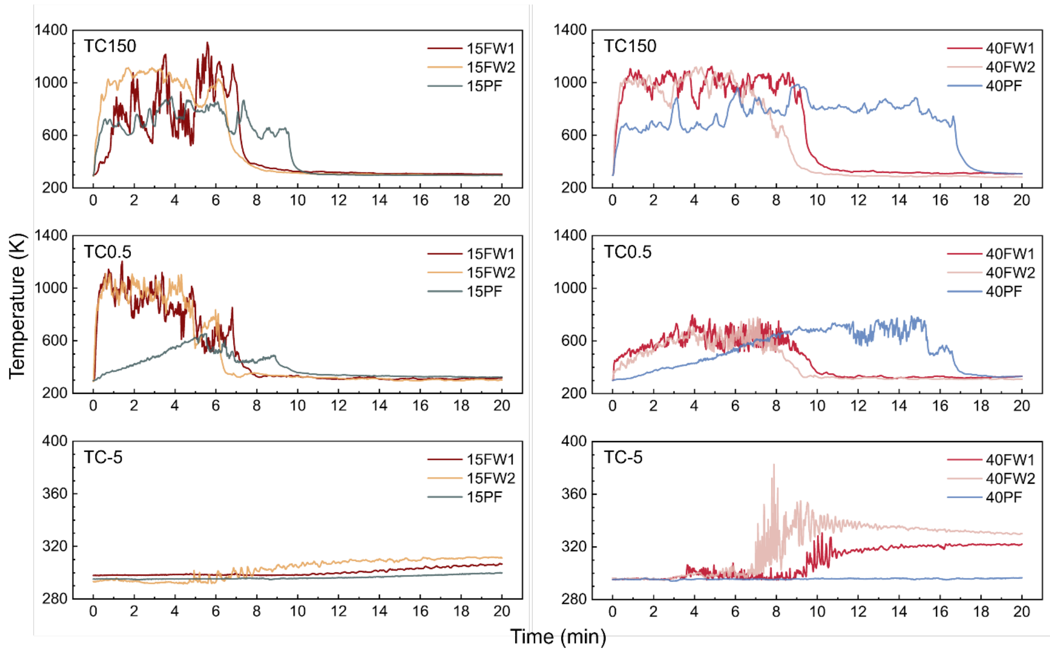

Figure 4.8: Temperature profiles at selected heights representing the temperature in the flame (TC150), in the oil layer (TC0.5), and in the water sublayer (TC-5).

to observed disruptions and deviations of the fire whirl from the pool's center, affirming the influence of dynamic fire behavior on heat flux measurements. All the above-mentioned heat flux values far exceed typical expectations, breaching the sensors' calibration range of up to 150 kW/m2. Notably, Sandia National Laboratory has performed heat flux measurements from fire whirls formed in a wind tunnel using a 1.77 m square fuel pan and measured up to 396 kW/m2 at the ceiling above the flame [83]. While the trends and differences between pool fires and fire whirls are clear, these results are still more than the calibration limit and should be interpreted with caution until further field-scale verification can be performed.

Figure 4.8 illustrates the temperature profiles at various heights within the flame, across the burning oil, and in the water sublayer. Thermocouple TC150, positioned 150 cm above the water surface, captured the typical flame temperature. Analysis reveals consistently higher flame temperatures in fire whirl experiments compared to pool fires, corroborating findings from previous research [94]. Fire whirl flames are typically taller than those in pool fires, and the flame inclination of the pool fire is more easily perturbed by wind. Figure 4.7(b) further interprets flame temperatures at a normalized height (z/H) of 0.3, comparing values at 1.5 m for fire whirls against 1 m for pool fires. Previous large-scale experiments found that fire whirl flame temperatures began to peak at this z/H value of 0.3 [87]. In our experiments, the highest temperature recorded in fire whirls was 1308 K, exceeding that in pool fires by 25%, which was 987 K. This increase corroborates with previous research, indicating that such an elevation in flame temperatures for fire whirls can be expected, despite the potential for even higher readings not captured in these experiments because of the flame displacement. During the pouring of the oil, the oil-water interface can become misaligned with the designed position of the thermocouples shown in Figure 4.2(d), on average by about 1 cm. Thermocouple TC0.5, monitoring within the slick layer of burning oil, recorded temperature variations indicative of a more rapid increase during fire whirl conditions as opposed to pool fires. This suggests an intensified heat transfer from the flame back to the fuel surface in fire whirl experiments. Thermocouple TC-5, recording temperatures less than 5 cm beneath the water surface, captured the extent of thermal penetration. As shown in Figures 4.8 and Figure 4.7(c), the data reveal greater thermal penetration depths in fire whirl experiments compared to pool fires, however the extreme localization of the increased temperature leads to heightened sensitivity to sensor placement. In experiments 40FW1 and 40FW2, a more substantial thermal penetration was noted, with increased volumes of water reaching boiling temperatures. These findings are in agreement with experimental observations showing a pronounced release of water vapor from the pool surface as the flames extinguished in these experiments, implying a direct relationship between deeper thermal penetration and the observed vapor emissions.

The primary goals of deploying fire whirls for in-situ burning include enhancing the burning rate and fuel consumption efficiency, alongside diminishing soot emissions, positively validated in prior small-scale studies utilizing a 10 cm diameter fuel pan [7, 20]. Figure 4.7(d) illustrates a juxtaposition of fuel consumption efficiency and related burning parameters determined from the large-scale experiments using crude oil. Fuel consumption efficiency is quantified by the ratio of fuel mass combusted to the initial fuel mass [20]. Among all conducted experiments using crude oil, fire whirl experiment 15FW1 exhibited the highest fuel consumption efficiency at 95%. For the other oil slick of 15 mm, 15FW2 presented marginally lower fuel consumption efficiency compared to its pool fire counterparts, while for the 40 mm slick thickness, fire whirl experiments showed lower fuel consumption efficiency. Comparing the fuel consumption efficiency between slick thicknesses, fire whirl experiments of 15 mm slick thickness showed higher values than those of 40 mm slick thickness, whereas pool fire experiments showed the opposite results, with the 40 mm condition achieving greater efficiency than the 15 mm. However, in previous laboratory settings, augmenting slick thickness has been linked to higher fuel consumption efficiency, with fire whirl configurations outperforming pool fires [7]. Although large-scale fire whirl experiments demonstrated enhanced burning parameters as measured by heat flux and temperature, a notable decrease in fuel consumption efficiency observed in experiments 15FW2, especially 40FW1 and 40FW2, have cast uncertainty on the scaling of the methodology. The factors affecting fuel consumption efficiency are multifaceted, potentially affected by the size and configuration of the setup, ambient wind conditions, variations in boilover behavior, or a combination of these factors. Due to the fact that one fire whirl presented the highest fuel consumption, it is hypothesized that fire whirls still have the potential for peak efficiency but that factors influencing the burning process disrupted these conditions at some point during subsequent fire whirl experiments. In particular, the experimental observations suggest that external influences may have contributed to the premature extinguishment of the fire whirl. Potential external factors are thus investigated to determine the mechanisms that may impact efficiency.

To compare burning rates between fire whirls and pool fires, the surface mass flux was calculated as the ratio of mass consumption to the product of burn duration and unit fuel surface area [20]. As illustrated in Figure 4.7(e), fire whirls exhibit a significantly elevated surface mass flux relative to pool fires by around 41% during large-scale experiments, with a nominal increment observed as slick thickness increases. These results are consistent with established literature, which indicates that fire whirls demonstrate a higher burning rate than pool fires [20] and that, beyond an initial slick thickness of 10 mm, the burning rate exhibits independence from slick thickness [14]. Consequently, it is inferred that the increased burning rates in fire whirls are not attributable to the incomplete consumption of fuel. The elemental analysis of residue samples and the crude oil used in the experiments is outlined in Table 4.2 for carbon, hydrogen, and nitrogen. Oxygen was calculated from these measurements as the remaining unaccounted for percentage. The elemental analysis indicates that the original crude oil's carbon content decreased marginally from approximately 85.9% to 77.3-82.4% post-burn. This points to a relatively modest volatilization of the residual crude, implying that flame extinguishment prior to the combustion of remaining fuel constituents must play a significant role in the observed burning dynamics. Experimental observations

Table 4.2: Results of Elemental Analysis for Crude Oil and Post-Burn Residue

		C(%)	H(%)	N(%)	O(%)
Original		85.9 ± 0.2	12.6 ± 0.1	1.1 ± 0.1	0.4
Residue	15 mm FW	82.4 ± 0.2	11.3 ± 0.0	1.6 ± 0.1	4.7
	15 mm PF	77.3 ± 0.1	11.2 ± 0.0	1.0 ± 0.1	10.5
	40 mm FW	80.3 ± 0.2	11.4 ± 0.0	1.4 ± 0.1	6.8
	40 mm PF	81.2 ± 0.4	10.8 ± 0.0	0.5 ± 0.2	7.4

and heat flux measurements by HFG2 shown in Figure 4.6 confirm the significant downwind tilt of the flame. Elevated wind speeds can incline the flame close towards the fuel surface, enhancing heat transfer and therefore increasing the fuel consumption efficiency of pool fire burning [95]. Conversely, fire whirls are likely to experience asymmetric air entrainment due to these variable winds, leading to complex effects on burning parameters. The experimental observations point to wind-induced alterations in flame geometry and instability, precipitating changes in the combustion dynamics and, consequently, the fuel consumption efficiency. The second factor contributing to the variation in fuel consumption efficiency may pertain to the dimension of the fuel ring. Our laboratory experiments established an optimal ring radius/wall length ratio of 0.33, leading to a diameter of 1.2 m for the fuel ring in large-scale experiments. However, the actual construction on site resulted in a diameter of 1.5 m, due to the limitations of available materials, with no viable option to modify the size post-manufacture. Consequently, the fixed-size enclosure walls could not be adjusted to maintain the intended separation distance from the fuel ring, leading to an overly proximate placement of the fire whirl to the walls. This proximity likely restricted air entrainment, leading to an excessive fuel-to-air ratio and a potential compounding impact from wind-induced instability. The vortex's development may have been stymied by spatial constraints, resulting in collision with the wall, heat loss, distortion of structure, and diminished overall efficiency. Furthermore, if considering the flame dynamics similar to that of a Burger's vortex, the alteration of the radius could interfere with vortex generation, given the dependence of circulation on the radius. To illustrate the effect of improper sizing of the fuel pool diameter relative to the enclosure size, a brief battery of tests was run at the small scale in which a three-walled triangular enclosure, side length $S = 30$ cm, was compared to two square enclosures. One square enclosure had the same side length as the triangular enclosure, $S = 30$ cm, the other had dimensions such that the distance between the center of the fuel pool and the center of each wall was the same for both the triangular enclosures, $S = 20$ cm. The experiment was repeated three times each for three different heights of the walls forming the enclosure. The average mass loss rate and flame height are shown in Figure 4.9. In this figure, it is shown that decreasing the size of the enclosure relative to the size of the fuel diameter can cause a decrease in the mass loss rate and flame length for large enclosures. Additionally, the three-wall triangular generator at the small scale is most comparable to the square enclosure with the same side length. If one assumes that the magnitude of circulation in an enclosure is dependent on the velocity at the air inlet and the radius at which that air is imparted into the enclosure, then it is reasonable that the scaling parameter for the two geometries of fire whirl generator should be the side length, as that represents the distance from the fuel pool center at which the air is entrained. Ambient wind conditions and fuel ring dimensions are intrinsically linked to the critical parameters that govern fire whirl dynamics: circulation (Γ) and heat release rate ($\dot{Q}$) [6]. Previous research has employed these parameters to classify distinct forms of fire whirls [26, 59]; moreover the ratio of their nondimensional forms was used as an indicator to signal the influence of buoyancy and circulation on the dynamics of fire whirls [21]. In this research, $\dot{Q}$ was estimated as $\dot{Q} = \dot{m}\Delta H_C$, with $\dot{m}$ denoting the burning rate, calculated as mass consumed divided by burning time, and ΔH_C representing the fuel's lower heating value. For the assessment of circulation, it was estimated as $\Gamma_t = 2\pi r_{c,t} U_{\Theta,t}$, where $U_{\Theta,t}$ is the velocity at each inlet, and $r_{c,t}$ is the radius of circulation, which is quantified as the distance from the whirl center to the measuring point on the wall. The outdoor experimental setup, featuring three inlets with variable air entrainment and a shifting whirl center, necessitated that circulation at any particular moment be the mean of the values obtained from all inlets. As $\dot{Q}$ embodies the average heat release rate of the whole burning process, Γ is similarly determined as the mean circulation throughout the burn period. The nondimensional heat release rate, $\dot{Q}^*$, and nondimensional circulation Γ^* were estimated as

$$\dot{Q}^* = \frac{\dot{Q}}{\rho_\infty c_{p\infty} T_\infty \sqrt{gD^5}} \tag{4.1}$$

$$\Gamma^* = \frac{\Gamma}{\sqrt{gD^3}} \tag{4.2}$$

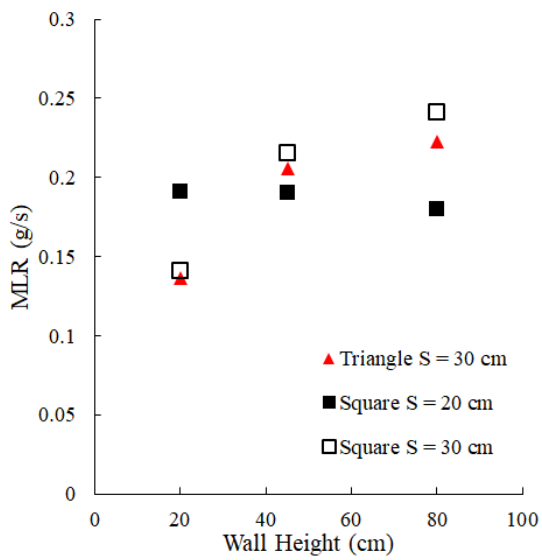

(a)

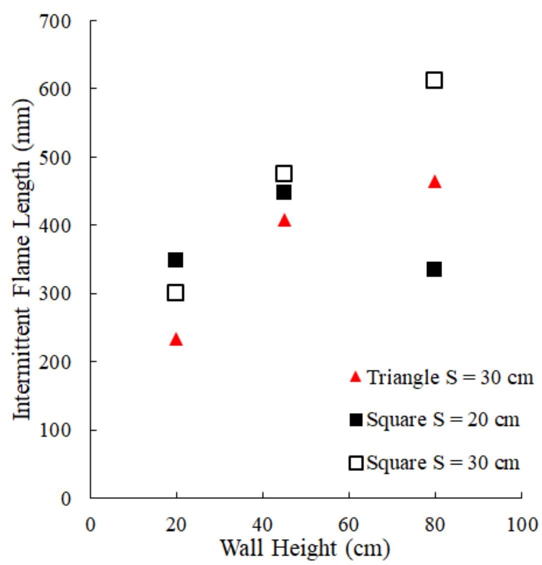

(b)

Figure 4.9: (a) Average mass loss rates and (b) intermittent flame heights for fire whirls at the small scale, with a duel diameter of 10 cm and a side length to the enclosure of either 20 cm or 30 cm. A triangular enclosure is compared to two four-sided square enclosures with varying side length.

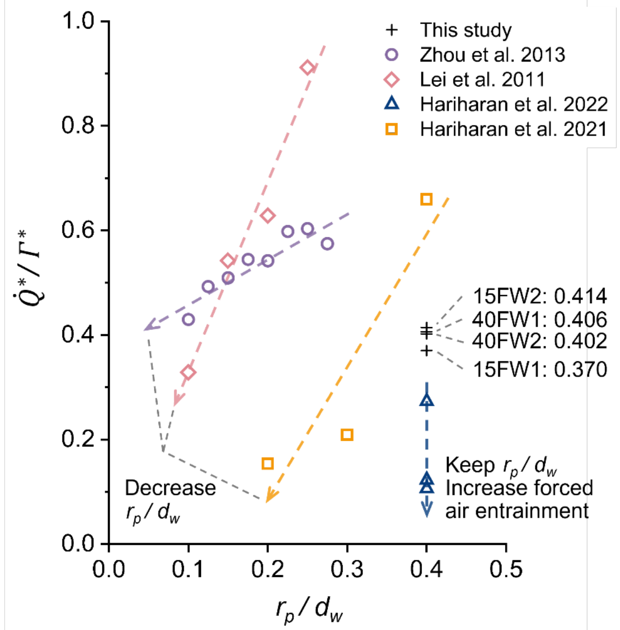

Figure 4.10: The ratio of nondimensional heat release rate $\dot{Q}^*$ and nondimensional circulation Γ^* for this study and values from the literature versus the ratio of the fuel pool radius r_p and the distance from center of the pool to wall structure d_w. Zhou et al. 2013 [30], Lei et al. 2011 [81], and Hariharan et al. 2021 [20] recorded $\dot{Q}$ and Γ with different combinations of r_p and d_w. Hariharan et al. 2022 [21] kept the dimensions of r_p and d_w, but increased the level of forced air entrainment for all inlets.

where ρ_∞, $c_{p\infty}$, and T_∞ are ambient air density, specific heat, and temperature, and D is the diameter of the fuel ring. Figure 4.10 presents the results of $\dot{Q}^*/\Gamma^*$ from this research alongside existing findings from the literature, examining the effects of varying fuel pan sizes and the application of forced air entrainment on fixed-frame fire whirls [20, 21, 30, 81]. The results indicate a reducing trend in the ratio $\dot{Q}^*/\Gamma^*$ as forced air entrainment intensifies, within a specific range. Additionally, the ratio declines as a proportional relationship between the radius of the fuel pool r_p and the distance to the wall structure d_w decreases. This reduction indicates an augmented role of circulation in influencing the behavior of fire whirls. In our experiments, utilizing an enlarged fuel ring for the fixed enclosure dimensions adversely impacted the circulation dynamics of the fire whirls, consequently affecting fuel consumption efficiency. The wind conditions led to irregular forced air entrainment, as opposed to uniform entrainment, causing instability and interruptions in circulation that altered the enhanced combustion characteristics of fire whirls.

The third factor causing variation in fuel consumption efficiency may be attributed to differences in pool boilover. Boilover, typically occurring when burning oil over water, involves the water beneath the oil layer becoming superheated, leading to a sudden and violent eruption of water vapor that ejects burning oil droplets into the flame, and hence intensifying the fire [47]. This complex, multi-phase process is influenced by the complicated interactions of water, oil, and gases. Previous studies have indicated that boilover dynamics are significantly influenced by variables such as pool diameter [74, 75], slick thickness [14, 75], boundary conditions [96, 97], and fuel properties [14, 75]. In the present study, the oil-water interface reached the boiling temperature under all experimental conditions, as evidenced by burning droplets, surface frothing, and water evaporating near the end of the experiments. Consistent with findings from the literature on pool fires, boilover intensity increases with layer thickness but decreases with larger pan diameters [47, 75]. Notably, the observed boilover in this study was less intense than that recorded during laboratory-scale experiments with a 10 cm diameter pan [20]. Temperature measurements taken just below the water's surface indicated enhanced thermal penetration in fire whirls with a 40 mm slick, leading to increased evaporation of water vapor from the pool. This elevated evaporation may contribute to flame extinction, potentially explaining some of the reduced fuel consumption efficiency observed in experiments 40FW1 and 40FW2. On the contrary, some laboratory studies have determined that slick thickness positively correlates with fuel consumption efficiency, noting that thinner slicks (2 – 20 mm) are more prone to pronounced boilover events, whereas thicker slicks (20 mm and above) tend to delay or prevent boilover, due to increased viscosity and insulation effects limiting superheating of the water below [14, 20]. These studies, however, were conducted with significantly smaller fuel pans, ranging from 10 to 16 cm in diameter, as opposed to the 1.5 m used in our large-scale experiments. Additionally, research involving the combustion of crude oil in ice cavities suggests that boilover occurs predominantly in cavities exceeding 25 cm in diameter, where smaller cavities dissipate heat more effectively, and larger ones experience greater in-depth heat conduction losses to the water sublayer due to an expanded oil-water interface [96]. This evidence emphasizes the extent to which scale and boundary conditions can influence the threshold for boilover. Extended burning durations enable greater heat accumulation in the water layer, facilitating deeper thermal penetration. Larger pan diameters may promote void formation at the fuel's surface as it thins during the burning process, particularly due to the increased viscosity, exposing water directly to the flame. While some laboratory studies may use a simplified fuel pan setup with only water beneath the fuel, our large-scale experiments simulate *in-situ* burning conditions with heat sinks encircling the fuel, leading to heating and evaporation of surrounding water surfaces. In experiments 40FW1 and 40FW2, an increased emission of water vapor from the pool coincided with flame decay. The influx of substantial water vapor into the flame has the potential to precipitate abrupt extinguishment. This is largely attributable to a constellation of interconnected mechanisms. Notably, the high heat capacity of water vapor allows it to absorb considerable thermal energy, exerting a cooling effect that may reduce the flame temperature below the minimum required to sustain combustion. Additionally, the sudden surge of water vapor into the flame zone can displace oxygen or dilute it within a fuel-rich environment, while its rapid expansion, particularly when coupled with enhanced turbulence, can obstruct air entrainment, accelerating the cooling and dilution effects. Given that the remaining fuel constituents are less combustible [14, 15], their interaction with water vapor results in an emulsified or diluted state, further impeding ongoing combustion. These combined influences of water vapor during boilover contribute to premature flame extinguishment, thereby compromising fuel consumption efficiency. In this large-scale study, we attempted to replicate open ocean conditions for in-situ burning by conducting experiments in a large pool; however, these conditions are not fully representative of actual marine scenarios. Previous investigations into the boilover phenomenon on turbulent surfaces have demonstrated that water turbulence significantly suppresses the phenomenon by reducing its intensity, delaying its onset, and shortening its duration, which might be a reason why boilover is rare in in-situ burning on open water [97]. As we have shown that fire whirls can significantly enhance surface mass flux, in open water conditions with more complicated environmental scenarios, the potential of increasing the fuel consumption efficiency by using fire whirls will be challenged by more factors. Nevertheless, further research is needed to understand the premature extinguishment in fire whirl dynamics across various environmental conditions, which holds potential for optimizing oil spill remediation strategies.

Gas and Particle Emissions

During the experiments, it was observed that fire whirls produced less voluminous and lighter-colored smoke compared to pool fires, suggesting a decrease in soot production. This finding aligns with previous laboratory studies that examined the impact of varying airflow on emissions from fire whirls [21]. The current study contributes substantial evidence at a large scale regarding the potential of fire whirls to reduce emissions. Emissions are quantified through the modified combustion efficiency, MCE, and the emission factor, EF. Traditionally, MCE is calculated using only the excess concentrations of CO_2 and CO, yielding a variation of less than 1% across different tests in this study. However, a new method adopted from the literature [78], which includes the carbon content in PM, is defined as:

$$MCE = \frac{\Delta CO}{\Delta CO_2 + \Delta CO + \Delta PM} \tag{4.3}$$

where ΔCO_2, ΔCO, and ΔPM represent the excess concentrations of CO2, CO, and carbon in PM, respectively. The incorporation of PM carbon content into MCE calculations resulted in a 4% variation (shown in Table 4.3), thereby illustrating the significance of particulate carbon in the discrepancy of combustion efficiency across tests.

In this study, EF was estimated using the carbon balance method, a widely adopted approach in field emission research [78]. The EF for a given species i is calculated as

$$EF(i) = F_c \times 1000(g/kg) \times \frac{\Delta i}{\Delta C} \tag{4.4}$$

where F_c signifies the fraction of carbon by mass in the fuel, and Δi and ΔC denote the excess concentration of species i and carbon emissions (kg/m3), respectively. Emission factors for

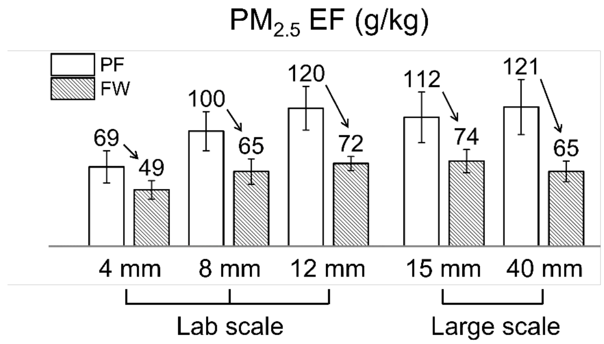

Figure 4.11: EFs of PM2.5 in this large-scale study and previous laboratory-scale study [7] burning HOOPS crude oil with different oil slick thickness.

CO2, CO, PM2.5, OC, EC and TC are collated in Table 4.3, with NS representing data not sampled. Comparative analysis indicates that fire whirls exhibit a higher combustion

Table 4.3: Summary of Emission Results for Experiments on Crude Oil

	CO_2 (g/kg)	CO (g/kg)	$PM_{2.5}$ (g/kg)	MCE	OC (g/kg)	EC (g/kg)	TC (g/kg)
15FW1	2672 ± 76	44 ± 4	76.6 ± 15	0.893	NS	NS	NS
15FW2	2757 ± 78	45 ± 4	72.1 ± 14	0.895	9.0 ± 2.4	67 ± 22	76.6 ± 23
15PF	2723 ± 69	45 ± 3	111.9 ± 22	0.874	14.7 ± 4.0	78.3 ± 25	92.9 ± 28
40FW1	2890 ± 82	44 ± 4	53.1 ± 11	0.897	11.2 ± 3.0	63.3 ± 20	74.5 ± 22
40FW2	2902 ± 82	43 ± 4	76.6 ± 15	0.913	9.8 ± 2.6	48.2 ± 15	58.0 ± 17
40PF	2566 ± 65	59 ± 4	120.7 ± 24	0.891	7.8 ± 2.1	65.0 ± 21	72.8 ± 22

efficiency than traditional pool fires. The EFs identified in this study are comparable in terms of the order of magnitude to those from previous studies involving the combustion of crude oil [15, 20, 78]. Analyses of filter samples suggest that approximately 75% of the PM2.5 mass is composed of carbon from crude oil in fire whirls, predominantly in the form of EC (86%). Figure 4.11 contrasts the $EF_{PM2.5}$ from large-scale fire whirl experiments with those from prior lab-based experiments using HOOPS crude oil [7]. On average, PM2.5 emissions from fire whirls were found to be 40% lower than from pool fires in large-scale experiments, in line with the findings from laboratory experiments. Nevertheless, discrepancies remain between large-scale and laboratory-scale studies concerning the influence of oil slick thickness on PM2.5 emissions, indicating a need for further experimentation to clarify this aspect. These large-scale fire whirl experiments are the largest to date in fire whirl studies for quantifying emissions. The data corroborated the hypothesis from laboratory-scale studies that fire whirls reduce particle emission levels compared to pool fires when scaled up [20].

However, questions persist regarding the fundamental interactions taking place in the gas phase and how these conditions affect the emissions of soot and other compounds. From the measurement of ambient conditions, flame geometry, and burning parameters, there are several interconnected factors to explain it. First, enhanced air entrainment in fire whirls leads to a leaner global equivalent ratio, resulting in higher average temperatures and more efficient combustion [34]. Second, improved heat feedback in fire whirls, both radiative and convective, contributes to higher fuel evaporation rates and consequently higher heat release rates, which further supports the combustion process [15, 24, 98]. The unique fluid dynamics of fire whirls, characterized by strong radial inflow at the bottom boundary layer and reduced turbulence, creates an environment that favors improved mixing and increased flame stretch, both of which are known to reduce soot formation in non-premixed combustion [51]. Finally, the unique structure of fire whirls allows for better oxygen availability along the height of the flame, potentially enabling the oxidation of soot particles formed in lower regions as they travel upwards through the oxidation zone of the flame [35]. Insights into the interactions between fire dynamics and emissions could help optimize configurations and conditions to minimize noxious emissions in in-situ burning, necessitating more future research to investigate these fundamental interactions across various conditions and scales.

4.4 Conclusions

While previous fire whirl research has been largely confined to laboratory settings with limited environmental application focus, this study makes several pioneering contributions. First, we conducted the first large-scale controlled fire whirl experiments specifically designed for oil spill remediation, successfully applying a three-wall structure design developed in laboratory small-scale setup to an outdoor environment for large-scale fire whirl generation. Second, we demonstrated the practical viability of fire whirl methodology for enhancing in-situ burning through significant improvements in burning efficiency and emissions reduction. The experiment revealed that, compared to traditional pool fires, fire whirls at times demonstrated enhanced performance in multiple aspects, including elevated flame height, increased flame and water temperatures, intensified surface heat and mass flux, improved combustion efficiency, and decreased particle emissions. These characteristics suggest that fire whirls could potentially offer a more effective method for in-situ burning of spilled oil over open water surfaces. Third, we provided comprehensive field-condition performance metrics across multiple parameters simultaneously, revealing the influence of ambient conditions, particularly wind direction and velocity, on fire whirl stability and formation. In our field experiment, fire whirls exhibited a tendency to displace toward the prevailing wind direction, indicating a complex relationship between ambient conditions and fire whirl dynamics. While the experiments suggested that fire whirls might be more effective in calm ambient conditions, further research is needed to fully understand their performance across a range of wind conditions and to explore potential design modifications that could enhance stability in variable environmental scenarios. The experiment highlighted several key considerations for future research and methodological improvements. One critical factor identified was the importance of optimizing the ring radius to wall length ratio, which plays an important role in fire whirl behavior. Additionally, the study revealed the need for improvements in instrumentation, including heat flux gauges with higher upper ranges to more accurately capture the intense heat fluxes associated with large-scale fire whirls, a better-structured method for measuring the temperature at oil-water interface to understand the boilover phenomenon, and more comprehensive emission quantifications to assess environmental impacts. Future work should also focus on exploring the factors contributing to the inconsistent observations of fuel consumption efficiency between fire whirls and pool fires, as this aspect has significant implications for the potential application of fire whirls in oil spill remediation. Moreover, as a pioneering large-scale field experiment in this area, valuable lessons were learned regarding experimental setup, data collection, and safety protocols, which will be instrumental in refining future studies and potentially scaling up to even larger experiments. While the findings of this study are promising, translating these results into real-world oil spill scenarios presents significant challenges. The experimental setup, involving three walls to generate fire whirls, is not directly applicable to open ocean environments where large oil spills typically occur. Future research should explore applicable methods for inducing fire whirls in open water conditions, possibly through the use of mobile or deployable structures, or by leveraging natural atmospheric conditions fitting for fire whirl formation. Additionally, the environmental impact of large-scale fire whirls needs to be thoroughly assessed before considering their application in real oil spill scenarios. Despite these challenges, the insights gained from this experiment provide a valuable foundation for developing innovative approaches to oil spill remediation.

Chapter 5

Conclusion

This work represents a series of experimental investigations into the characteristics of fire whirls at various scales. Fire whirls show their desirable properties for enhancing *in-situ* burning as scales increase from laboratory to field scale structures. The burning rate of the fire whirl increases as the thickness of the fuel layer increases until it reaches a critical thickness beyond which further fuel thickness does not increase burning rate. This is due to the insulating effect the fuel provides when it is over a layer of cold water. This behavior has been demonstrated in pool fires in the past, but the critical fuel insulation thickness for fire whirls is much greater than that for pool fires. While increasing fuel slick thicknesses do correlate to slightly higher emissions of soot per unit mass of fuel, the rate at which the emissions increase with slick thickness for pool fires remains much larger.

As fire whirl generators increase in size relative to the size of the fuel source, the flame length and burning rates also increase up until a critical value of wall height beyond which the fire shrinks and becomes weaker. Short walls, those on the order of the fuel pool diameter, create flames with higher mass loss rates for narrower enclosures, but do not greatly effect the other burning parameters or other enclosure sizes. As the height of the walls of the fire whirl generator enclosure increases, the emissions of particulate matter decrease to a minimum value for a given enclosure width.

One of the largest controlled fire whirl experiments yet conducted was enacted to prove the scalability of the fire whirl and the fixed-frame fire whirl generator. For a fuel pool 1.5 m wide and enclosure walls 5 m high, the fire whirl showed higher flame lengths and surface mass fluxes than the pool fire of the same diameter. Importantly, the fire whirl showed a decrease in particulate matter production of around 30% when compared to the pool fire. One factor of the field-scale fire whirl that cannot be anticipated at the laboratory-scale is the effect of weather, with ambient wind causing disturbances in the flame great enough to potentially cause early extinction. Appropriate sizing between the fuel pool and sidewalls is also important and may have affected available oxygen and stability at the large scale.

At all scales, the fire whirl produced less soot than a pool fire of the same diameter while also burning at a higher rate. The cause of this aspect of the fire whirl phenomenon is as yet not wholly understood. As the fuel surface experiences greater mass flux, more fuel is being consumed in the flame but without a commensurate increase in the yield of soot or products of combustion that indicate incompleteness. One mechanism to explain this may be that the fire whirl consumes a greater percentage of the soot that would be produced inside the flame before it can escape the flame tip.

Further work on this topic must be conducted to prove this hypothesis. Namely, an investigation into the size and morphology of the soot particles emitted from the fire whirl would be needed to make definitive conclusions as to the reason for the decreased particulate emissions. Following from this would be a study of the emissions from the fire whirl at different applied circulations in such a way that the heat release rate of the flame can be decoupled from the circulation.

The investigations presented here have taken a very practical approach to understanding the behavior of the fire whirl at varying scales from the view of an experimentalist. The fire whirl is one of the most beautiful and awe-inspiring sights in the field of fire science, and more questions about the structure and nature of the fire whirl remain to be answered by experimentalists and theoreticians alike.

Bibliography

[1] Jason M. Forthofer and Scott L. Goodrick. "Review of Vortices in Wildland Fire". In: *Journal of Combustion* 2011 (2011).

[2] California Department of Forestry and Fire Protection. *Burn Over Fatalities: July 26, 2018 Carr Incident*. Tech. rep. Cal Fire, 2018.

[3] S. Soma and K. Saito. "Reconstruction of fire whirls using scale models". In: *Combustion and Flame* (1991).

[4] Emily Conover. "Flaming fuel on water creates 'blue whirl' that burns clean". In: *ScienceNews* (2016). URL: `https://www.sciencenews.org/article/flaming-fuel-water-creates-blue-whirl-burns-clean`.

[5] Huahua Xiao, Michael J. Gollner, and Elaine S. Oran. "From Fire Whirls to Blue Whirls and Combustion with Reduced Pollution". In: *Proceedings of the National Academy of Science* 113.34 (2016).

[6] Ali Tohidi, Michael J. Gollner, and Huahua Xiao. "Fire Whirls". In: *Annual Review of Fluid Mechanics* (2018).

[7] J.L. Dowling et al. "Fire whirl emissions and burning rates for crude oil slicks of varying thicknesses". In: *Fuel* (2025).

[8] *Short Term Energy Outlook*. Tech. rep. United States Energy Information Administration, Nov. 6, 2025.

[9] *Worldwide Rig Count Report*. Tech. rep. Baker Hughes, Nov. 7, 2025.

[10] A. Jernelöv. "The Threats from Oil Spills: Now, Then, and in the Future". In: *AMBIO* (2010).

[11] Alan A. Allen et al. "The Use of Controlled Burning during the Gulf of Mexico Deepwater Horizon MC-252 Oil Spill Response". In: *International Oil Spill Conference*. 2011.

[12] Alan A. Allen. "Contained Controlled Burning of Spilled Oil During the Exxon Valdez Oil Spill". In: *Spill Technology Newsletter* 15 (1990).

[13] Merv F. Fingas. "In-Situ Burning of Oil Spills - An Overview". In: *Spill Technology Newsletter* 23 (1998).

[14] Laurens van Gelderen et al. "Importance of the slick thickness for effective *in-situ* burning of crude oil". In: *Fire Safety Journal* 78 (2015).

[15] L. van Gelderen, L.M.V. Malmquist, and G. Jomaas. "Vaporization order and burning efficiency of crude oils during in-situ burning on water". In: *Fuel* (2017).

[16] D.D. Evan et al. "In Situ Burning of Oil Spills". In: *Journal of research of the National Institute of Standards and Technology* (2001).

[17] I. Buist et al. "In-situ burning". In: *Pure and Applied Chemistry* (1999).

[18] M. Szwangruber et al. "Occupational exposure to air pollutants emitted from in situ burning of offshore oil spills: a large-scale field study". In: *International Maritime Health* (2022).

[19] J.S. Brown et al. "Thoracic and respirable particle definitions for human health risk". In: *Particle and Fibre Toxicology* (2013).

[20] SB Hariharan et al. "Comparison of particulate-matter emissions from liquid-fueled pool fires and fire whirls". In: *Combustion and Flame* 227 (2021).

[21] Sriram Bharath Hariharan et al. "Effects of Natural and Forced Air Entrainment on PM Emissions from Fire Whirls". In: *Environmental Science and Technology* (2022).

[22] H.W. Emmons and S.J. Ying. "The fire whirl". In: *Symposium (International) on Combustion* 11 (1967).

[23] Wilfried Coenen et al. "Observed dependence of characteristics of liquid-pool fires on swirl magnitude". In: *Combustion and Flame* 205 (2019).

[24] Jiao Lei et al. "Burning Rates of Liquid Fuels in Fire Whirls". In: *Combustion and Flame* 159 (6 2012).

[25] Ritsu Dobashi et al. "Experimental Study on Flame Height and Radiant Heat of Fire Whirls". In: *Fire Technology* 52 (2016).

[26] J. Lei et al. "Experimental investigation on flame patterns of buoyant diffusion flame in a large range of imposed circulations". In: *Proceedings of the Combustion Institute* (2017).

[27] Kazunori Kuwana et al. "Fire whirls: A Combustion Science Perspective". In: *Combustion Science and Technology* 195.13 (2023).

[28] E.E. Zukoski, T. Kubota, and B. Cetegen. "Entrainment in fire plumes". In: *Fire Safety Journal* (1981).

[29] The burning rate's effect on the flame length of weak fire whirls. "K. Kuwana and S. Morishita and R. Dobashi and K.H. Chuah and K. Saito". In: *Proceedings of the Combustion Institute* (2011).

[30] K. Zhou et al. "Effect of flow circulation on combustion dynamics of fire whirls". In: *Proceedings of the Combustion Institute* (2013).

[31] A.Y. Snegirev et al. "Numerical studies and experimental observations of whirling flames". In: *International Journal of Heat and Mass Transfer* (2004).

[32] R.I. Emori and K. Saitoh. "A study of scaling laws in pool and crib fires". In: *Combustion Science and Technology* (1983).

[33] I.M. Kennedy, W. Kollmann, and J.-Y. Chen. "A model for soot formation in a laminar diffusion flame". In: *Combustion and Flame* (1990).

[34] B.S. Haynes and H.G. Wagner. "Soot formation". In: *Progress in Energy and Combustion Science* (1981).

[35] Irvin Glassman. "Soot formation in combustion processes". In: *Symposium (International) on Combustion* 22.1 (1989), pp. 295–311. ISSN: 0082-0784. DOI: `https://doi.org/10.1016/S0082-0784(89)80036-0`. URL: `https://www.sciencedirect.com/science/article/pii/S0082078489800360`.

[36] J. Du and R.L. Axelbaum. "The effect of flame structure on soot-particle inception in diffusion flames". In: *Combustion and Flame* (1995).

[37] J.H. Kent and H.G. Wagner. "Why do diffusion flames emit smoke?" In: *Combustion Science and Technology* (1984).

[38] S. Ukleja. "Production of smoke and carbon dioxide in underventilated enclosure fires". PhD thesis. University of Ulster, 2012.

[39] R.J. Yokelson, D.W.T. Griffith, and D.E. Ward. "Open-path Fourier transform infrared studies of large-scale laboratory biomass fires". In: *Journal of Geophysical Research* (1996).

[40] V. Babrauskas. "Heat Release in Fires". In: Elsevier Science Publishers LTD., 1992. Chap. Simple cases of Heat Release Rates.

[41] George M. Byram and Robert E. Martin. "Fire Whirlwinds in the Laboratory". In: *Fire Control Notes* 23.1 (1962).

[42] A.O. Ekperusi et al. "In-Situ Burning as an Oil Spill Control Measure and Its Effect on The Environment". In: *SPE Nigeria Annual International Conference and Exhibition.* 2019.

[43] Jr. Bruce A. Benner et al. "Polycyclic Aromatic Hydrocarbon Emissions from the Combustion of Crude Oil on Water". In: *Environmental Science and Technology* 24 (1990).

[44] S.E. Petty. "Combustion of crude oil on water". In: *Fire Safety Journal* 5 (1983).

[45] J. Garo et al. "Determination of the Thermal Efficiency of Pre-Boilover Burning of a Slick of Oil on Water". In: *Spill Science and Technology Bulletin* 5.2 (1999).

[46] Yuhang Chen et al. "Pool fire dynamics: Principles, models and recent advances". In: *Progress in Energy and Combustion Science* (2023).

[47] J.P. Garo, J.P. Vantelon, and A.C. Fernandez-Pello. “Boilover Burning of Oil Spilled on Water”. In: *Twenty Fifth Symposium (International) on Combustion*. 1994.

[48] A.D. Weiss et al. “A model for the constant-density boundary layer surrounding fire whirls”. In: *Journal of Fluid Mechanics* 900 (2020).

[49] Richard I. Emori and Kozo Saito. “Model experiment of hazardous forest fire whirl”. In: *Fire Technology* 18 (1982).

[50] R. J. Santoro et al. “The Transport and Growth of Soot Particles in Laminar Diffusion Flames”. In: *Combustion Science and Technology* 53.2-3 (1987), pp. 89–115. DOI: 10.1080/00102208708947022.

[51] Y.R Sivathanu and G.M. Faeth. “Soot Volume Fractions in the Overfire Region of Turbulent Diffusion Flames”. In: *Combustion and Flame* 81 (1990).

[52] Joseph L. Dowling, Mohammedhadi Hajilou, and Michael J. Gollner. “Experimental Characterization of Enhanced In-situ Burning Using Fire Whirls on a Three-wall Structure”. In: *44th AMOP Technical Seminar on Environmental Contamination & Response*. 2022.

[53] Pengfei Wang et al. “Experimental Study on Flame Wander of Fire Whirl”. In: *Fire Technology* 54 (2018).

[54] *ANS17Y*. ExxonMobil Refining and Supply Crude Oil Assay. 2018.

[55] *HOOPS16F*. ExxonMobil Refining and Supply Crude Oil Assay. 2018.

[56] Jiao Lei, Naian Liu, and Kohyu Satoh. “Buoyant pool fires under imposed circulations before the formation of fire whirls”. In: *Proceedings of the Combustion Institute* 35 (3 2015).

[57] Longhua Hu. “A review of physics and correlations of pool fire behaviour in wind and future challenges”. In: *Fire Safety Journal* 91 (2017).

[58] Bernd Broeckmann and Hans-Georg Schecker. “Heat Transfer Mechanisms and Boilover in Burning Oil-Water Systems”. In: *Journal of Loss Prevention in the Process Industries* 8.3 (1995).

[59] Jiao Lei et al. “Turbulent cylindrical fire whirl”. In: *Combustion and Flame* (2023).

[60] K. Kuwana et al. “Scaling Fire Whirls”. In: *Fire Safety Journal* (2008).

[61] K.H. Chuah et al. “Inclined fire whirls”. In: *Proceedings of the Combustion Institute* (2011).

[62] W. Cui et al. “Large-scale field experiements on enhancing in-situ burning with fire whirls”. In: *Fuel* (2026).

[63] J. Lei et al. “Experimental research on flame revolution and precession of fire whirls”. In: *Proceedings of the Combustion Institute* (2013).

[64] K.A. Hartl and A.J. Smits. “Scaling of a small scale burner fire whirl”. In: *Combustion and Flame* (2016).

[65] K.A. Hartl and A.J. Smits. "Comparing burner fire whirls to pool fire whirls". In: *Combustion and Flame* (2023).

[66] J.L. Dowling. "Effect of Fire Whirl Generator Dimensions on Flame Length and Burning Rate". MA thesis. University of Maryland, College Park, 2020.

[67] R. Zhou and Z.N. Wu. "Fire whirls due to surrounding flame sources and the influence of the rotation speed on flame height". In: *Journal of Fluid Mechanics* (2007).

[68] P. Wang et al. "Fire whirl experimental facility with no enclosure of solid walls: design and validation". In: *Fire Technology* (2014).

[69] G. Heskestad. *SFPE Handbook of Fire Protection Engineering*. Springer, 2016. Chap. Fire Plumes, Flame Height, and Air Entrainment.

[70] M.G. Barron et al. "Long-Term Ecological Impacts from Oil Spills: Comparison of Exxon Valdez, Hebei Spirit, and Deepwater Horizon". In: *Environmental Science and Technology* (2020).

[71] C.H. Peterson et al. "Long-Term Ecosystem Response to the Exxon Valdez Oil Spill". In: *Science* (2003).

[72] Q. Lin et al. "In-Situ Burning of Oil in Coastal Marshes. 2. Oil Spill Cleanup Efficiency as a Function of Oil Type, Marsh Type, and Water Depth". In: *Environmental Science and Technology* (2005).

[73] J. Fritt-Rasmussen et al. "Coastline in-situ burning of oil spills, analysis of a Greenland field experiment". In: *Journal of Hazardous Materials* (2023).

[74] H. Koseki and G.Q. Mulholland. "The effect of diameter on the burning of crude oil pool fires". In: (1991).

[75] J.L. Torero et al. "Determination of the Burning Characteristics of a SLick of Oil on Water". In: *Spill Science and Technology Bulletin* (2003).

[76] L. Hu. "A review of physics and correlations of pool fire behaviour in wind and future challenges". In: *Fire Safety Journal* (2017).

[77] A.S. Rangwala N.G. Sauer K.S. Arsava. "Burning capability of the flame refluxer under the influence of waves". In: *Fire Safety Journal* (2023).

[78] J. Aurell et al. "Analysis of emissions and residue from methods to improve efficiency of at-sea, in situ oil spill burns". In: *Marine Pollution Bulletin* (2021).

[79] Y. Iga et al. "Open-field scale-model experiments of fire whirls over L-shaped line fires". In: *Progress in Scale Modelling, and International Journal* (2021).

[80] W.K. Chow, Z. He, and Y. Gao. "Internal Fire Whirls in a Vertical Shaft". In: *Journal of Fire Sciences* (2011).

[81] J. Lei et al. "Experimental research on combustion dynamics of medium-scale fire whirl". In: *Proceedings of the Combustion Institute* (2011).

[82] C. Pinto et al. "C. Pinto and D. Viegas and M. Almeida and J. Raposo". In: *Fire Safety Journal* (2017).

[83] A. Luketa. *Fire Whirl Investigation*. Tech. rep. Sandia National Laboratory, 2018.

[84] C. Ji et al. "Effect of initial generating eddy height on temperature, velocity and air entrainment of fire whirl". In: *Combustion and Flame* (2024).

[85] G.M. Byram and R.E. Martin. "The Modeling of Fire Whirlwinds". In: *Forest Science* (1970).

[86] A. Darwish Ahmad et al. "Large-scale fire whirl and forest fire disasters: Awareness, implications, and the need for developing preventative methods". In: *Frontiers in Mechanical Engineering* (2023).

[87] J. Lei et al. "Radiative characteristics of large-scale fire whirl: An experimental study". In: *International Journal of Thermal Sciences* (2024).

[88] I. Buist et al. "In-situ Burnin in Ice-Affected Waters: State of Knowledge Report". In: *Arctic Response Technology* (2013).

[89] J. Aurell et al. "Wildland fire emission sampling at Fishlake National Forest, Utah using an unmanned aircraft system". In: *Atmospheric Environment* (2021).

[90] J. Aurell and B.K. Gullet. *In-Situ Oil Burns Fire Whirls*. Tech. rep. U.S. Environmental Protection Agency, 2024.

[91] L. Carmignani. "Flame Tracker: An image analysis program to measure flame characteristics". In: *SoftwareX* (2021).

[92] X. Ju et al. "Effect of circulation on flame heights over liquid fuel pools". In: *Combustion and Flame* (2022).

[93] G. Heskestad. "Luminous flame heights of turbulent diffusion flames". In: *Fire Safety Journal* (1983).

[94] J. Lei et al. "Temperature, velocity and air entrainment of fire whirl plume: A comprehensive experimental investigation". In: *Combustion and Flame* (2015).

[95] V. Blinov and G. Khudyakov. *Diffusion burning of Liquids*. Tech. rep. U.S. Army Engineering Research and Development Laboratories, 1961.

[96] X. Shi et al. "Experimental study of burning behavior of large-scale crude oil fires in ice cavities, Fire Safety Journal". In: *Fire Safety Journal* (2022).

[97] L. Chang and A.S. Rangwala. "Experimental study of crude oil slick burning on a turbulent water surface". In: *Combustion and Flame* (2022).

[98] P. Wang et al. "An experimental study on thermal radiation of fire whirl". In: *International Journal of Wildland Fire* (2017).